Instituto de Química
Programa de Pós-Graduação em Química

TESE DE DOUTORADO

ORIGIN OF *NON*-ARRHENIUS KINETICS FOR THE TETRAATOMIC HYDROGEN EXCHANGE REACTIONS OF OH WITH HCl, HBr AND HI: *AB INITIO* MOLECULAR DYNAMICS

Nayara Dantas Coutinho Carvalho

Prof. Dr. Heibbe Cristhian B. de Oliveira
Prof. Dr. Vincenzo Aquilanti

Brasília, DF
2018

Instituto de Química
Programa de Pós-Graduação em Química

TESE DE DOUTORADO

ORIGIN OF *NON*-ARRHENIUS KINETICS FOR THE TETRAATOMIC HYDROGEN EXCHANGE REACTIONS OF OH WITH HCl, HBr AND HI: *AB INITIO* MOLECULAR DYNAMICS

Nayara Dantas Coutinho Carvalho

Prof. Dr. Heibbe Cristhian B. de Oliveira
Prof. Dr. Vincenzo Aquilanti

Brasília, DF
2018

Folha de Aprovação

Comunicamos a aprovação da Defesa de Tese do (a) aluno (a) **Nayara Dantas Coutinho Carvalho**, matrícula nº **14/0107762**, intitulada "***ORIGIN OF NON-ARRHENIUS KINETICS FOR THE TETRAATOMIC HYDROGEN EXCHANGE REACTIONS OF OH WITH HCl, HBr AND HI: AB INITIO MOLECULAR DYNAMICS***", apresentada no (a) Auditório Azul do Instituto de Química (IQ) da Universidade de Brasília (UnB) em 20 de abril de 2018.

Prof. Dr. Angelo Henrique de Lira Machado
Presidente de Banca (IQ/UnB)

Prof. Dr. Demétrio Antônio da Silva Filho
Membro Titular (IF / UnB)

Prof. Dr. José Roberto dos Santos Politi
Membro Titular (IQ/UnB)

Prof. Dr. Luciano Ribeiro
Membro Titular (UnUCET/UEG)

Prof. Dr. Hamilton Barbosa Napolitano
Membro Suplente (UnUCET/UEG)

Em 20 de abril de 2018.

To my Family

ACKNOWLEDGEMENTS

Thanks to God for being my refuge and my fortress throughout PhD.

To my parents, Orgacy José Coutinho and Márcia Freire Dantas Coutinho, for always prioritizing my education. Thank you also for unconditional love and for being examples of dedication and integrity in my life. I love you so much!!!

To my brothers Vinícius Dantas Coutinho and Victor Dantas Coutinho, for all their support and companionship during this trajectory. You are very special to me.

To professor Kleber Mundim, who without even realizing it, motivated me at various moments; his enthusiasm, dedication and passion for science are contagious. Thank you also for the great and valuable discussions about *non*-Arrhenius problems, which were of great value.

To professor Vincenzo Aquilanti, for his example as a scientist and professor. During all this time I appreciated his love for what he does and his competence. More than an excellent researcher, I have the honor to work beside sensational human being, and on many occasions, I learned from him about humility, charity and care for others. Thank you for the great teaching and discussions about this thesis and the receptivity in Perugia. I look forward to our next meetings with caipirinhas, barbecue, good conversation and science. I would like to thank the University of Perugia for providing me with exceptional experiences. I hope to go back soon.

To Professor Ademir João Camargo for introducing me to the academic world and for presenting *ab initio* molecular dynamics to me. Thank you for the discussions and contributions to this thesis.

To laboratory colleagues, Arsênio Pereira Vaconcelos Neto, Ana Gabriela Coelho Oliveira, Thiago Oliveira Lopes, Daniel Francisco Scalabrini Machado, Fernanda Ferrari and Sandro Francisco Brito for moments of discussion, learning and for good coffee times. Thanks very much, guys!!

To my friends Jackeline Souza D'Abadia and Bruno Magalhães D'Abadia for accommodation in Brasilia, but mainly for friendship. To have them as my friends is God's gift.

To the University of Brasília, represented by the postgraduate program in Chemistry, for institutional support.

To the Coordenação de Aperfeiçoamento de Pessoal de Nível Superior and the Fundação de Apoio à pesquisa do Distrito Federal for financial support.

Special thanks go to my husband Valter Henrique Carvalho Silva, for love and companionship. But mainly because of the great incentive during those years. Your support was fundamental for me to become a researcher today. Besides having an excellent husband, I am fortunate to have one of the best researchers in chemical kinetics in Brazil by my side. Thank you very much for the discussions and for thesis review, you are FANTASTIC. I have the greatest love in the world for you!

ABSTRACT

The reaction $OH + HX \longrightarrow H_2O + X\,(X = \text{Halogen})$ is very important in atmospheric chemistry because it belongs to a class of processes producing halogen atoms that are destroyers of ozone. Additionally, these four-body reactions are also of basic relevance for chemical kinetics. Its kinetics has manifested *non*-Arrhenius behavior: the experimental rate constants for the OH + HCl reaction, when extended to low temperatures, show a strong concave curvature in the Arrhenius plot, a phenomenon designated as *sub*-Arrhenius behavior, while reactions with HBr and HI are considered as typical processes that exhibit negative temperature dependence of the rate constants (*anti*-Arrhenius behavior). From a theoretical point of view, these reactions have been studied in order to obtain the potential energy surface and to reproduce these complex rate constants using the Transition State Theory. Here, in order to understand the change of *anti*-Arrhenius to *sub*-Arrhenius behavior after the simple halogen replacement, we performed a blend of first-principles Born-Oppenheimer molecular dynamics and high-level Transition-State-Theory modified to account for quantum tunneling conditions. In the Born-Oppenheimer molecular dynamics approach, the trajectories are step-by-step generated on a potential energy surface that was quantum mechanically calculated on-the-fly, and they are thermostatically equilibrated to correspond to a specific temperature. We considered four temperatures – 50, 200, 350 and 500 K. For OH + HI and OH + HBr, the visualizations of rearrangements of bonds along trajectories showed how molecular reorientation occurs in order that the reactants encounter a mutual angle of approach favorable for them to proceed to reaction. Besides the demonstration of the crucial role of stereodynamics, additional documentation was also provided on the interesting manifestation of the roaming phenomenon, both regarding the search for reactive configurations sterically favorable to reaction and the subsequent departure involving vibrational excitation of products. For the OH + HCl reaction, We find that the theoretical rate constants calculated with Bell tunneling corrections are in good agreement with extensive experimental data available for this reaction in the ample temperature range from 200 to 2000 K using an insightful approach more direct than previous treatments. Furthermore, the Born-Oppenheimer molecular dynamics simulation showed the role of molecular orientation in promoting this reaction is minor than in the HBr and HI, and dominating is the effect of quantum mechanical penetration through the of energy barrier along the reaction path on the potential energy surface. The discussion of these results provides clarification of the origin of different *non*-Arrhenius mechanisms involved in the series of reactions.

RESUMO

As reações $OH + HX \longrightarrow H_2O + X\ (X = \text{Halogênio})$ tem um papel importante para a química da atmosfera, uma vez que pertencem a uma classe de processos que produzem átomos de halogênios que destroem a camada de ozônio. Adicionalmente essas reações de quatro corpos também têm relevância fundamental para a química cinética. As reações entre o radical hidroxil e os haletos de hidrogênio apresentam comportamento cinético não-Arrhenius. Os dados cinéticos disponíveis para a reação entre o radical hidroxil e o cloreto de hidrogênio tem mostrado uma forte curvatura côncava para baixas temperaturas, fenômeno descrito como *sub*-Arrhenius, enquanto que as reações entre o radical hidroxil e as moléculas de HBr e HI são considerados processos típicos que apresentam dependência negativa da temperatura na constante cinética (comportamento *anti*-Arrhenius). De um ponto de vista teórico, essas reações têm sido estudadas com o objetivo de descrever a superfície de energia potencial e reproduzir essas complexas taxas de reação usando a Teoria do Estado de Transição. Neste trabalho, com objetivo de compreender a transição do comportamento *anti*-Arrhenius para o *sub*-Arrhenius após uma simples substituição de halogênios, realizamos cálculos de dinâmica molecular de Born-Oppenheimer e teoria do estado da transição com correção de tunelamento. Na dinâmica molecular de Born-Oppenheimer as forças que atuam sobre as partículas são obtidas a partir de cálculos de estrutura eletrônica executados em tempo real, à medida que a trajetória da dinâmica é gerada. Nestes estudos foram consideradas quatro temperaturas - 50, 200, 350 e 500 K. Para as reações OH + HI e OH + HBr, as visualizações das trajetórias em função das coordenadas que correlacionam as ligações quebradas e formadas durante a reação evidenciam que há uma mudança de mecanismo em função da temperatura: enquanto que, para temperaturas mais baixas os reagentes se orientam em torno da direção reativa, à medida que a temperatura aumenta, o efeito *roaming* fica mais pronunciado, provocando um “atraso” no processo reativo. Para a reação OH + HCl, as constantes cinéticas teóricas calculadas utilizando a correção de tunelamento de Bell estavam em acordo com os dados experimentais para a faixa de temperatura entre 200 e 2000 K, com um mínimo de esforço quando comparado com tratamentos muito mais elaborados. Adicionalmente, as simulações de dinâmica molecular de Born-Oppenheimer mostraram que o processo de orientação é menos efetivo do que o observado para as reações OH + HI e OH + HBr, enfatizando, assim, o papel do efeito do tunelamento quântico na penetração da barreira de energia no caminho de reação ao longo da superfície de energia potencial. A discussão desses resultados fornece esclarecimentos sobre a origem de diferentes mecanismos não-Arrhenius envolvidos na série de reações.

LIST OF FIGURES

Figure 1: Temperature dependence of the rate constant for the OH + HBr reaction..... 2

Figure 2: Reactive cross-sections as a function of collision energy for the OH +HBr. Isotropic distributions for the vibrational states, $\nu 1, \nu 2 = (0,0), (0,1)\ \text{and}\ (1,1)$ of the produced water are indicated by circles, squares and triangles, respectively. The shaded area shows the acceptable error in the experiment and the uncertainty of analysis. Figure copied from reference 25. 4

Figure 3: (a) The orange area represents the experimental results for acceptable angle. (b) Spatial distribution of electrons in HOMO orbital obtained from calculations at B3LYP/6-311++G (d, p) level. Figure copied from Ref. 23. 4

Figure 4: Energy profile with stationary points for the OH + HBr reaction. The energies are in kcal.mol^{-1}. Figure adapted from REF. 31. 6

Figure 5: Temperature dependence of the rate constant for the OH + HI reaction. 7

Figure 6: Pictorial view of comparison of the stationary points on the potential energy surfaces for the $OH + HX \longrightarrow H_2O + X$ (X= Halogen) reaction, adapted from Ref. [63]. 10

Figure 7: The experimental rate constants[64], which discriminate the transition from anti-Arrhenius (HI and HBr) to *sub*-Arrhenius. From our knowledge, there are no experimental values for the HF + OH reaction. 11

Figure 8: The linear behavior of the Arrhenius model, in the Arrhenius plot. The slope of the line provides the activation energy. 13

Figure 9: Representation of dependence of $\ln k$ by reciprocal temperature $1/T$, showing the super-Arrhenius and *sub*-Arrhenius behavior. Adapted by Ref.29. 14

Figure 10: Representation of dependence of Ea by reciprocal temperature $1/T$. The temperature directly influences the activation energy behavior. Adapted from Ref.29 15

Figure 11: Schematic representation of the potential energy profile showing the main stationary points along the IRC path for exothermic reaction. 19

LIST OF ABREVIATIONS

AIMD	*Ab Initio* Molecular Dynamics
BOMD	Born Oppenheimer Molecular Dynamics
CMD	Classical Molecular Dynamics
CPMD	Car-Parrinello Molecular Dynamics
DFT	Density functional Theory
EMD	Ehrenfest Molecular Dynamics
HOMO	Highest Occupied Molecular Orbital
IUPAC	International Union of Pure and Applied Chemistry
MD	Molecular Dynamics
KIE	Kinetics isotopic effects
PES	Potential Energy Surface
PIMD	Path Integrals Molecular Dynamics
QCT	Quasi-Classical Trajectories
RBA	Rotating Bond Aproximation
RPMD	Ring Polymer Molecular Dynamics
TS	Transition State
TST	Transition State of Theory
VTST	Variational Transition State theory

CONTENTS

1 INTRODUCTION 1

1.1 Motivation 1

1.1 Plan of the thesis 9

2 Theoretical approach 12

2.1 Chemical Reaction Rates 12

2.1.1 The basic theory 12

2.2 *Non*-Arrhenius Behavior 14

2.2.1 Arrhenius law deformation 16

2.3 Computational Chemistry 17

2.3.1 Brief description of the static methodology 17

2.3.2 Potential Energy surface 17

2.3.3 Transition State Theory 19

2.4 Molecular Dynamics Simulations 21

2.4.1 Molecular Dynamics: The idea 21

2.4.2 Integrating the Equations of Motion 22

2.4.3 Born-Oppenheimer Molecular Dynamics 24

3 PAPERS 26

4 CONCLUSIONS 84

REFERENCES 87

PUBLICATIONS AND EVENTS 96

1 INTRODUCTION

1.1 Motivation

Reactive halogen species play a crucial role in atmospheric chemistry by disturbing the natural equilibrium processes that create and destroy ozone in the stratosphere. For example, depletion of ozone through the reaction with halogen atoms occurs through efficient catalytic cycles. These atoms react with ozone molecules to yield halogen monoxide (XO) and oxygen molecules (O_2).[1,2]

In particular, the $OH + HX \longrightarrow H_2O + X$ $(X = F, Cl, Br \text{ and } I)$ reactions have been extensively studied because they are major providers of the halogens in the atmosphere. Further understanding of these reactions is important from the technological point of view, for example, in the kinetic study of the role of iodine in light water reactor accidents, where volatile fission products such as iodine can be released from fuel into an atmosphere of hydrogen and vapor, upon reacting with the these species can cause accidents.[3] Additionally, these four-body reactions are also of basic relevance for both experimental and theoretical chemical kinetics.

The rate constants for most rate processes depend on absolute temperature according to the Arrhenius law: however, for reactions of OH radical with hydrogen halides, when extended to low temperatures, deviations are observed: the kinetics data available for the reaction with HCl[4,5] show a strong concave curvature for low temperatures, a phenomenon described as *sub*-Arrhenius behavior, while reactions with HBr[6–12] and HI[13–17] are considered as typical processes that exhibit negative temperature dependence of the reaction rate (*anti*-Arrhenius behavior).

The direct and inverse reactions

$$OH + HBr \underset{k_{-1}}{\overset{k_1}{\rightleftharpoons}} H_2O + Br \qquad (1)$$

and its their isotopic variants have been exhaustively studied in recent years, both from a theoretical and an experimental point of view, by different research groups. The kinetic data obtained from the reaction between the hydroxyl radical and hydrogen bromide have shown that there is a strong negative temperature dependence for values below 200 K. The first kinetic data obtained for range of temperature were measured by Ravishakara and co-workers[6] for the temperature range from 249 to 416 K. The authors found that the rate constant was independent of temperature and equal to $k = 1.19(\pm 0.14) \cdot 10^{-11} \mathrm{cm^3 s^{-1}}$. Before the work of Ravishakara *et al*.[6], some other authors had obtained the rate constant value for isolated temperatures: Takacs and Glass (298 K),[18] Smith and Zellner (298 K)[19] and Wilson and co-workers (1925 K)[20].

However, the first kinetic study that was able to identify the negative dependence on temperature was developed by Sims *et al*.[7] for the temperature range from 23 to 295 K. This same behavior was observed by Atkinson *et al*.[8] for the range of temperature from 76 to 242 K. The only discrepancy between these last two studies was whether the rate constant really was dependent on

the temperature for values above 150 K. In order to solve this uncertainty, in 2002, the experimental groups of Rowe and Smith, in Rennes and Tucson, made new measurements for the rate constants in the temperature range between 23 and 416 K. This study present two forms of global fits:[12]

$$k(T) = 1.11 \cdot 10^{-11} \left(\frac{T}{298}\right)^{-0,91} \text{cm}^3\text{molecules}^{-1}\text{s}^{-1} \quad (2)$$

$$k(T) = 1.06 \cdot 10^{-11} \left(\frac{T}{298}\right)^{-1,09} \cdot \exp\left(\frac{-10.5\ \text{K}}{T}\right) \text{cm}^3\text{molecules}^{-1}\text{s}^{-1} \quad (3)$$

The autors demonstrated that both of which accurately describe the negative temperature dependence for OH + HBr reaction. Figure 1 shows the dependence on temperature of the rate constant for the OH + HBr reaction and summarizes the mainly experimental results:

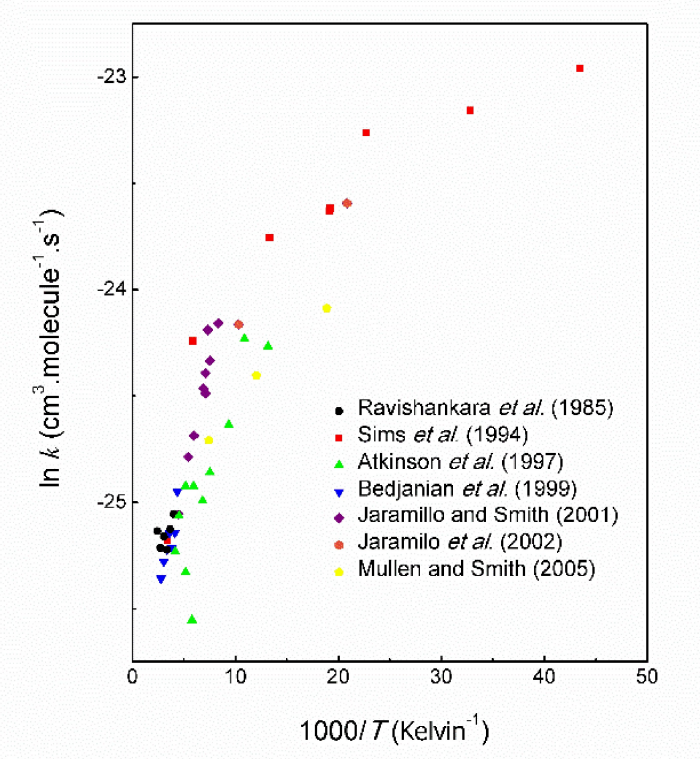

Figure 1: Temperature dependence of the rate constant for the OH + HBr reaction.

Concomitantly, several other studies have been published with the objective of understanding the isotopic effect on the rate constant of the OH + HBr reaction. This effect was initially investigated for temperatures above 230 K by Bedjanian *et al.*9. The isotopic variations for Reaction 1 are described as:

$$\text{OD} + \text{HBr} \xrightarrow{k_2} \text{HOD} + \text{Br}, \quad (4)$$

$$OH + DBr \xrightarrow{k_3} HOD + Br, \quad (5)$$

$$OD + DBr \xrightarrow{k_4} D_2O + Br. \quad (6)$$

In the study of Bedjanian *et al.*[9] (230-360 K), both primary kinetics isotopic effects (KIE), $\left({}^{k_1}/_{k_3}\right)$ and $\left({}^{k_2}/_{k_4}\right)$, are found near 1.8, and for both secondary isotopic kinetics effects, $\left({}^{k_1}/_{k_2}\right)$ and $\left({}^{k_3}/_{k_4}\right)$, the measured values were near to 1. In 2001, Jaramillo *et al.*[10] proposed the study the KIE for a different temperature range. The values obtained for 120 K for $\left({}^{k_1}/_{k_3}\right)$ were 1.00($\pm$0.17) and $\left({}^{k_2}/_{k_4}\right)$ 0.46 ($\pm$0.08), while, for secondary effect $\left({}^{k_1}/_{k_2}\right)$ and $\left({}^{k_2}/_{k_4}\right)$, they were 0.94($\pm$0.20) and 0.43($\pm$0.05), respectively. The authors observed that for the temperature of 120 K the deuterated reactants reacted as fast or faster than the neutral hydrogen isotope. Mullen and Smith[21] selected the temperature range between 53 and 135 K and found that the KIE was temperature independent, taking into account the experimental error, and that the mean value for the primary isotopic kinetic effect $((k_H/k_D)_{MED})$ was equal to 1.64, and for the secondary effect $((k_H/k_D)_{MED})$ it was equal to 0.87.

The KIE can be a good experimental criterion for elucidating the tunneling effect in a chemical reaction. Generally, the reactions that have tunneling effect have high values for primary KIE.[22] Due to the low values found for primary KIE for the OH + HBr reaction, it can be concluded that the tunneling effect is negligible.

Another important phenomenon in this reaction, the stereodynamic aspects had been convincingly revealed in experiments, where in order to understand orientational effects, The Osaka group[23–26] studied the OH + HBr reaction using crossed molecular beams for higher than thermal energy (0.05-0.026 eV). This result indicated that the cross-section decreased, increasing the collision energy (Figure 2), and suggested that reorientation effects of the reagents strongly favor the reactivity. That is, if reorientation effects are present in the OH + HBr reaction, they are probably more pronounced for small values of the collision energy, since reagents have more time to reorient before the reactive process.

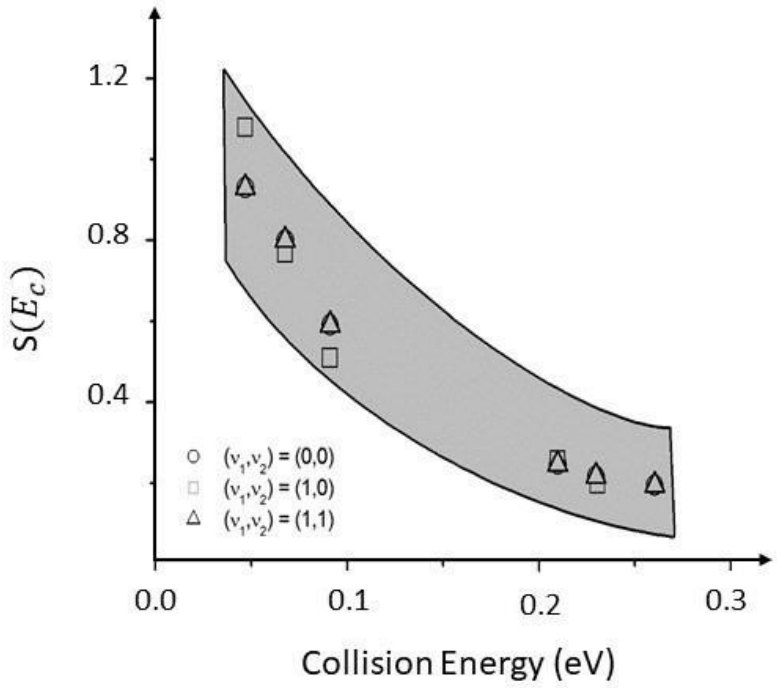

Figure 2: Reactive cross-sections as a function of collision energy for the OH +HBr. Isotropic distributions for the vibrational states, $(v_1, v_2) = (0,0), (0,1)$ and $(1,1)$ of the produced water are indicated by circles, squares and triangles, respectively. The shaded area shows the acceptable error in the experiment and the uncertainty of analysis. Figure copied from Ref. 25.

More recently, in 2010 Tsai and co-workers[23] continued the experimental studies for the OH + HBr reaction in order to prove the energy dependence of reorientation effects and to extract information on the ratio of the O-end, H-end and sideways collisions, Osaka group used an orientating hexapole electrostatic field. Regarding the relative importance of the reactive sites, it was found that the O-end attack is most favored for this reaction than the H-end attack by a factor of 3.4 ± 2.3; they also suggested a cone of acceptance with a limiting angle[23] of $\alpha = 117 \pm 13$ degrees for the reaction to occur (see Figure 3). The authors also suggested that the orientation effect may be related to the spatial distribution of the HOMO electron of the OH radical.

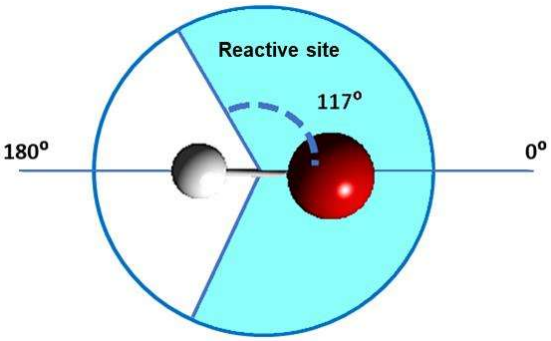

Figure 3: The blue area represents the experimental results for acceptable angle. Figure adapted from Ref. 23.

From a theoretical point of view, the OH + HBr reaction has been studied under a focus on the calculation of the rate constants and on the interpretation of *anti*-Arrhenius behavior. Clary and co-workers,[27] using rotationally adiabatic capture theory with a long-range electrostatic interaction potential, predicted a maximum for the rate constant at temperatures of 20 K. In 1994, Clary *et al*. performed quantum scattering calculation, within rotating bond approximation (RBA).[28] The simple potential energy surface (PES) as a functional London-Eyring-Polanyi-Sato was constructed. This surface showed that between the reactants and the products there is a transition state with energy slightly less than the reactants. These calculations also suggested the existence of dependence of the reaction cross-section in the initial rotational quantum number of OH, and the authors proposed that this effect may be responsible for the negative dependence of the rate constant as a function of temperature. Subsequently, Nizamov and co-workers[29] obtained similar results with an additional PES and quasi-classical trajectories (QCT).

Liu *et al*. [30] performed a direct dynamic study over a wide range of temperatures, 23-2000 K. The information on the accurate potential energy surface, including geometries, energies and vibrational frequencies of the stationary points and some extra points along the minimum energy pat, was obtained directly from *ab initio* electronic structure calculations. The results show that at the side of the reactants, there is an entrance complex with an energy less than that of the reactants, so the reaction system passes through a transition state with an energy slightly higher than that of the reactants, contradicting the previous results[27–29]. Furthermore, they calculated the rate constants using Variational Transition State theory (VTST) and attributed the *anti*-Arrhenius behavior to tunneling effects of the barrier with 0.85 kcal mol^{-1}.

Recently, Oliveira-Filho and co-workers[31,32] calculated an accurate potential energy surface, and using high-level electronic structure calculations, the authors found a saddle point with less energy than the reactants and the presence of a van der Waals well (See Figure 4), which they suggested as being responsible for the negative activation energy observed in experimental kinetic data. Then, the same authors published a complementary study where they introduced quasi-classical trajectories (QCT), obtained information about the cross-section and found a good description of the rate constants for the range of temperature 5-500 K.[32]

In 2014 using QCT, Ree *et al.*[33] calculated the rate constants using an analytical form for two, three and four bodies and a long-range potential. The authors found that, at low temperatures the reaction is driven by attractive forces and occurs with the formation of a BrH-OH entrance complex, which presents a sufficient life-time that guarantees the tunneling of the hydrogen atom. Additionally, they applied tunneling corrections and obtained a rate in accordance with the experimental data. Simultaneously, Zang *et al*.[34] studied five stationary points on the potential energy surface that included entrance and exit complexes, as well as the transition state using the CCSD(T)/cc-pV5Z-PP calculation level. Even using a different methodology, the values for energy and geometric parameters were consistent with those obtained by Oliveira-Filho *et al*.[31,32]. However, none of these authors discussed the importance of the favored stereodynamic effect at low temperatures observed in the Osaka experiments.[23–26]

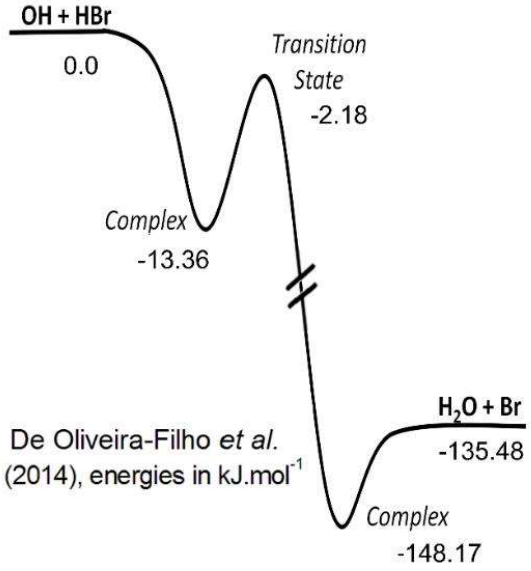

Figure 4: Energy profile with stationary points for the OH + HBr reaction. The energies are in kcal.mol^{-1}. Figure adapted from Ref. 31.

Although important in the technological and atmospheric context, the experimental studies for hydroxyl radical and hydrogen iodine are limited: just a few values are available for rate constants near 300 K.[13–16] Takacs and Glass[13], using fast flow system found for a temperature of 295 K, found the rate constant equal to $1.3 \cdot 10^{-11}\,\mathrm{cm^3 molecule^{-1} s^{-1}}$. Mac Leod *et al.*[14], using a laser photolysis-resonance fluorescence (LP-RF) apparatus, measured the rate constant at 298 K and found $k = 2.7 \cdot 10^{-11}\,\mathrm{cm^3 molecule^{-1} s^{-1}}$. In 1990, Lancar, Mellouki and Poulet[15] experimentally measured the rate constant at 298 K using discharge-flow reactors coupled to electron paragmagnetic resonance (EPR) and mass spectrometry for analysis and found that the rate constant was $3.3(\pm 0.2) \cdot 10^{-11}\,\mathrm{cm^3 molecule^{-1} s^{-1}}$. In 1999, Jost Campuzano-Crowley[17] measured the rate constants at room temperature and, in order to solve the discrepancies in the literature, extended the study to a small temperature range between 246 and 353 K. Under these conditions, the authors haven shown that the rate constants had a negative dependence on temperature (Figure 5), the same *anti*-Arrhenius behavior observed for the reaction between OH and HBr. As a result, this study produced the following adjustment of the rate constants:

$$k\ (246 - 353\ \mathrm{K}) = 7.0 \cdot 10^{-11} \left(\frac{T}{298}\right)^{-1.5 \pm 0.5}\ \mathrm{cm^3 molecule^{-1} s^{-1}} \qquad (7)$$

In a contribution to the understanding of the detailed microscopic dynamics of the OH + HI reaction, Moise and co-workers used crossed molecular beam experiments to measure relative state-to-state cross-section and steric asymmetries, and present a comparison with the previously studied systems OH-HCl and OH-HBr[35]. They discussed the relevance of the potential energy surface of these molecular systems in the reactive process. From a theoretical perspective, the direct and reverse reactions have been of interest for some time. In 1997, Inada and Akagane[43] predicted the

activation energy for the $\mathrm{I} + \mathrm{H_2O} \longrightarrow \mathrm{OH} + \mathrm{HI}$ reaction using the quadratic configuration interaction method with single and double substitutions (QCISD)[36].

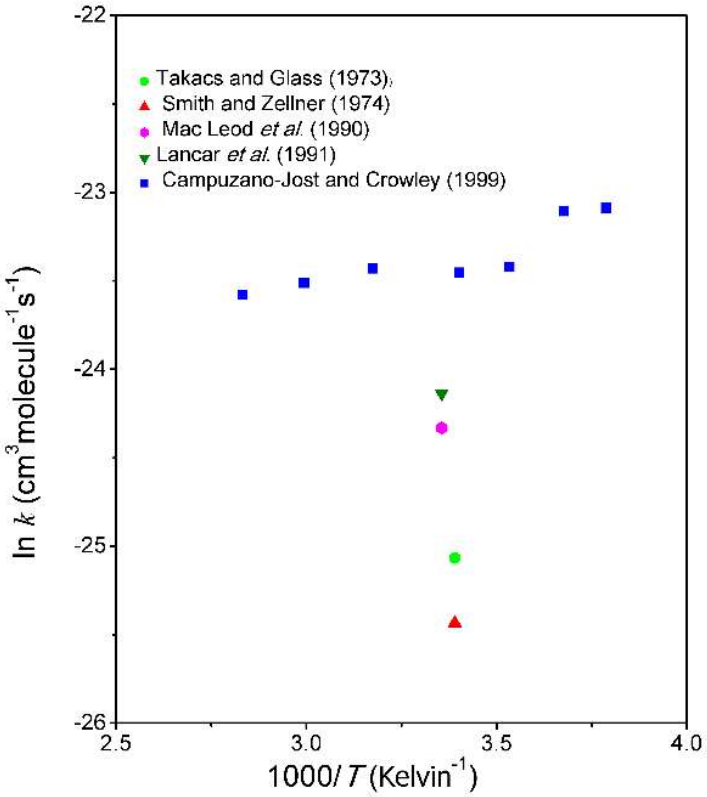

Figure 5: Temperature dependence of the rate constant for the OH + HI reaction.

Canneaux, Xerri, Louis and Cantrel[37] obtained a potential energy profile of the I + H_2O reaction, showing that the relative energy of products is lower than that of transition state, and they determined the quantitative rate constants for the reactions involving iodine-containing species, using the canonical transition state theory with a simple Wigner tunneling correction. Recently, the stationary points, zero-point vibrational energies and vibrational frequencies for the I + H_2O potential energy surface have been predicted with the high-level *ab initio* CCSD(T) method, with the spin–orbit coupling corrections[38]. However, all previous studies neglect the understanding of *anti*-Arrhenius behavior.

On variance with Arrhenius law and unlike OH + HBr and OH + HI, the rate constant for the OH + HCl[19,39–47] reaction, when extended to low temperatures, shows a strong concave curvature in the Arrhenius plot: a phenomenon designated as *sub*-Arrhenius behavior (see Figure 6).[48,49.] Generally, there is a consensus in the literature that processes exhibiting *sub*-Arrhenius behavior are intrinsically dominated by the quantum tunneling effect of penetration of an energy barrier along the reaction path on the potential energy surface[50,51]. Further observation for the OH + HCl reaction is that of a large primary KIE[52].

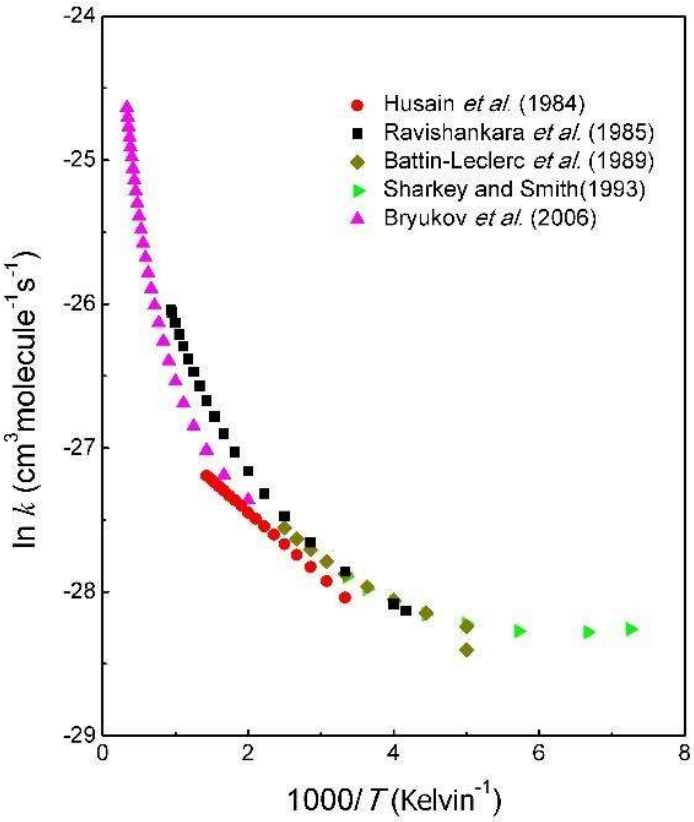

Figure 6: Temperature dependence of the rate constant for the OH + HI reaction

From a theoretical perspective, much effort has been dedicated to obtaining the potential energy surface (PES) and rate constants for this reaction. Recently, the Schaefer group obtained a potential energy profile of the OH + HCl reaction by CCSD(T) method with correlation consistent basis sets through cc-pVQZ, showing energy, geometry and frequencies for five stationary points along the reaction path.[53] The Guo group calculated a full-dimensional global PES generated by fitting ca. 25,000 multi-reference configuration interaction points using a permutation invariant polynomial method.[54] Later, they calculated the thermal rate constant for a wide range of temperatures using ring-polymer molecular dynamics and observed the deviations in the rate constant with available experimental data for low temperatures.[55]

In order to improve the more accurate full-dimensional global PES, the Guo group fitted a new set of *ab initio* points obtained by (UCCSD(T)-F12b/AVTZ), and the rate constant was calculated by canonical variational transition state theory. The authors found a lower barrier for forward reaction than that of previous PES,[54] and the rate constant was in better agreement with experimental values, at least for high temperatures; however, for low temperatures the disagreement was still significant[5]. Recently, the Guo Group[56] presented a study using ring polymer molecular dynamics for the title reaction and its deuterium analogue. The calculated RPMD rate constants are in excelent agreement with experimental data confirming the accuracy of the potential energy surface. Recently, the investigation of the catalytic effect of NH_3 and HCO_2H on the reaction between OH and HCl found

both *sub*-Arrhenius and *anti*-Arrhenius plots of rate constants, depending on the reactive channel analysed.[57]

From a quasi-classical trajectory method, the Guo group has shown that for the OH + HCl reaction, the vibrational excitation of the HCl reactant greatly increased the reactivity, while the OH vibrational is essentially a spectator.[58] This result was assessed as contradicting Polanyi's rule, which suggests that the translational energy is more efficient than vibrational energy in enhancing an early barrier reaction. However, they explained that this violation can be elucidated by a sudden vector projection model, which attributes the promotional effect of the HCl vibration to its strong coupling with the coordinate in the transition state.[58,59]

Relevant from our view point are the quasi-classical trajectory calculations by Bonnet *et al*.[60] who demonstrated unexpected reaction pathways involving strong reorientation of the reagents, and shown that the most important channels were far from the reaction path, using a dynamical extension of the notion of cone of acceptance to rationalize the stereodynamic effects.[60]

An alternative source of important information comes from molecular beam scattering experiments with oriented reactants. Only a non-reactive experiments is available: Cireasa and collaborators[61] reported stereodynamical features in the inelastic collisions between OH and HCl molecule, showed that H-end attack is favoured for the inelastic collision system. They define a "steric asymmetry factor" and found it negative, in contrast with the analogous four-body reaction, OH + HBr, for which the O-end attack is more favourable by a factor three over that at the H-end.[23,24]

1.1 Plan of the thesis

In Figure 7, a pictorial view of the potential energy surface for $\mathrm{OH} + \mathrm{HX} \longrightarrow \mathrm{H_2O} + \mathrm{X}$ (X = Halogen) can been seen. The reactions with hydroxyl radical and hydrogen iodine, hydrogen bromide and hydrogen chloride are highly exothermic, with ΔH^0 equal to -47.70, -31.43 and -15.82 Kcal/mol, respectively, while the reaction with hydrogen fluoride is endothermic (ΔH^0 =17.6 kcal/mol). These differences revolve around the fact that the energy of dissociation of HF is much greater than that for the other hydrogen halides. As seen for four reactions, there is an entrance complex, followed by a saddle-point barrier and exit complex in the product channel; however, as expected, the energies of stationary points change in function of hydrogen halide. The transition-state barrier has a positive energy for the OH + HF and OH + HCl reaction, while for the other two reactions the transition state is energetically lower than the entrance channel (negative activation energy).

The anisotropic forces generated by electrostatic and dispersion interactions promote the formation of the wells in the reactant in the PES. However, differently from the entrance complex (HO—HX), the origin of stability of the exit complex (X—H_2O) cannot be explained by electrostatic or dispersion interaction, since neither the geometry nor the energy encodes with this type of interaction. Guo group[62] showed strong evidence that the interactions between halogens and water have a

covalent origin due to the two-center-electron bond formed between an unpaired electron of the halogen atom and a lone pair of H_2O.

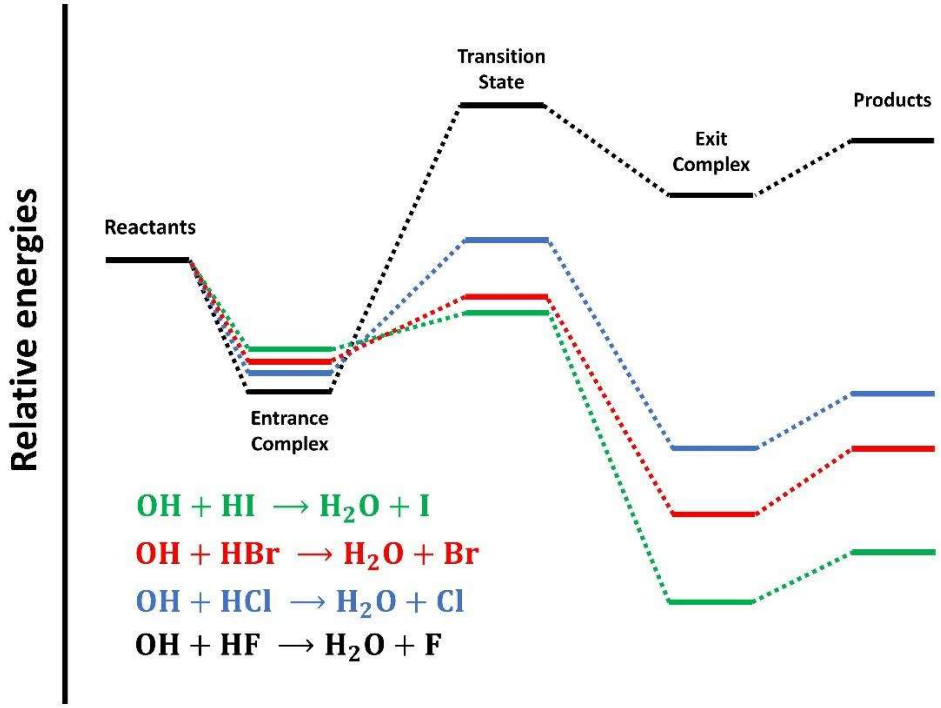

Figure 7: Pictorial view of comparison of the stationary points on the potential energy surfaces for the $OH + HX \longrightarrow H_2O + X$ (X= Halogen) reaction, adapted from Ref. [63].

Figure 8 shows the comparison of rate constants for OH + HI, OH + HBr and OH + Cl reactions; nevertheless, for the endothermic reaction there is no kinetic data available. As can be seen, among three reactions, the HI molecules were found to have the highest rate constant for the range of temperature available, and the HCl molecule had the smallest reactive reaction in almost the entire temperature range. Additionally, as already mentioned, the reaction between HCl and OH has a *sub*-Arrhenius behavior, while the other two reactions have *anti*-Arrhenius behavior.

Here, inspired by the results from oriented molecular-beam experiments for OH + HBr[23,24,64] and in order to understand this transition from *anti*-Arrhenius behavior for OH + HI and OH + HBr to *sub*-Arrhenius behavior for OH + HCl after the simple halogen replacement, in this work we perform a blend of *ab-initio* molecular dynamics thermalized at four temperatures for $OH + HX \longrightarrow H_2O + X\ (X = I, Br \text{ and } Cl)$ reactions and high-level Transition-State-Theory. The main strategy that we follow is to use the Born-Oppenheimer molecular dynamics.[65–67]technology to carry out numerical experiments that simulate the reaction in a box, which we consider as our first-principles "nanoreactor" in the spirit, *e.g.*, of Ref. 68: the reactant molecules introduced in the box explore the potential energy surface at a specified temperature, enforced by a Nosé-Hoover thermalizing bath and therefore representing a 'canonical' ensemble[69].

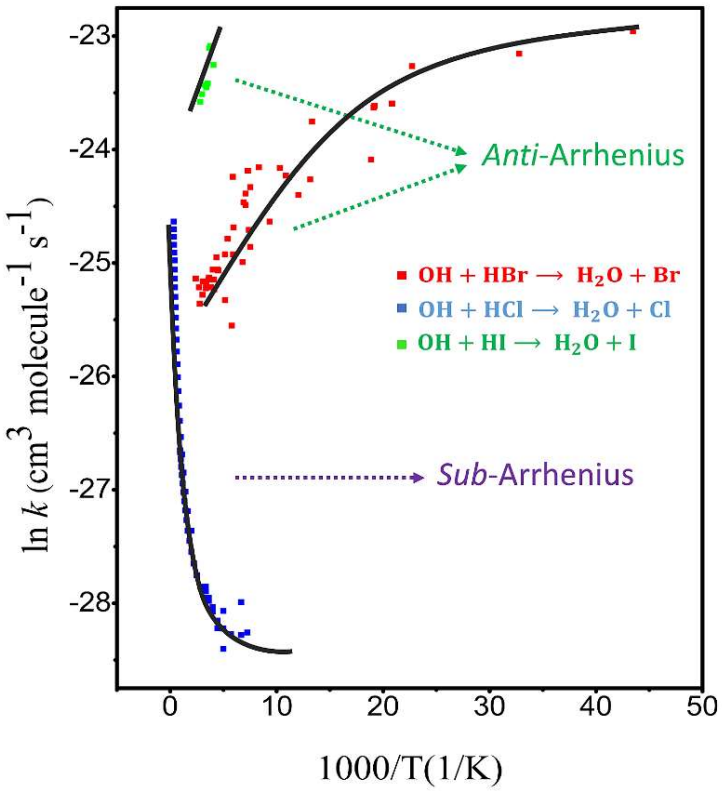

Figure 8: The experimental rate constants[70], which discriminate the transition from *anti*-Arrhenius (HI and HBr) to s*ub*-Arrhenius. From our knowledge, there are no experimental values for the HF + OH reaction.

This thesis is organized as follows. The next chapter is devoted to a description of theoretical methods where we present Arrhenius formalism and provide interpretations for the negative activation energy, as well as the theory involved in the formulation of the *ab initio* molecular dynamics method, more specifically the Born-Oppenheimer molecular dynamics. In section 3, we present the four papers produced during the study of the $OH + HX \longrightarrow H_2O + X\ (X = I, Br\ and\ Cl)$ reactions, where the results are presented and discussed. The conclusions are given in the final section.

2 Theoretical approach

2.1 Chemical Reaction Rates

For understanding, monitoring and controlling the physical chemistry processes of materials, as well as the biophysics of the environment, thorough knowledge is needed of the mechanism and kinetics of the elementary processes involved, specifically on their rates—often in a wide range of conditions and notably as a function of temperature. At the end of the 19th century, phenomenological studies began to be developed, mainly through the famous Arrhenius equation, and in the mid-1930s, the heuristic formulation of the transition state theory was presented to the scientific community. However, the development of experimental techniques and the current ability to measure the rate of physical-chemistry processes, for a wide range of temperatures, mainly at low temperatures, have demanded alternative paradigms. In this section, the fundamental theories will be presented, as well as the progress that has been developed in this area of science.

2.1.1 The basic theory

One of the most important contributions to chemical kinetics was made by Van't Hoff.[71] In 1884 he published the famous textbook on chemical dynamics (*Etudes de Dynamique Chimique*). In this study, he accounted the kinetic data available and formulated the laws of unimolecular and bimolecular reactions. Additionally, he made a comprehensive discussion on the influence of temperature on the reaction thermodynamic parameters, and demostrated that there is a correlation between equilibrium constant, reaction enthalpy and temperature:[72]

$$\frac{d \ln K_{eq}}{d\left(\frac{1}{T}\right)} = -\frac{\Delta H}{R}, \tag{8}$$

where K_{eq} is the equilibrium constant, ΔH is the enthalpy of reaction and R the gas constant.

Svante A. Arrhenius,[73] inspired by Van't Hoff's formulation, proposed a correlation between the reaction rate and the temperature, providing a physical interpretation, based on molecular collisions, for all reaction parameters. Arrhenius started out from the application of the equilibrium formulation to a simple first order reaction:

$$A \underset{k_I}{\overset{k_D}{\rightleftharpoons}} B \tag{9}$$

where *A* is the reagent, *B* the product, k_D the forward rate constant and k_I the reverse rate constant. For this reaction, the equilibrium constant is written as:

$$K_{eq} = \frac{[B]_{eq}}{[A]_{eq}} = \frac{k_D}{k_I}. \tag{10}$$

Combining equations (8) and (10) and considering that $\Delta H = E_D - E_I$, where E_D and E_I are the internal energy variations during forward and reverse reaction between the activated complex, the Van't Hoff formulation can be rewritten as:

$$\frac{d \ln k_D}{dT} = \frac{E_D}{RT^2}, \tag{11}$$

$$\frac{d \ln k_I}{dT} = \frac{E_I}{RT^2}. \tag{12}$$

The famous Arrhenius equation is obtained integrating equations (11) and (12):

$$k_D = A_D e^{-\frac{E_D}{RT}} \tag{13}$$

and

$$k_I = A_I e^{-\frac{E_I}{RT}}, \tag{14}$$

where, $E\ is$ activation energy and can be interpreted as the energy necessary for a molecular rearrangement with enough energy to make product formation viable, usually represented by E_a. The parameter A is known as a pre-exponential factor and is directly related to the total frequency of molecules that may collide during the reaction.

The great advantage of the Arrhenius model is the possibility of making predictions of the reactive microscopic dynamics from experimental kinetic data; thus, taking the experimental data concerning the kinetic constant (k) and the temperature (T), it is possible to calculate the activation energy and the pre-exponential factor of a given reaction. In practice, this procedure is performed by adjusting the logarithm of the kinetic constant by the inverse of the temperature, the Arrhenius plot, such as:

$$\ln k = \ln A - \frac{E_a}{RT}, \tag{15}$$

so that the curvature of the Arrhenius plot provides the activation energy and the intercept provides the pre-exponential factor, as shown in Figure 9:

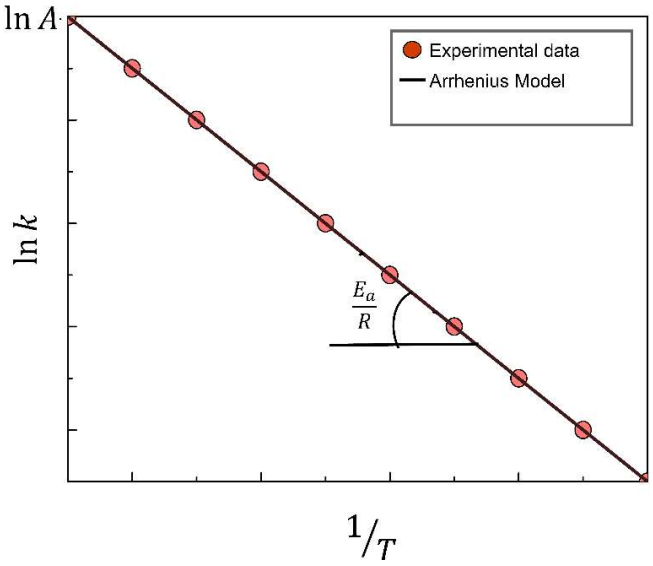

Figure 9: The linear behavior of the Arrhenius model, in the Arrhenius plot. The slope of the line provides the activation energy.

2.2 *Non*-Arrhenius Behavior

Due to the need to obtain a description of the mechanisms involved in physico-chemical transformations, the Arrhenius equation has been applied in several kinetic studies to a large number of processes that are not restricted only to elemental chemical reactions,[74–76] for example, particle diffusion in supercooled,[77,78] electrical conductivity in ionic liquidsionicos[79,80] and food preservation processes.[81,82] However, the development of advanced experimental techniques and the current capacity to obtain kinetic data for a wider range of temperatures has revealed that the Arrhenius model needs to be reformulated.

The deviations observed on the Arrhenius plot lead to two different regimes, denoted by *sub*-Arrhenius and *super*-Arrhenius. When the deviation observed in the Arrhenius plot leads to a concave curvature, this behavior is classified as *sub*-Arrhenius; however, when the curvature is convex it is referred to as *super*-Arrhenius (See Figure 10).

There is a consensus in the literature that processes involving *sub*-Arrhenius behavior are related to quantum effects, whereas the *super*-Arrhenius behavior may be related to contributions of classical collective phenomena, where transport of particles plays an important role.[50]

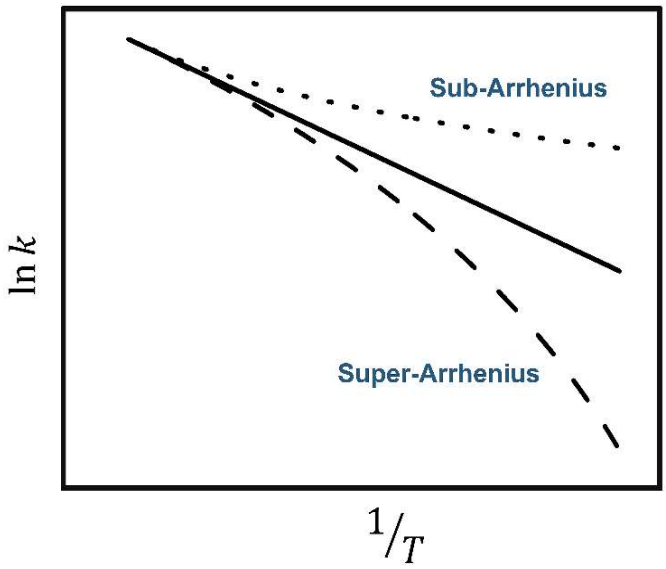

Figure 10: Representation of dependence of $\ln k$ from reciprocal temperature $(1/T)$, showing the *super*-Arrhenius and *sub*-Arrhenius behavior. Adapted by Ref. 50.

According to the Arrhenius equation, the activation energy is constant and independent of temperature. However, nonlinear behaviors observed in the Arrhenius plot interfere in the behavior of the activation energy (Figure 11). Therefore, a more comprehensive definition for the activation energy is needed. Currently, the most general definition accepted by the International Union of Pure and Applied Chemistry (IUPAC) is given by:

$$E_a = -R\frac{\mathrm{d}\ln k}{\mathrm{d}\left(\frac{1}{T}\right)} \tag{16}$$

It is worth mentioning that the activation energy obtained experimentally can be different from the height of the energy barrier for a reaction. In 1920 Tolman[83] proposed an interpretation for activation energy based on statistical formulations. In this formulation the activation energy is the difference between the average energy of the successful chemical collisions and the total kinetic energy of the gas where the reaction occurs. Usually this amount is attributed to the meaning of an energy requirement for the reaction to occur; however, it is only in particular cases, specifically in temperature ranges where the activation energy is constant or varies slowly, that this interpretation is valid, recovering Arrhenius formulation.

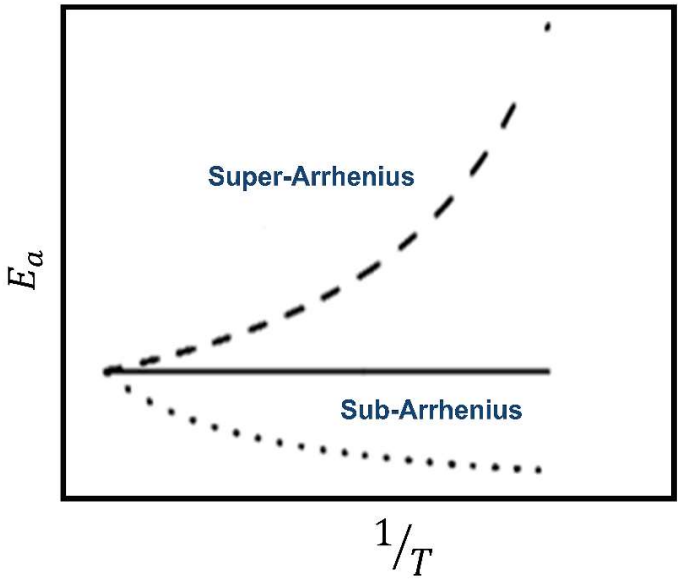

Figure 11: Representation of dependence of $\mathrm{E_a}$ by reciprocal temperature $\left(1/\mathrm{T}\right)$. The temperature directly influences the activation energy behavior. Adapted from Ref. [50].

Another known *non*-Arrhenius behavior, which differs totally from those presented previously, shows negative dependence on temperature for the rate constant, which impacts on the existence of negative activation energy. This phenomenon is often found in bimolecular reactions that have radicals as reagents. Most papers refer to reactions between small free radicals centered by carbon or silicon atoms with hydrogen halide$(\mathrm{HX},\ \mathrm{X} = \mathrm{I}, \mathrm{Br\ and\ Cl})$ or halogens $(\mathrm{X_2})$, reaction type as $\mathrm{R}\cdot + \mathrm{HX} \longrightarrow \mathrm{RH} + \mathrm{X}\cdot$ or $\mathrm{R}\cdot + \mathrm{X_2} \longrightarrow \mathrm{RX} + \mathrm{X}\cdot$, as well as reactions between hydroxyl radicals and bromine or iodine halides. Some examples can be seen in Table 1

Table 1. Reactions with negative activation energy. Adapted from [84].

Reactants	E_a(kcal/mol)	Reference
CH_3/HBr	-0.38	85
CH_3/HI	-0.29	86
C_2H_5/HBr	-1.00	85
C_2H_5/HI	-0.77	86
i-C_3H_7/HBr	-1.53	85
t-C_4H_9/HBr	-1.89	85
CH_3/Br_2	-0.39	87
C_2H_5/Br_2	-0.82	87
i-C_3H_7/Cl_2	-0.49	88
OH/acetone	-0.84	89

Usually, the negative activation energy is interpreted in terms of the formation of a stable intermediate complex. Wolfgang[90] was one of the first kinetic chemists who saw the importance of forming these complexes and in 1969 wrote about the reactions that proceeded through the formation of stable intermediates. In 1984, Mozurkewich and Benson[91] made a correlation between the formation of stable complexes and the presence of negative activation energy, presenting in their paper physical arguments for the formation of these complexes and an explanation for the phenomenon based on Rice-Ramsperger-Kassel-Marcus theory (RRKM).

2.2.1 Arrhenius law deformation

In order to obtain a phenomenological model that best describes *non*-Arrhenius behaviors, Aquilanti and co-workers[48,92] proposed the deformation of the Arrhenius equation (d-Arrhenius), considering the deformation of the Euler exponential:

$$\exp(x) = \lim_{n\to\infty}\left(1-\frac{x}{n}\right)^n. \tag{17}$$

The parameter d is a continuous generalization of $1/n$, so the d-exponential can be defined as:

$$\exp_d(x) = (1 \mp dx)^{\frac{1}{d}}. \tag{18}$$

When d tends to zero, the d-exponential equation tends to conventional exponential. Thus, knowing the behavior of Equation (18), the rate constant was defined by:

$$k_d(T) = A\exp_d\left[1-\frac{E_0}{RT}\right] = A\left[1-d\frac{E_0}{RT}\right]^{\frac{1}{d}}, \tag{19}$$

where, A, E_0 and d are phenomenological parameters. Only the last parameter does not appear in the familiar Arrhenius equation. The d parameter provides the degree of deformation of the exponential function: when $d \to 0$, equation (19) tends to the Arrhenius equation. Taking the logarithm of Equation (19) the expression of Arrhenius plot is obtained:

$$\ln k_d = \ln A + \frac{1}{d}\ln\left[1 - d\frac{E_0}{RT}\right]. \quad (20)$$

Parameter *d* governs the *sub*-Arrhenius behavior for values of $d < 0$ and *super*-Arrhenius for values of $d > 0$. In this work, the deformation of the Arrhenius equation was extended to *anti*-Arrhenius behaviors, corresponding to negative values of the activation energy, E_a. Applying the definition of IUPAC activation energy, according to the equation below, E_a is given by:

$$\frac{1}{E_a} = \frac{1}{E_0} - \frac{d}{RT}. \quad (21)$$

2.3 Computational Chemistry

2.3.1 *Brief description of the static methodology*

The increase in computer performance over the last few decades, along with advances in mathematics, chemistry and physics, has led to the birth of a new way of doing science, which is at the intersection of theory with experiment, referred to as computational science, which allows computational experiments to be run under perfectly controllable and reproducible conditions. Currently, the results obtained through computational simulations are increasingly consistent with the experimental results, and in some cases, make good predictions about data that are not easily measurable.[93]

From the theoretical-computational point of view, the most consolidated theories in the study of chemical reactions are static and dynamic. The first method consists basically in the determination and analysis of the potential energy surface and the application of statistical theories, such as the Transition State of Theory (TST). And the second consists in the solution of the equations of motion under the influence of quantum potential or not. Both methods have advantages and disadvantages, and together they have been of great importance for the development of modern chemistry. Their bases will be presented in more detail in subsequent sections.[94]

2.3.2 Potential Energy Surface

The potential energy surface (PES) is critical to understanding the dynamics of chemical reactions. The PES represents the dependence of the potential energy on the coordinates of the system and is calculated by solving the Electronic Schrödinger equation for fixed values of the nuclear coordinates (**R**), which arises naturally from the Born-Oppenheimer approximation, given by:

$$\hat{H}_{ele}\psi_{ele}(\boldsymbol{r};\mathbf{R}) = E_{ele}\psi_{ele}(\boldsymbol{r};\mathbf{R}), \quad (22)$$

where ψ_{ele} is the electronic wave function that depends on the electronic coordinates, $\boldsymbol{r}$, and parametrically by fixed nuclear positions, $\mathbf{R}$, and E_{ele} is the electronic energy. For the Hamiltonian, $\hat{H}_{ele}$, the nuclei are considered punctual charges and, therefore, contribute only to the generation of an electrostatic potential to attract the electrons.

For a chemical reaction between two reactants containing N atoms, the PES will be described by $3N-6$ dimensions (or $3N-5$ for linear systems). Therefore, for a very simple reaction involving only three atoms, $\mathrm{A}+\mathrm{BC}\longrightarrow\mathrm{AB}+\mathrm{C}$, at least three $(3\cdot 3-6=3)$ coordinates are required to describe the system, two interatomic distances and an angle between the bonds. This means that the representation of potential energy is a function of the three parameters, and therefore provides a four-dimensional diagram, which in practice is difficult to visualize, if not impossible. To overcome this difficulty, the graphic representation is made as a function of only one or two internal coordinates, keeping the remaining coordinates at fixed values. [95]

The most important information in a reactive process on the potential energy surface is the reaction path that connects reagents and products through the transition state on the surface. Several reaction paths are possible in the PES; however, the intrinsic reaction path (IRC) corresponds to the path of minium energy in the PES, and therefore is most likely to happen. From the mathematical point of view, the IRC can be defined by a line in the coordinate space in PES, which connects two minimums through a saddle point, also known as the transition state. The example of a potential energy profile (potential energy as a function of only one reaction coordinate) relating the intrinsic path of reaction is shown in Figure 12.[95]

In the static methodology, the reactional mechanism study and calculation of rate constant is done by geometric analyses, and by energy and frequencies of stationary points on the IRC. In practice, the following steps are necessary: (i) calculation of potential energy as a function of atomic positions; (ii) obtaining important stationary points that connect reagents and products (transition states and chemical intermediates); (iii) determination of the IRC and (iv) calculation of the rate constant using quantum-mechanical statistical theories.

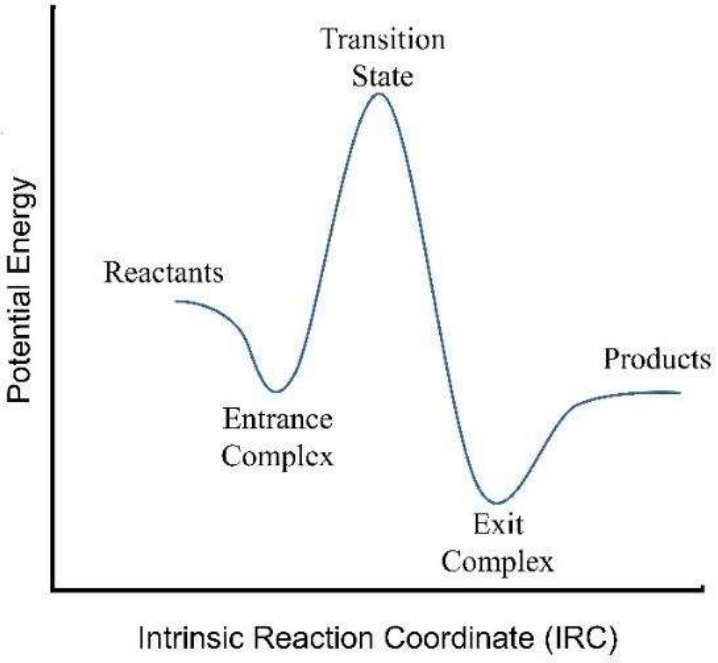

Figure 12: Schematic representation of the potential energy profile showing the main stationary points along the IRC path for exothermic reaction.

2.3.3 Transition State Theory

Transition state theory is one of the most reliable and widely applied methods in calculating rate constants in chemical reactions. The conventional TST was developed by Eyring, Evans and Polanyi in 1935 and is based on statistical assumptions. However, the applicability of this theory requires that the chemical reaction obey some criteria.[95–97]

- The reaction should occur in electronically adiabatic states and in the ground state;
- No quantum effects should occur. Effects such as tunneling are added *posteriori.*
- The energy states of the reagents and transition state should follow a Maxwell-Boltzmann statistical distribution;
- The molecules of the reagents that cross the hypersurface dividing the reagents of the products through the transition state towards the products cannot return in the direction of the reagents; that is, there may be barrier recrossing.
- After the formation of the transition state, there must be product formation.

For example, considering a general bimolecular reaction such as:

$$R_1 + R_2 \rightleftharpoons [TS^{\dagger}] \longrightarrow \text{Products}$$

where R_1 and R_1 are the reactants that are in equilibrium with the transition state $[TS^{\dagger}]$, which immediately forms the products. The rate constant predicted by the formulation of the transition state theory is given by[96,98]:

$$k^{TST} = \frac{k_B}{h}\frac{Q^{\dagger}}{Q_1 Q_2}\exp\left(\frac{E_0}{k_B T}\right), \tag{23}$$

where, Q_1, Q_2 and $Q^{\dagger}$, the total partition functions for reagents 1 and 2 and for the transition state, respectively; k_B is the Boltzmann's constant; h is the Planck's constant; T is the absolute temperature the temperature and E_0 the height of the potential barrier, defined as the difference between the energy of the transition state and reactants, interpreted as the energy threshold for a reaction to occur.

In practice, the rate constants via TST are obtained by first calculating the electronic structure of the reagents and products and by searching for the transition state on the potential energy surface. The TS search methods are based on the location of a molecular arrangement in the reaction pathway between the reagents and the products with only a negative frequency (mathematical characterization of the saddle point). Information on the geometry, electronic energy and frequency obtained are used to calculate the partition function of each of the molecular entities.

In order to include quantum tunneling effects along the reaction coordinate, it is used the tunneling Bell 1935, and 1958 tunneling correction[22] (κ) and *deformed* theory (d-TST - k_d^{TST})[51] as follows:

$$\kappa_{Bell\ 1935} = \frac{\left[\frac{E_0}{\hbar\nu^{\dagger}} - \frac{E_0}{k_B T}\exp\left(\frac{E_0}{k_B T} - \frac{E_0}{\hbar\nu^{\dagger}}\right)\right]}{\frac{E_0}{\hbar\nu^{\dagger}} - \frac{E_0}{k_B T}} \tag{24}$$

$$\kappa_{Bell\ 1958} = \frac{\left(\frac{\hbar\nu^{\dagger}}{2k_B T}\right)}{\sin\left(\frac{\hbar\nu^{\dagger}}{2k_B T}\right)} - \frac{E_a \exp\left(\frac{E_0}{k_B T} - \frac{E_0}{\hbar\nu^{\dagger}}\right)}{\left(\frac{E_a k_B T}{\hbar\nu^{\dagger}} - E_a\right)} \tag{25}$$

$$k_d^{TST} = \frac{k_B T}{h}\frac{Q^{\dagger}}{Q_1 Q_2}\left(1 - d\frac{E_0}{k_B T}\right)^{1/d}, \qquad d = -\frac{1}{3}\left(\frac{h\nu^{\dagger}}{2E_0}\right)^2 \tag{26}$$

where $\nu^{\dagger}$ is the imaginary frequency for crossing the barrier and d is deformed parameter. The tunnelling regime can be characterized considering the crossover temperature parameter ($T_c = h\nu^{\dagger}/2\pi k_B$) as: negligible ($T > 4T_c$), moderate ($T_c < T < 2T_c$) and deep ($T < T_c$).

Even though it is a very successful and easy-to-apply theory, TST tends to fail when the reactive trajectories do not follow the minimal energy path in PES or when redistribution of internal vibrational energy is not complete. Another alternative for describing systems to which these effects are observed may come from the use of *ab-initio* molecular dynamics.

2.4 Molecular Dynamics Simulations

The history of Molecular Dynamics began in the 1950s, when the first computers performed a simulation of simple systems.[99] In the last two decades the growth of this technique has been exponential, and in 2013 researchers in this area won the Nobel Prize in Chemistry.[100]

One of the major challenges of Molecular Dynamics is the calculation of interatomic forces.[101,102] In classical simulations, interatomic forces are calculated from empirical functions which reproduce experimental data or are obtained from electronic structure calculations.[93,101] The equations used to obtain the positions and velocities of the atoms in the system are based on Newton's laws. These equations are integrated numerically, and the results are the positions and velocities of the atoms. Due to the simplicity of the equations involved in Classical Molecular Dynamics (CMD), this is an excellent tool in the study of large systems, providing a relatively short calculation time when compared to quantum and semi quantum dynamics.[67,101]

However, Classical Molecular Dynamics has some limitations. Essentially quantum phenomena, such as tunneling and chemical reaction, cannot be described. Another difficulty of CMD is the anticipated need for determination of fixed potentials. Despite the progress in developing these potentials, the possibility of transferability to different systems from which they have been provided is often restricted.

In order to eliminate such difficulties, *ab initio* molecular dynamics (AIMD) has been very attractive. In AIMD the forces acting on the nucleus are calculated from electronic structure calculations that are executed in real time (on-the-fly) as the trajectory is generated. Unlike DMC, in *ab initio* dynamics the electronic variables are calculated at each step of the simulation and no longer defined *a priori* as fixed interaction potentials. The four *ab initio* Molecular Dynamics methods most used have been: Ehrenfest Molecular Dynamics (EMD), Born Oppenheimer Molecular Dynamics (BOMD), Car-Parrinello Molecular Dynamics (CPMD) and Path Integrals Molecular Dynamics (PIMD).[67,103]

2.4.1 Molecular Dynamics: The idea

Molecular dynamics is based on the principles of classical mechanics and basically consists of the numerical solution, step-by-step, of the classical equations of motion. Considering a system with N particles moving under the influence of a potential U, and that these particles can be described by their $\mathbf{R}$ positions and by the moment $\mathbf{P} = M\mathbf{v}$, the union of all positions (or moment) is defined as $\mathbf{R}^N(\mathbf{P}^N)$. Thus, the Hamiltonian H of the system is defined as:

$$H(\mathbf{R}^N, \mathbf{P}^N) = \sum_{I=1}^{N} \frac{\mathbf{P}_I^2}{2M_I} + U(\mathbf{R}^N). \tag{27}$$

The forces in each particle are derived from the potential:

$$F(\boldsymbol{R}^N) = -\frac{\partial U(\boldsymbol{R}^N)}{\partial \boldsymbol{R}_I} \tag{28}$$

Thus, the equations of motion can be obtained from the classical formulation of Hamilton,

$$\dot{\mathbf{R}}_I = -\frac{\partial H}{\partial \boldsymbol{P}_I} = \frac{\boldsymbol{P}_I}{M_I}, \tag{29}$$

$$\dot{\mathbf{P}}_I = -\frac{\partial H}{\partial \boldsymbol{R}_I} = \boldsymbol{F}_I(\boldsymbol{R}^N). \tag{30}$$

The equations of motion can also be derived from Lagrangian formalism. The Lagrangian:

$$\mathcal{L}(\mathbf{R}^N, \dot{\mathbf{R}}^N) = \sum_{I=1}^{N} \frac{1}{2} M_I \dot{\mathbf{R}}_I^2 - U(\mathbf{R}^N) \tag{31}$$

and the associated Euler-Lagrange equation:

$$\frac{d}{dt}\frac{\partial \mathcal{L}}{\partial \dot{\mathbf{R}}_I} = \frac{\partial \mathcal{L}}{\partial \mathbf{R}_I}, \tag{32}$$

lead to the same result. The two formulations are equivalent; however, it is more common in the literature to use Lagrangian formalism to describe *ab initio* molecular dynamics.[103]

The standard procedure for solving the equations of motion consists in discretizing the coupled differential equations, that is, transforming them into finite differences.[101] Thus, it starts from the conjecture that the interaction potential, and therefore the forces between the particles, are continuous and differentiable functions. If the initial conditions of the system at time t_0 are known, position and velocity and any other dynamic variable can be determined later at $t + \Delta t$ with the appropriate precision. This process is known as numerical integration.

2.4.2 Integrating the Equations of Motion

The main objective of the numerical integration of the equations of motion is to find an expression that defines the positions $\mathbf{R}(t + \Delta t)$ in terms of the already known positions at time t. There is a huge variety of algorithms, all based on Taylor expansion. Due to simplicity and precision, the most widely used algorithms in molecular dynamics are Verlet and Velocity Verlet.[67,101] The Verlet algorithm uses the positions and accelerations of the atoms at time t and the positions of the previous step $\mathbf{R}(t - \Delta t)$, to determine the new positions at time $t + \Delta t$, according to:

$$\mathbf{R}(t + \Delta t) = \mathbf{R}(t) + \mathbf{v}(t)\Delta t + \frac{1}{2}\boldsymbol{a}(t)\Delta t^2 + \frac{1}{3!}\boldsymbol{a}(t)\Delta t^3 \tag{33}$$

(34)

$$\mathbf{R}(t-\Delta t) = \boldsymbol{R}(t) - \mathbf{v}(t)\Delta t + \frac{1}{2}\boldsymbol{a}(t)\Delta t^2 - \frac{1}{3!}\boldsymbol{a}(t)\Delta t^3$$

Summing these two equations and isolating $\mathbf{R}(t+\Delta t)$, the following is obtained:

$$\mathbf{R}(t+\Delta t) = 2\mathbf{R}(t) - \mathbf{R}(t-\Delta t) + \boldsymbol{a}(t)\Delta t^2. \tag{35}$$

Replacing the acceleration in Equation (35), the following is obtained:

$$\boldsymbol{R}(t+\Delta t) = 2\mathbf{R}(t) - \mathbf{R}(t-\Delta t) + \frac{\boldsymbol{F}}{M}(t)\Delta t^2 \tag{36}$$

The forces can be calculated using equation $\mathbf{F} = -\nabla U(\mathbf{R}^N)$. This algorithm has the advantage of being simple, accurate, stable and very popular among simulators. However, it has the disadvantage of not calculating velocities directly from the forces. Although the velocities are not required to find the new positions, their knowledge is sometimes necessary, for example, to calculate the kinetic energy E_C, whose evaluation is necessary to test the conservation of the total energy and verify that the MD simulations are proceeding from correct form. In the Verlet algorithm the velocities can be calculated as:

$$\mathbf{v}(t) = \frac{\boldsymbol{R}(t+\Delta t) - \boldsymbol{R}(t-\Delta t)}{2\Delta t} \tag{37}$$

As mentioned above, the main problem of the Verlet algorithm is that the velocities at time t are only calculated after obtaining the positions at time $t+\Delta t$, causing a large storage of data in the memory of the computer.

In order to overcome this difficulty, modifications in the Verlet algorithm were made, giving rise to Velocity Verlet. The positions at time $t+\Delta t$ are derived using the Taylor expansion:

$$\mathbf{R}(t+\Delta t) = \mathbf{R}(t) + \mathbf{v}(t)\Delta t + \frac{\boldsymbol{a}(t)}{2}\Delta t^2. \tag{38}$$

The equation (38) depends on the velocities, which can be calculated as follows:

$$\mathbf{v}(t+\Delta t) = \mathbf{v}(t) + \boldsymbol{a}(t)\Delta t + \frac{\boldsymbol{a}'(t)}{2}\Delta t^2. \tag{39}$$

Using the finite-difference method, $\boldsymbol{a}'(t)$ is obtained:

$$\boldsymbol{a}'(t) = \frac{a(t+\Delta t) - \boldsymbol{a}(t)}{\Delta t}. \tag{40}$$

Replacing (40) in (41):

$$\mathbf{v}(t+\Delta t) = \mathbf{v}(t) + \boldsymbol{a}(t)\Delta t + \frac{\boldsymbol{a}(t+\Delta t) - \boldsymbol{a}(t)}{2\Delta t}\Delta t^2, \tag{41}$$

$$\mathbf{v}(t+\Delta t) = \mathbf{v}(t) + \frac{\boldsymbol{a}(t+\Delta t) + \boldsymbol{a}(t)}{2}\Delta t, \tag{42}$$

$$\mathbf{v}(t+\Delta t) = \mathbf{v}(t) + \frac{\mathbf{F}(t+\Delta t) + \mathbf{F}(t)}{2M}\Delta t. \tag{43}$$

This algorithm is certainly one of the most frequently used in molecular simulations, mainly due to its ease of implementation. An overall strategy is as follows:

1. Given $\mathbf{R}(t)$ and $\mathbf{v}(t)$ at time t, the force is first calculated on each particle, using the force field;
2. The new positions and velocities are calculated by Equations (38) and (43), respectively;
3. New forces are calculated for new positions;
4. Go back to step 1.

After knowing the particle trajectories in the phase space, the next step is to obtain the macroscopic properties of the system. Starting from the hypothesis of ergodicity, these properties can easily be obtained by realizing time averages from the solution of the equations of motion.

In this way, thermodynamic properties, such as thermal capacity, free energy, entropy and pressure, as well as the microscopic structure of the system, can be determined at finite temperatures, for example, which involve connection length and distribution of connection angles.

2.4.3 Born-Oppenheimer Molecular Dynamics

A good approximation for adding quantum effects to molecular dynamics simulations is to solve the problem of static electronic structure for each step of the dynamics, given a set of fixed nuclear positions for a given instant. Thus, the electronic part of the system is reduced in the solution of the time-independent quantum problem, that is, the nuclei are propagated using the laws of classical mechanics while the electrons are solved simultaneously using the Schrödinger equation independent of time. In this way, the temporal dependence of the electronic part of the system is imposed and dictated by the parametric dependence of the dynamics of the nuclei.[104]

Then, the separation of the electronic and nuclear degrees of freedom allows the time evolution of the nuclei under the influence of a potential $U(\mathbf{R}^N)$ calculated for each configuration of the nuclei, given by:

$$U(\mathbf{R}^N) = \min_{\Psi_0}\{\langle\Psi_0|H_e|\Psi_0\rangle\}. \tag{44}$$

Thus, the Lagrangian of the Born-Oppenheimer molecular dynamics can be defined as:

$$\mathcal{L}_{BO} = \sum_I^N \frac{1}{2} M_I \dot{\mathbf{R}}_I^2 - \min_{\Psi_0}\{\langle\Psi_0|H_e|\Psi_0\rangle\}. \tag{45}$$

And the equations of motion are:

$$M_I \ddot{\mathbf{R}}_I = -\nabla \left[\min_{\Psi_0} \{ \langle \Psi_0 | H_e | \Psi_0 \rangle \} \right], \tag{46}$$

$$E\Psi_0 = H_e \Psi_0. \tag{47}$$

In principle, any electronic structure method can be used to solve Born-Oppenheimer molecular dynamics equations. However, in practice, it is necessary to make a careful choice of the method to be used, considering the aggregate computational cost. One of the most widely used methods is Density Functional Theory (DFT), since it offers a good balance between computational cost and accuracy of the calculated parameters[104].

As discussed in the previous section, Born-Oppenheimer molecular dynamics is based on the Born-Oppenheimer approximation; therefore, this methodology presents limitations in the description of real systems. *Non*-adiabatic transitions and quantum effects, such as tunneling, cannot be described by these simulations.

3 PAPERS

The hydroxyl radical is the major free radical responsible for converting hydrogen halides to halogen atoms in the stratosphere via the reaction:

$$\mathrm{OH} + \mathrm{HX} \longrightarrow \mathrm{H_2O} + \mathrm{X} \ \ (\mathrm{X} = \mathrm{halogen})$$

Halogen atoms can catalytically destroy the ozone layer, and for this reason, these reactions play an important role in atmospheric chemistry. The rate constants have been extensively measured in a large range of temperatures. The rate constants deviate significantly from the Arrhenius limit at a low temperature: while the reaction with HBr and HI has an *anti*-Arrhenius behavior the HCl reaction has *sub*-Arrhenius behavior and large kinetic isotope effect, suggesting the presence of quantum tunneling effect. In this thesis, these *non*-Arrhenius mechanisms were investigated using *ab initio* molecular dynamics. A total of four papers are presented here as results of an investigation into the balance of stereodynamic and tunneling effect for these four-body systems.

The first and second papers were dedicated to the $\mathrm{OH} + \mathrm{HBr} \longrightarrow \mathrm{H_2O} + \mathrm{Br}$ reaction. In these works, the role is documented of the adjustment of the reactants' mutual orientation to encounter the entrance into the "cone of acceptance" for reactivity. The aperture angle of this cone is dictated by a range of directions of approach compatible with the formation of the specific angle of the product water molecule; and consistently the adjustment is progressively less effective, the higher the kinetic energy. Additionally, the extraction of thermal rate constants from molecular dynamics approach is discussed, and systematic sampling of the canonical ensemble is indicated as needed for quantitative comparison with the kinetic experiments.

In the third paper, in order to assess the *anti*-Arrherrius mechanism, we extended this study for the $\mathrm{OH} + \mathrm{HI} \longrightarrow \mathrm{H_2O} + \mathrm{I}$ reaction. Again, we have shown that negative dependence of the rate constant on temperature is explained by the stereodynamic effect, which is more pronounced at low temperatures.

Finally, in the fourth paper, we expand the strategy to understand the transition to *sub*-Arrhenius behavior after the simple halogen replacement. The $\mathrm{OH} + \mathrm{HCl} \longrightarrow \mathrm{H_2O} + \mathrm{Cl}$ reaction was studied by a blend of Born-Oppenheimer molecular dynamics and high-level Transition-State-Theory modified to account for tunneling conditions. The simulations showed that the role of the molecules orientation process is important for this reaction, although this is less than in *anti*-Arrhenius cases and compared to that of quantum mechanical through the penetration of energy barrier along the reaction path on the potential energy surface. The discussion of these results provides clarification of the occurrence of the different *non*-Arrhenius mechanisms involved in the series of reactions.

PAPER 1:

COUTINHO, ND, SILVA, VHC, de OLIVEIRA, HCB, CAMARGO, AJ, MUMDIM, KC, AQUILANTI, V. **Stereodynamical Origin of *Anti*-Arrhenius Kinetics: Negative Activation Energy and Roaming for a Four-Atom Reaction.** The Journal of Physical Chemistry Letters, 2015, 6, pp 1553-1558.

Among the processes involving four atoms, the reaction between the radical hydroxyl and the hydrogen bromide is one of the most studied experimentally: the kinetic data show that as the temperature increases the rate constants decreases, kinetic behavior known as Anti-Arrhenius. From a theoretical point of view, this reaction has already been studied by several levels of theory where the main objective has been to describe the potential energy surface and theoretically reproduce these complex rate constants using mainly the reformulations of Transition State Theory. However, the motivations that led us to study this system revolve around the results obtained by molecular-oriented beams experiments. We propose to study the OH + HBr reaction using the Born-Oppenheimer molecular dynamics approach. Trajectories are step-bystep generated on a potential energy surface quantum mechanically calculated on-the-fly and are thermostatically equilibrated to correspond to a specific temperature. Several trajectories were simulated for temperatures of 50 and 500 K. The visualizations of the trajectories as a function of the coordinates that correlate the broken and formed bonds during the reaction and the approach angles showed that there is a mechanism change as a function of temperature: while, for lower temperatures the reagents are oriented around the reactive direction, as the temperature increases, the roaming effect becomes more pronounced, where "delay" in the reactive process was observed.

My contribution in this study was to perform Born-Oppenheimer molecular dynamics simulations and perform all relevant analyzes, as well as contribute to the discussions and in the paper writing. Acknowledgment to the other authors who contributed to the development of this investigation. To professor Ademir Carmargo for the help in the development of the methodology, to professor Kleber Mundim for the discussions about the *non*-Arrhenius behavior and by developed to computational code to generate 3D surface used for representation free energy surface, to the professors Valter H. Carvalho-Silva, Heibbe Cristhian B. de Oliveira and Vincenzo Aquilanti for the results discussions and the paper revision and to Professors T. Kasai, K.-C. Lin, D.-C. Che, L. Bonnet and P.-Yu Tsai for discussion of their molecular-oriented beams experiments.

Special thanks to the American Chemical Society for the reprinted the paper in my theses.

Title: Stereodynamical Origin of Anti-Arrhenius Kinetics: Negative Activation Energy and Roaming for a Four-Atom Reaction

Author: Nayara D. Coutinho, Valter H. C. Silva, Heibbe C. B. de Oliveira, et al

Publication: Journal of Physical Chemistry Letters

Publisher: American Chemical Society

Date: May 1, 2015

PERMISSION/LICENSE IS GRANTED FOR YOUR ORDER AT NO CHARGE

This type of permission/license, instead of the standard Terms & Conditions, is sent to you because no fee is being charged for your order. Please note the following:

- Permission is granted for your request in both print and electronic formats, and translations.
- If figures and/or tables were requested, they may be adapted or used in part.
- Please print this page for your records and send a copy of it to your publisher/graduate school.
- Appropriate credit for the requested material should be given as follows: "Reprinted (adapted) with permission from (COMPLETE REFERENCE CITATION). Copyright (YEAR) American Chemical Society." Insert appropriate information in place of the capitalized words.
- One-time permission is granted only for the use specified in your request. No additional uses are granted (such as derivative works or other editions). For any other uses, please submit a new request.

BACK CLOSE WINDOW

THE JOURNAL OF PHYSICAL CHEMISTRY Letters

Letter

pubs.acs.org/JPCL

Stereodynamical Origin of Anti-Arrhenius Kinetics: Negative Activation Energy and Roaming for a Four-Atom Reaction

Nayara D. Coutinho,[†,‡] Valter H. C. Silva,[*,†] Heibbe C. B. de Oliveira,[‡] Ademir J. Camargo,[†] Kleber C. Mundim,[‡] and Vincenzo Aquilanti[*,§,∥,⊥]

[†]Unidade Universitária de Ciências Exatas e Tecnológicas, 75001-970, Anápolis, and Unidade de Ipameri, Ipameri, Universidade Estadual de Goiás, 75780-000 Goiás, Brazil

[‡]Instituto de Química, Universidade de Brasília, Caixa Postal 4478, 70904-970 Brasília, Brazil

[§]Dipartimento di Chimica, Biologia e Biotecnologie, Università di Perugia, Via Elce di Sotto 8, 06123 Perugia, Italy

[∥]Instituto de Física, Universidade Federal da Bahia, 40210 Salvador, Brazil

[⊥]Istituto di Struttura della Materia, Consiglio Nazionale delle Ricerche, 00185 Rome, Italy

Supporting Information

ABSTRACT: The OH + HBr → H_2O + Br reaction, prototypical of halogen-atom liberating processes relevant to mechanisms for atmospheric ozone destruction, attracted frequent attention of experimental chemical kinetics: the nature of the unusual reactivity drop from low to high temperatures eluded a variety of theoretical efforts, ranking this one among the most studied four-atom reactions. Here, inspired by oriented molecular-beams experiments, we develop a first-principles stereodynamical approach. Thermalized sets of trajectories, evolving on a multidimensional potential energy surface quantum mechanically generated on-the-fly, provide a map of most visited regions at each temperature. Visualizations of rearrangements of bonds along trajectories and of the role of specific angles of reactants' mutual approach elucidate the mechanistic change from the low kinetic energy regime (where incident reactants reorient to find the propitious alignment leading to reaction) to high temperature (where speed hinders adjustment of directionality and roaming delays reactivity).

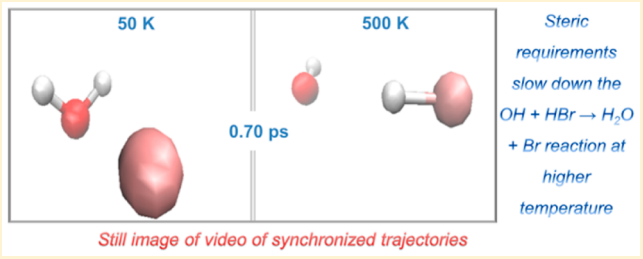

The reaction OH + HBr → H_2O + Br is considered as a benchmark elementary process that exhibits negative temperature dependence of the reaction rate[1−7] (anti-Arrhenius behavior). Recently, quantum chemical calculations of an accurate global potential energy surface[8] and extensive classical trajectory simulations[9] reproduced the behavior, whereas a review[10] pointed out at existing evidence from molecular beam scattering experiments with oriented reactants[11,12] of the key role of stereodynamics, establishing the ground for a mechanistic interpretation.

This reaction is of relevance in atmospheric modeling because it belongs to a class of processes producing halogen atoms that are destroyers of ozone.[13] At thermal energies, it proceeds through a negligible barrier and its cross section decreases as the collision energy increases.[14,15] From a theoretical viewpoint, this observed negative collision energy dependence could not be explained by the average long-range dipole−dipole attraction between the reactants; we argue that a relevant molecular reorientation occurs and the effect becomes less pronounced as the collision energy increases and reactants have less time to rotate toward the reactive direction. This paper reports numerical experiments to document this effect.

Motivations and background information are illustrated with reference to Figure 1. Left panels define the geometrical parameters for the configuration of this four-atom system; the reaction profile is drawn according to recent accurate quantum chemical calculations:[8] the van der Waals-type entrance channel well leads to a transition state at lower an energy than that of the reagents. Cross section data are from crossed beam experiments[14,15] and show a dramatic drop as a function of collision energy; stereodynamical information is also provided[11,12] on role of mutual direction of approaching reactants: a relevant angle θ, also defined in the figure, serves to discuss the effect. On the right, we present an Arrhenius plot for a selection of available experimental rate constants[1−7] showing the unusual temperature dependence fitted by the d-Arrhenius formula recently introduced[16−19] for sub- and super-Arrhenius cases, and here extended to anti-Arrhenius behavior (see Supporting Information). The addition of the parameter d accounts for deviations from linearity of the plot. The apparent activation energy, E_a, is extracted and seen to be temperature dependent and negative.

The strategy that we follow is to use the Born−Oppenheimer molecular dynamics (BOMD)[20,21] approach to visualize the

Received: February 22, 2015
Accepted: April 7, 2015
Published: April 7, 2015

DOI: 10.1021/acs.jpclett.5b00384
J. Phys. Chem. Lett. 2015, 6, 1553−1558

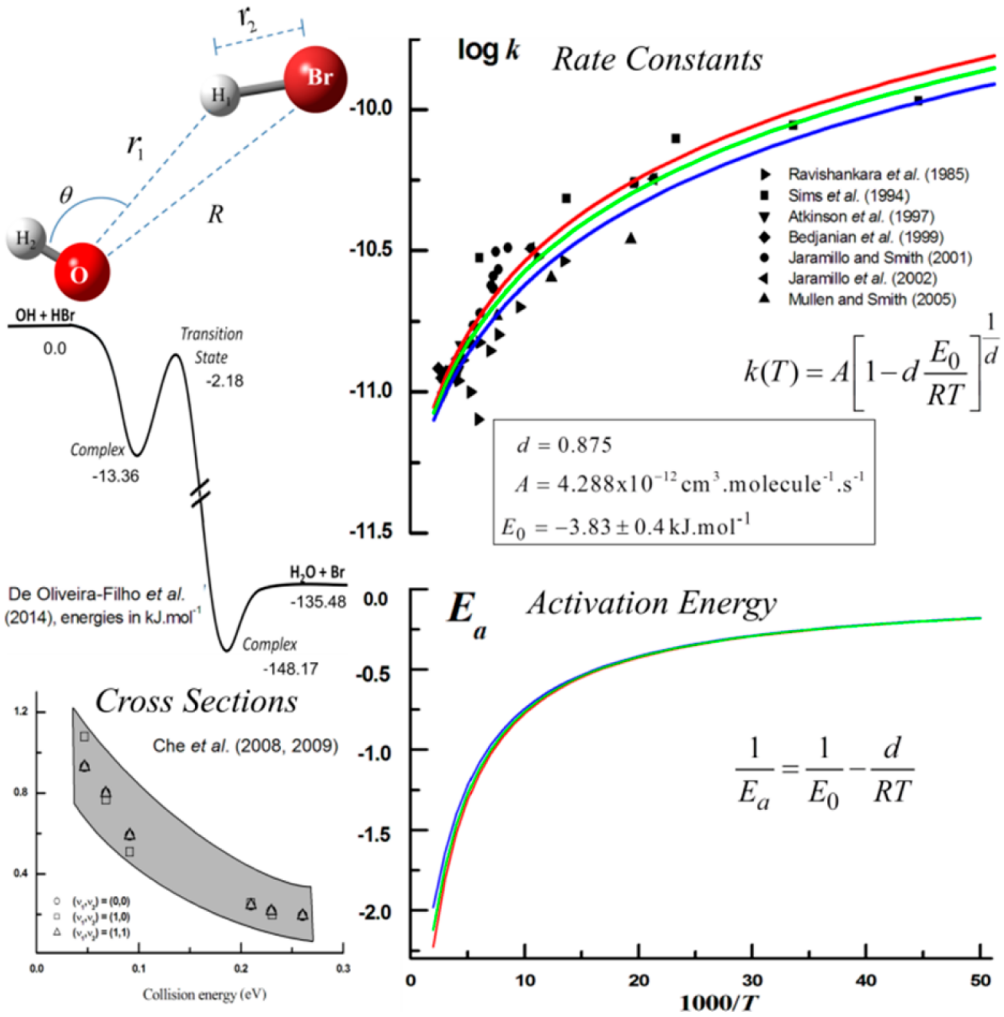

Figure 1. Coordinates, energy profile, cross sections for specific vibrational states of product H_2O, Arrhenius plots of rate constants and temperature dependence of activation energy. To give a view of the general trend, we show a fit of selected kinetic data with the *d*-Arrhenius formula describing curvatures in Arrhenius plots.[16−19] The central curves correspond to the best fit for E_0, the others show those corresponding to its estimated limiting values.

reaction in a box, our "nanoreactor" in the spirit of ref 22, whereby the system explores the potential energy surface at a specified temperature, simulated by a Nosé−Hoover thermalizing bath.[23] Although computations of the potential energy surface on-the-fly are time-consuming, we can scrutinize trajectories at different configurations and will examine comparatively their behavior at two extreme temperatures, according to this sequence: (i) by having a global look to obtain information on selective sensitivity to the features of the free energy surface when explored at slow or fast speed; (ii) by focusing on three exemplarily selected trajectories to follow in time rupture and formation of bonds; (iii) by showing how trajectories exhibit molecular reorientation for favorable reactivity, and document interesting manifestations of the roaming phenomenon and of the crucial role of stereodynamics. A movie showing the synchronized progress of two trajectories with the same initial configurations at two given temperature contributes to the visualization of these concepts (see the video in Supporting Information).

Anti-Arrhenius Behavior and Negative Activation Energy. For this four-atom system, archetypal of four-center reactions: (i) accurate computation and fitting of six-dimensional PES is demanding, (ii) exact quantum close coupling state-to-state dynamics is prohibitively expensive, and (iii) even for reduced dimensionality models benchmark cross sections are difficult to obtain and rate constants out-of-reach. Although this reaction involves hydrogen exchange, tunneling is arguably not influential, according to deuterium substitution experiments[5] and the accepted reaction profile[8] (see Figure 1). The latter is a cut of a recent potential energy surface on which classical trajectory calculations[9] of reaction rates provided agreement with the temperature dependent experimental data. The unusual barrier at an energy lower than that of reactants arising from the pronounced van der Waals well for the approaching reactants is pointed out as important for the apparent negative activation energy. However, the authors do not discuss any role of stereodynamics in favoring low temperature reactivity and disfavoring high-temperature reactive outcomes.

The importance of stereodynamical aspects had been convincingly revealed in experiments, where in order to understand orientational effects, the Osaka group[11,12,14,15] studied this reaction using crossed molecular beams for higher than thermal energy (0.05−0.26 eV): the results indicated that the cross section decreases, increasing the collision energy (Figure 1) and suggest that reorientation effects of the reagents

DOI: 10.1021/acs.jpclett.5b00384
J. Phys. Chem. Lett. 2015, 6, 1553−1558

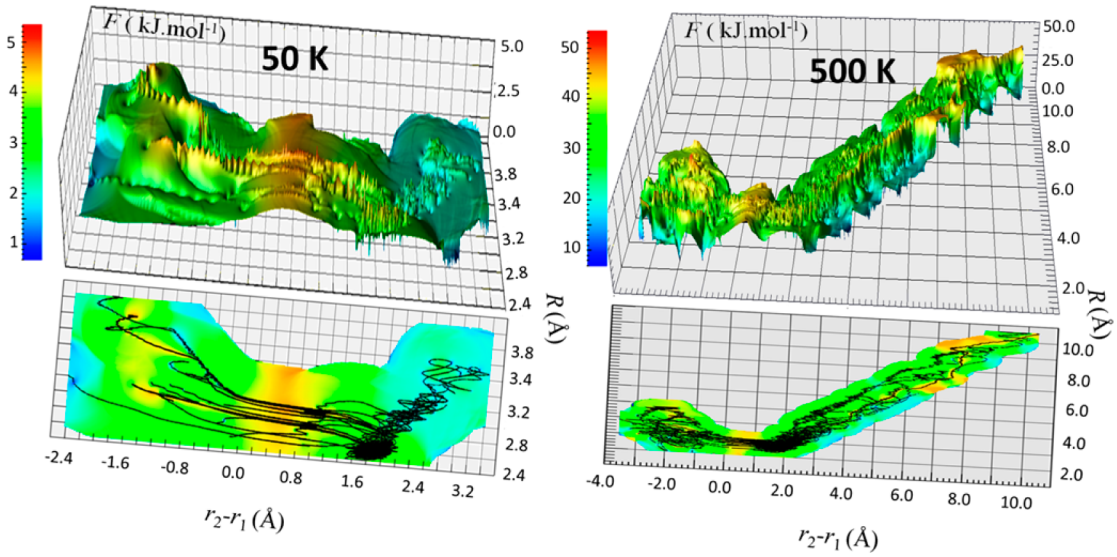

Figure 2. "Canonical" trajectories in the reactive box: reconstruction of free energy surfaces as sampled by several trajectories at low (50 K, left panels) and high (500 K, right panels) temperatures.

strongly favor the reactivity. To test the energy dependence of reorientation effects and to extract information on the relative reactivity of the O-end, H-end, and sideways collisions, the Osaka group used an orienting hexapole electrostatic field. Regarding the relative importance of the reactive sites, it was found that the O-end attack is most favored for this reaction than that of H-end attack by a factor 3.4 ± 2.3; they also suggested a cone of acceptance with a limiting angle[11] of α = 117 ± 13 degrees for the reaction to occur (their $\alpha = \pi - \theta$, where θ is defined in Figure 1). Our results provide a theoretical framework for this effect confirming the experimentally derived suggestion that the negative temperature dependence of the OH + HBr has a stereodynamical origin, overlooked by previous theoretical studies.

First-Principles Approach. First-principles molecular dynamics is presented here for the first time for this prototypical halogen generating reaction. For a pioneering investigation of a reaction involving an OH radical, see ref 24, where Car−Parrinello dynamics was used. However, with respect to the original Car−Parrinello type of approaches, where motion of the nuclei in the on-the-fly dynamics occurs in the potential generated by the electrons and governed by classical mechanics, the wave functions here are converged at every step, making trajectory calculations much more expensive but arguably more accurate.[21]

Interatomic forces are not preassigned but are obtained through electronic structure calculations, and chemical reactions occur as the electronic structure adjusts to the evolving atomic positions. In this way, it is possible to determine reaction mechanisms with no reference to previously determined reaction pathways. Rather, the exploit of the automatic focusing of trajectories on regions actually sampled during the process provides information on parts of the multidimensional potential energy surface that demand more accuracy for realistic simulations of the dynamics. Randomly generated initial conditions and procedures for equilibration with respect to thermal baths (see details in Supporting Information) permit to efficiently bypass the often severe bottlenecks of computational dynamics, such as both the impact parameter integration to provide total cross sections, and their Boltzmann kinetic energy averaging; this allows us to directly express results at a specific temperature: our choice was to consider two extremes of the experimentally relevant range, at low (50 K) and high (500 K) temperatures.

Figure 2 is an overview of results for trajectories within the reactive box. We define these trajectories as "canonical" being intended as evolving at given temperatures[23] (those trajectories found as nonreactive were stored for further analysis): the reconstruction of free energy surfaces (upper panels) as sampled by several trajectories is shown at low and high temperatures: although arguably valid within a close neighborhood, the graphical extension is intended to visually help the readers' perception. A table in Supporting Information lists the initial configurations of the trajectories that are reported but not distinguishable in Figure 2: they will be discussed in detail later. The horizontal coordinate is the difference between lengths of the bond that is progressively broken r_2 and of the one which is concertedly formed r_1 (Figure 1). The transverse coordinate R, the length of the bond between O and Br, can be regarded as approximately proportional either to the principal moment of inertia of this nearly oblate top system or else to the hyperradius of the hyperspherical approach. The lower panels show the bunch of the reactive trajectories on the R, $r_2 - r_1$ plane (the identification of each of them with the corresponding initial conditions listed in the Table of Supporting Information is not attempted here but is discussed graphically in the following).

At low temperature, all reactive trajectories are seen to enter the box in the upper left corner and evolve, whereas the R coordinate attains a range of minimum values in the closest approach configurations, where the $r_2 - r_1$ coordinate changes sign; then they continue downhill (the vibrational excitation of the newly formed bond appears as wavelets in the graph) until they exit the box toward product formation in the lower right corner of the figure. The free energy landscape from left to right shows an early stage, exhibiting a decreasing tendency to a small basin due to the intermolecular attraction between the reactants, then the ascent to a barrier, followed by the fall into the basin of the intermolecular interactions between the incipiently departing products. Eventually, they separate with

DOI: 10.1021/acs.jpclett.5b00384
J. Phys. Chem. Lett. 2015, 6, 1553−1558

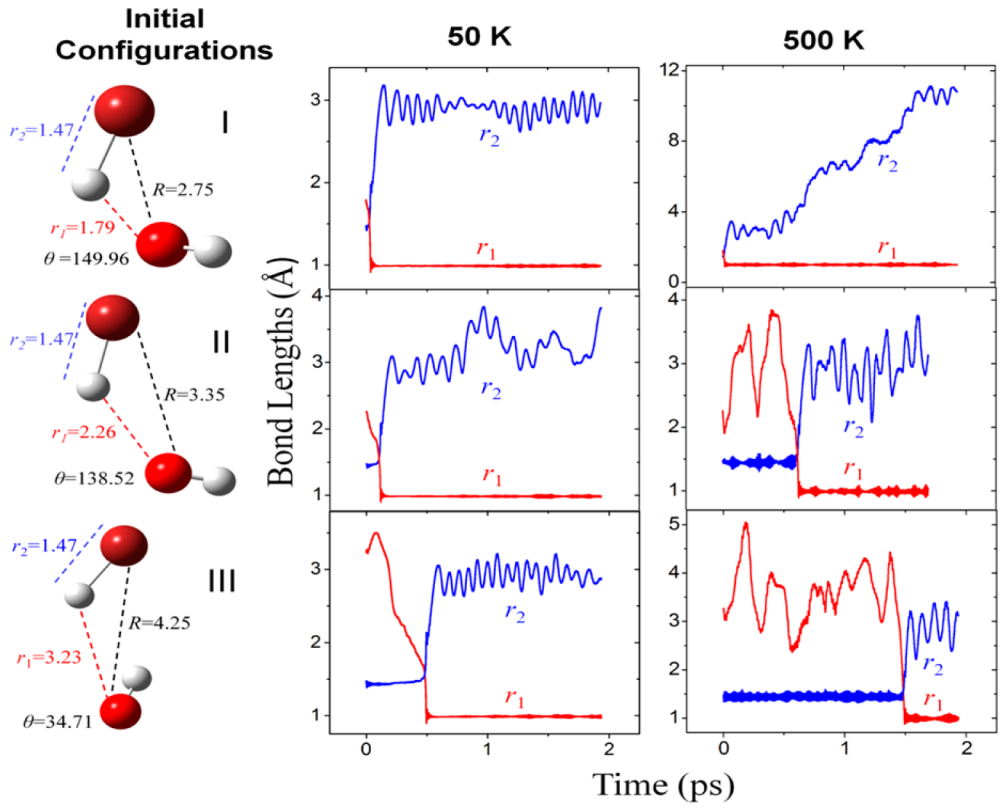

Figure 3. Exemplary "canonical" trajectories at two temperatures for three initial configurations I, II and III, chosen among those that are found to lead to reaction. Estimated switching times (in picoseconds) are, respectively: 0.05, 0.11, 0.50 at 50 K and 0.01, 0.64, 1.50 at 500 K.

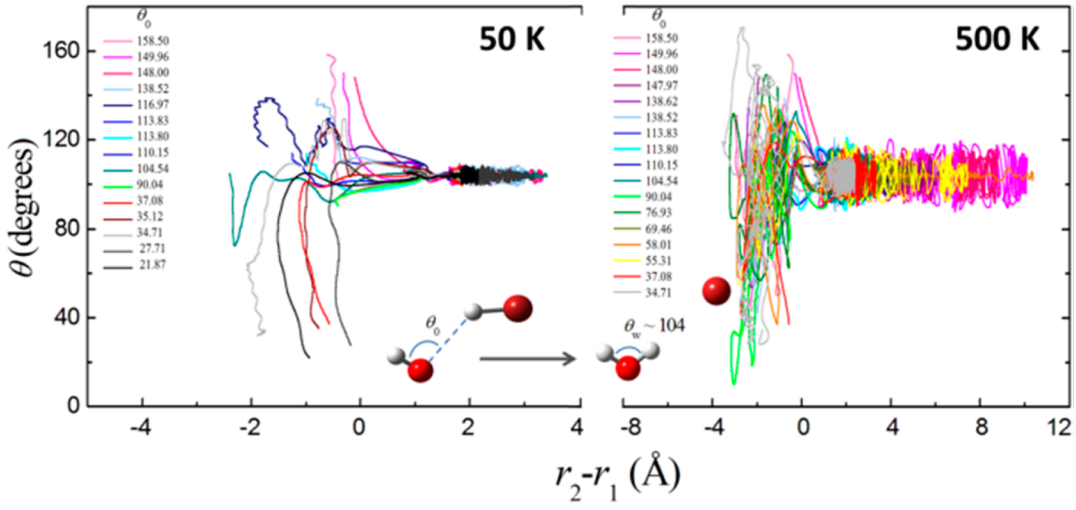

Figure 4. Evolution at two temperatures of the stereodynamical angle of approach θ defined in Figure 1 for "canonical" trajectories (see Table in Supporting Information). Colors indicate the initial value of θ, denoted by θ_0.

large vibrational energy in the newly formed bond of the water molecule. This progression is a manifestation of the minimum energy path profile for this exothermic reaction (Figure 1), characterized by van der Waals-like complexes in the reactant and product channels and by a transition-state barrier energetically lower than the entrance channel.

At high temperature, reactive trajectories are seen that, after entering the box from different directions, only subsequently find their relatively narrow way toward product formation, and are much less sensitive to the details of the reaction profile.

Delayed Reactivity and Roaming. The three initial configurations shown in Figure 3, correspond to the given geometrical parameters (see also Table in Supporting Information); the lengths of the bond that is broken r_2 and of the bond that is formed r_1 are reported as a function of time. After hydrogen exchange, the interatomic distance r_1 is seen tending fast to the asymptotic value ca. 1 Å that correspond to the length of the OH bond of water, with some vibrational stretching at 500 K. For I, where reactants enter the reactive box with a favorable configuration, reaction occurs suddenly. For II and III, where the dynamics is started with increasingly larger initial

DOI: 10.1021/acs.jpclett.5b00384
J. Phys. Chem. Lett. 2015, 6, 1553−1558

elongation for r_1, reaction is delayed, and roaming in the entrance channel manifests with ample oscillations. Initial values for R and θ similarly contribute, and the effect is dramatically enhanced at high temperature, where interesting signatures of "roaming" also are particularly evident as increasingly ample vibrations of the bond being broken, whereas bromine tends to move away.

For the following discussion, interesting is the "switching" time, occurring when along trajectories, $r_1 = r_2$, that to a very rough approximation can be considered as the moment that reaction occurs. The main visual impression (see also the video in Supporting Information) is the evident delayed reactivity for trajectories in the search of encountering proper paths, a phenomenon that is impeded at high temperature. More pronounced is also seen the apparent "roaming" in vibrational modes in search of favorable outcomes when initial r_1 is stretched, to be contrasted for example to the round-about mechanism seen in S_N2 reaction dynamics.[25]

The "roaming" effect can often be attributed to the manifestation of nonadiabatic transitions and has been individuated and documented as the occurrence in photodissociation experiments of alternative routes to molecular fragmentation channels[26,27] that avoid passing through the transition state. The presence of these alternative pathways can be inferred by the properties of the energy distribution of the product fragments and indicates that attention be devoted to regions of the potential energy surfaces other than those in the neighborhoods of saddle points along minimum energy paths: eventually this leads to discovery avenues to reaction beyond the venerable transition state theory approach.[10,27]

The origin of roaming as a rearrangement between weakly bound reactants is connected to high-lying reaction channels.[28] In refs 29 and 30, observed roaming was perpetuated by pronounced bond elongation in methyl formate[29] emerging from a conical intersection: similarly, in the present case, it is favored by trajectories originating at elongated r_1. However, exothermicity appears not to be used for appreciable vibrational excitation of the formed bond.

Stereodynamics and Excitation of Bending for the Water Product. Figure 4 provides documentation of the role of stereodynamics in the peculiar kinetics of this reaction. The "canonical" reactive trajectories, as a function of the variable $r_2 - r_1$, are distinguished by different colors as listed and arranged in decreasing order of θ_0, the initial values for the θ angle (the other parameters characterizing the initial configurations are reported in the Table in Supporting Information). The figure shows that when the dynamics is started with those values of θ_0 close to that directly leading to the formation of the bending angle of water, the system finds an easier way to products, and possible reorientation facilitating the process is impeded at high temperature. Note again the "roaming" effect as the search of a favorable approaching angle for reactivity (see video in Supporting Information).

Remarkably, substantial energy appears to dispose as excitation in the bending mode of the product water, as it is visually clear to a much greater extent for the higher temperature (see ref 31 for experimental comparisons). The range of values of the θ angle can be analyzed in terms of the energy disposal into the bending mode.

In retrospect, results from this paper describing reactivity in a four-atom system are insightful in view of the enormous difficulties that are encountered to provide theoretically benchmark rate constants. Great effort is needed to go all the way from the intermolecular interactions to rate constants, through state-to-state coupled-channel Schrödinger dynamics (to obtain scattering matrices), followed by sums over angular momenta (to obtain differential and integral cross sections) and finally by Boltzmann averaging to obtain the rates. Only recently, this has been achieved for a triatomic system and predictions[32] have been verified experimentally for very low temperature reactivity.[33] However, comparison of results for this four-atom reaction with related three-atom processes is interesting: de Oliveira-Filho et al.[9] commented on the reaction O + HBr; in addition, we indicate as insightful to consider also the H + HBr reaction, for which Pomerantz et al.[34] gave experimental and computational evidence of reactive trajectories far from minimum energy path, an unnoticed signature of "roaming" in the sense of our discusson of Figure 3.

The involved computational effort forced us to limit the number of trajectories and thus the statistical validity of our sampling. However, we did not present here very numerous nonreactive events: the data are stored and available for future analysis within an extension of this work to more quantitative investigations, which are in progress for this and other reactions of analogous complexity. Nevertheless an order-of-magnitude estimate of rates can be of interest: in our numerical experiments, we place one molecule of both OH and HBr in a cubic box of 6 Å in size under periodic boundary conditions, amounting to a concentration of $\sim 3 \times 10^{21}$ molecules cm^{-3} for each reactant. From the decay times of the order of 1 ps at 50 K and 2 ps at 500 K, one estimates bimolecular rates of order $\sim 3 \times 10^{-11}$ and 1.5×10^{-11} cm^3 $molecules^{-1}$ s^{-1}, respectively, in a range compatible with experimental values (Figure 1).

■ ASSOCIATED CONTENT

Supporting Information

Details of the theoretical and computational methods. Movie (MOV format) with synchronized trajectories of the OH + HBr reaction at low and high temperatures. This material is available free of charge via the Internet at http://pubs.acs.org.

■ AUTHOR INFORMATION

Corresponding Authors

*E-mail: vincenzoaquilanti@yahoo.it.

*E-mail: fatioleg@gmail.com.

Notes

The authors declare no competing financial interest.

■ ACKNOWLEDGMENTS

The authors acknowledge grants from Brazilian CAPES, FAPEG, CNPQ and FINATEC. V. Aquilanti thanks CAPES for the appointment as Professor Visitante Especial at Instituto de Fisica, Universidade Federal da Bahia, Salvador (Brazil) and T. Kasai, K.-C. Lin, D.-C. Che, L. Bonnet and P.-Yu Tsai for discussion of their oriented molecular beams experiments.

■ REFERENCES

(1) Ravishankara, A. R.; Wine, P. H.; Wells, J. R. The OH + HBr Reaction Revisited. *J. Chem. Phys.* **1985**, *83*, 447−448.

(2) Sims, I. R.; Smith, I. W. M.; Clary, D. C.; Bocherel, P.; Rowe, B. R. Ultra-Low Temperature Kinetics of Neutral-Neutral Reactions—New Experimental and Theoretical Results For OH + HBr Between 295 and 23 K. *J. Chem. Phys.* **1994**, *101*, 1748−1751.

(3) Atkinson, D. B.; Jaramillo, V. I.; Smith, M. A. Low-Temperature Kinetic Behavior of the Bimolecular Reaction OH + HBr (76−242 K). *J. Phys. Chem. A* **1997**, *101*, 3356−3359.

DOI: 10.1021/acs.jpclett.5b00384
J. Phys. Chem. Lett. 2015, 6, 1553−1558

(4) Bedjanian, Y.; Riffault, V.; Le Bras, G.; Poulet, G. Kinetic Study of the Reactions of OH and OD with HBr and DBr. *J. Photochem. Photobiol., A* **1999**, *128*, 15−25.
(5) Jaramillo, V. I.; Smith, M. A. Temperature-Dependent Kinetic Isotope Effects in the Gas-Phase Reaction: OH + HBr. *J. Phys. Chem. A* **2001**, *105*, 5854−5859.
(6) Jaramillo, V. I.; Gougeon, S.; Le Picard, S. D.; Canosa, A.; Smith, M. A.; Rowe, B. R. A Consensus View of the Temperature Dependence of the Gas Phase Reaction: OH + HBr → H_2O + Br. *Int. J. Chem. Kinet.* **2002**, *34*, 339−344.
(7) Mullen, C.; Smith, M. A. Temperature Dependence and Kinetic Isotope Effects for the OH + HBr Reaction and H/D Isotopic Variants at Low Temperatures (53−135 K) Measured Using a Pulsed Supersonic Laval Nozzle Flow Reactor. *J. Phys. Chem. A* **2005**, *109*, 3893−3902.
(8) De Oliveira-Filho, A. G. S.; Ornellas, F. R.; Bowman, J. M. Quasiclassical Trajectory Calculations of the Rate Constant of the OH + HBr → Br + H_2O Reaction Using a Full-Dimensional Ab Initio Potential Energy Surface Over the Temperature Range 5 to 500 K. *J. Phys. Chem. Lett.* **2014**, *5*, 706−712.
(9) De Oliveira-Filho, A. G. S.; Ornellas, F. R.; Bowman, J. M. Energy Disposal and Thermal Rate Constants for the OH + HBr and OH + DBr Reactions: Quasiclassical Trajectory Calculations on an Accurate Potential Energy Surface. *J. Phys. Chem. A* **2014**, *118*, 12080−12088.
(10) Kasai, T.; Che, D.-C.; Okada, M.; Tsai, P.-Y.; Lin, K.-C.; Palazzetti, F.; Aquilanti, V. Directions of Chemical Change: Experimental Characterization of the Stereodynamics of Photodissociation and Reactive Processes. *Phys. Chem. Chem. Phys.* **2014**, *16*, 9776−9790.
(11) Tsai, P.-Y.; Che, D.-C.; Nakamura, M.; Lin, K.-C.; Kasai, T. Orientation Dependence in the Four-Atom Reaction of OH + HBr Using the Single-State Oriented OH Radical Beam. *Phys. Chem. Chem. Phys.* **2010**, *12*, 2532−2534.
(12) Tsai, P.-Y.; Che, D.-C.; Nakamura, M.; Lin, K.-C.; Kasai, T. Orientation Dependence for Br Formation in the Reaction of Oriented OH Radical with HBr Molecule. *Phys. Chem. Chem. Phys.* **2011**, *13*, 1419−1423.
(13) Saiz-Lopez, A.; von Glasow, R. Reactive Halogen Chemistry in the Troposphere. *Chem. Soc. Rev.* **2012**, *41*, 6448−6472.
(14) Che, D.-C.; Matsuo, T.; Yano, Y.; Bonnet, L.; Kasai, T. Negative Collision Energy Dependence of Br Formation in the OH + HBr Reaction. *Phys. Chem. Chem. Phys.* **2008**, *10*, 1419−1423.
(15) Che, D.-C.; Doi, A.; Yamamoto, Y.; Okuno, Y.; Kasai, T. Collision Energy Dependence for the Br Formation in the Reaction of OD + HBr. *Phys. Scr.* **2009**, *80*, 048110.
(16) Aquilanti, V.; Mundim, K. C.; Elango, M.; Kleijn, S.; Kasai, T. Temperature Dependence of Chemical and Biophysical Rate Processes: Phenomenological Approach to Deviations from Arrhenius Law. *Chem. Phys. Lett.* **2010**, *498*, 209−213.
(17) Aquilanti, V.; Mundim, K. C.; Cavalli, S.; De Fazio, D.; Aguilar, A.; Lucas, J. M. Exact Activation Energies and Phenomenological Description of Quantum Tunneling for Model Potential Energy Surfaces. The F + H_2 Reaction at Low Temperature. *Chem. Phys.* **2012**, *398*, 186−191.
(18) Silva, V. H. C.; Aquilanti, V.; de Oliveira, H. C. B.; Mundim, K. C. Uniform Description of Non-Arrhenius Temperature Dependence of Reaction Rates, and a Heuristic Criterion for Quantum Tunneling vs Classical Non-Extensive Distribution. *Chem. Phys. Lett.* **2013**, *590*, 201−207.
(19) Cavalli, S.; Aquilanti, V.; Mundim, K. C.; De Fazio, D. Theoretical Reaction Kinetics astride the Transition between Moderate and Deep Tunneling Regimes: The F + HD Case. *J. Phys. Chem. A* **2014**, *118*, 6632−6641.
(20) Marx, D.; Hutter, J. Ab Initio Molecular Dynamics: Theory and Implementation. In *Modern Methods and Algorithms of Quantum Chemistry*; Grotendorst, J., Ed.; John-von-Neumann-Inst. for Computing: Jülich, Germany, 20001301449
(21) Paranjothy, M.; Sun, R.; Zhuang, Y.; Hase, W. L. Direct Chemical Dynamics Simulations: Coupling of Classical and Quasiclassical Trajectories with Electronic Structure Theory. *Wiley Interdiscip. Rev.: Comput. Mol. Sci.* **2013**, *3*, 296−316.
(22) Wang, L.-P.; Titov, A.; McGibbon, R.; Liu, F.; Pande, V. S.; Martínez, T. J. Discovering Chemistry with an Ab Initio Nanoreactor. *Nat. Chem.* **2014**, 1044−1048.
(23) Martyna, G. J.; Klein, M. L.; Tuckerman, M. Nosé−Hoover Chains: The Canonical Ensemble via Continuous Dynamics. *J. Chem. Phys.* **1992**, *97*, 2635.
(24) Frank, I.; Parrinello, M.; Klamt, A. Insight into Chemical Reactions from First-Principles Simulations: The Mechanism of the Gas-Phase Reaction of OH Radicals with Ketones. *J. Phys. Chem. A* **1998**, *102*, 3614−3617.
(25) Mikosch, J.; Trippel, S.; Eichhorn, C.; Otto, R.; Lourderaj, U.; Zhang, J. X.; Hase, W. L.; Weidemüller, M.; Wester, R. Imaging Nucleophilic Substitution Dynamics. *Science* **2008**, *319*, 183−186.
(26) Townsend, D.; Lahankar, S. A.; Lee, S. K.; Chambreau, S. D.; Suits, A. G.; Zhang, X.; Rheinecker, J.; Harding, L. B.; Bowman, J. M. The Roaming Atom: Straying from the Reaction Path in Formaldehyde Decomposition. *Science* **2004**, *306*, 1158−1161.
(27) Bowman, J. M. Roaming. *Mol. Phys.* **2014**, *112*, 2516−2528.
(28) Herath, N.; Suits, A. G. Roaming Radical Reactions. *J. Phys. Chem. Lett.* **2011**, *2*, 642−647.
(29) Tsai, P.-Y.; Chao, M.-H.; Kasai, T.; Lin, K.-C.; Lombardi, A.; Palazzetti, F.; Aquilanti, V. Roads Leading to Roam. Role of Triple Fragmentation and of Conical Intersections in Photochemical Reactions: Experiments and Theory on Methyl Formate. *Phys. Chem. Chem. Phys.* **2014**, *16*, 2854−2865.
(30) Nakamura, M.; Tsai, P.-Y.; Kasai, T.; Lin, K.-C.; Palazzetti, F.; Lombardi, A.; Aquilanti, V. Dynamical, Spectroscopic and Computational Imaging of Bond Breaking in Photodissociation: Roaming and Role of Conical Intersections. *Faraday Discuss.* **2015**, No. 10.1039/C4FD00174E, DOI: 10.1039/C4FD00174E.
(31) Butkovskaya, N. I.; Setser, D. W. Chemical Dynamics of H Abstraction by OH Radicals: Vibrational Excitation of H_2O, HOD, and D_2O Produced in Reactions of OH and OD with HBr and DBr. *J. Phys. Chem.* **1996**, *100*, 4853−4866.
(32) Aquilanti, V.; Cavalli, S.; Fazio, D.; De Volpi, A.; Aguilar, A.; Lucas, J. M. Benchmark Rate Constants by the Hyperquantization Algorithm. The F + H_2 Reaction for Various Potential Energy Surfaces: Features of the Entrance Channel and of the Transition State, and Low Temperature Reactivity. *Chem. Phys.* **2005**, *308*, 237−253.
(33) Tizniti, M.; Le Picard, S. D.; Lique, F.; Berteloite, C.; Canosa, A.; Alexander, M. H.; Sims, I. R. The Rate of the F + H_2 Reaction at Very Low Temperatures. *Nat. Chem.* **2014**, *6*, 141−145.
(34) Pomerantz, A. E.; Camden, J. P.; Chiou, A. S.; Ausfelder, F.; Chawla, N.; Hase, W. L.; Zare, R. N. Reaction Products with Internal Energy beyond the Kinematic Limit Result from Trajectories far from the Minimum Energy Path: An Example from H + HBr → H_2 + Br. *J. Am. Chem. Soc.* **2005**, *127*, 16368−16369.

DOI: 10.1021/acs.jpclett.5b00384
J. Phys. Chem. Lett. 2015, 6, 1553−1558

Associated Content

Stereodynamical Origin of Anti-Arrhenius Kinetics: Negative Activation Energy and Roaming for a Four-Atom Reaction

Nayara D. Coutinho[†,‡], Valter H. C. Silva[†*], Heibbe C. B. de Oliveira[‡], Ademir J. Camargo[†], Kleber C. Mundim[‡] and Vincenzo Aquilanti[┼*]

[†]Unidade Universitária de Ciências Exatas e Tecnológicas, 75001-970, Anápolis, and Unidade de Ipameri, 75780-000, Ipameri, Universidade Estadual de Goiás, Goiás, Brazil.

[‡]Instituto de Química, Universidade de Brasília, Caixa Postal 4478, 70904-970, Brasília, Brazil.

[┼]Dipartimento di Chimica, Biologia e Biotecnologie, Università di Perugia, Via Elce di Sotto 8, 06123, Perugia, Italy. Instituto de Física, Universidade Federal da Bahia, 40210 Salvador, Brazil. Istituto di Struttura della Materia, Consiglio Nazionale delle Ricerche, Rome, Italy.

I. PREVIOUS THEORETICAL APPROACHES

The main text emphasizes that because of its unusual kinetic behavior, this reaction had been previously extensively investigated. We amply cited the very recent references[1,2] where classical trajectories were run on a state-of-the art potential energy surface reproducing the unusual reactivity features and confirming previous work that indicated that the mechanism is indeed bimolecular and involves the role of a van der Waals pre-reactive complex [3–6].

Other remarkable approaches are here noted. Clary *et al.*[3] used a statistical adiabatic capture model, providing a maximum to the experimental rate constant at very low temperatures and predicting the rate constant at 20 K, and later[4] employed the rotation bond approximation in quantum scattering calculations for thermal energies. A simple PES was constructed for the reaction on the basis of a London-Eyring-Polanyi-Sato function and an accurate H_2O potential and it was shown that between the reactants and

products, there is a transition state with energy slightly less than that of the reactants, as accepted now (Fig. 1). Although agreement with available experimental data was not satisfactory, these calculations also suggested a strong cross-section dependence of the initial rotational state of the OH radical and that this effect may be responsible for the negative dependence of the reaction rate on temperature. Afterwards, Nizamov *et al.*[5] obtained similar results on additional PES using classical trajectories.

Liu *et al.*[6] calculated an *ab initio* PES, including geometries, energies, gradients, and force constants of the stationary points and some extra points along the minimum energy path, showing again that at the reactant side there is a hydrogen-bonded complex with energy lower than that of the reactants, and that from the complex to the products, the reaction system passes through a reactant-like transition state with energy slightly higher than that of the reactants, so that they could calculate the rate constants using Variational Transition State Theory. A just accepted manuscript[7] providing an extensive trajectory study on a novel PES differs in approach from our on-the-fly one and in spirit principally because of neglect of the stereodynamical perspective.

II. THEORETICAL AND COMPUTATIONAL DETAILS

To describe the experimental kinetic data in Fig. 1, where what can be defined an anti-Arrhenius behavior was observed, we used the equation

$$k(T) = A\left[1 - d\,\frac{E_0}{RT}\right]^{\frac{1}{d}}. \qquad (1)$$

Equation (1) contains three phenomenological parameters, A, E_0 and d, only the latter appearing besides the familiar two of the Arrhenius equation. The parameter d provides the degree of deformation of the exponential function: in fact, for the deformation

parameter $d \to 0$, Equation (1) tends to the Arrhenius equation, $k(T) = A\exp(-E_0 / RT)$, where E_0 is a temperature independent activation energy. In Refs. [8–11], we introduced (1) and classified cases where $d > 0$ and $d < 0$ correspond to processes that we defined as Super- and Sub-Arrhenius, respectively, offering a general phenomenology for deviation of linearity in ln *k vs* 1/*T* plots. Equation (1) bears a formal relationship with a non-Boltzmann distribution law occurring in non-extensive thermodynamics[12].

In this application, we extended Equation (1) to an anti-Arrhenius behavior, corresponding to negative values of the activation energy, E_a. E_a is obtained by the application of the current (IUPAC) definition [13] to Equation (1), as follows:

$$E_a = -R\frac{\mathrm{d}\ln k}{\mathrm{d}\left(1/T\right)}, \qquad (2)$$

which, when rearranged gives the inverse-activation-energy-inverse-temperature linear relationship (Fig.1) where *d* is seen to appear as the linearizing parameter, as follows:

$$\frac{1}{E_a} = \frac{1}{E_0} - \frac{d}{RT}. \qquad (3)$$

All the *ab initio* BOMD simulations used in this paper were carried out using the CPMD 3.17.1 suite of programs (Copyright IBM, 2012). The electronic structure was treated within density functional theory (DFT), through the Perdew-Burke-Ernzerhof (PBE) functional[14]. The level of these calculations is admittedly lower than that of the recent Refs. [1,2], but it is a useful compromise for the demanding computational requirements of the on-the-fly dynamics. The wave functions were represented by plane waves with a plane-wave cutoff of 70 Ry; the core electrons were described using Troullier-Martins pseudopotentials[15]. The equations of motion were integrated using the Velocity Verlet scheme with a time step of 0.05 fs. The temperatures of the system were controlled by Nosé-Hoover thermostats scheme[16] at 50 and 500 K. One HBr molecule and one OH radical were placed inside a 6 Å cubic cell and periodic boundary conditions were imposed for each trajectory reaching the walls of the cell. The Table lists for the trajectories discussed in this paper the randomly generated starting configurations on the NVT[16] ensemble: they were run at both low (50 K) and high (500 K) temperatures. The intermolecular orientation of the two molecules was not

optimized; that is, the starting geometries do not represent local minima of the global potential surface. A total simulation time of 2 ps was used for each trajectory, although for 50 K calculations 1 ps maximum was generally sufficient. For those cases in which the reaction did not take place at any the two examined temperatures, the corresponding trajectories were stored but their discussion is beyond the scope of this paper. The vertical coordinate F in Fig. 2 is the calculated Helmholtz free energy surface, obtained by the trajectory data in the configuration range actually sampled, $F = -k_B T \ln\left[\int P(R, r_2 - r_1)\, dR\right]$, where k_B is Boltzmann constant, T is the simulation temperature and $P(R, r_2 - r_1)$ is a distribution as a function of R and $r_2 - r_1$, as calculated from the molecular dynamics simulations[17,18]. The issue, about the maintenance of an equilibrium distribution all the way from reactants to products also beyond the transition state - a concern for example of Refs [19,20] is arguably not influential to the main conclusions of this paper.

We developed a computational code to generate 3D surface based on the open source code OpenDX. IBM Open Visualization Data Explorer (OpenDX) is an application and development software package for visualizing data, especially 3D vector field from simulations. It uses a Graphical User Interface based on X windows. It comes with a complete set of standard visualization tools for looking at data. We used two modules from this package, the Autogrid to interpolate the data and the Rubbersheet to create a continuous 3D surface based on 3D vector field with components (R, $r_2 - r_1$, F).

Table S1 Initial values of the coordinates for reactive trajectories[(a)], arranged in decreasing order of the stereodynamical angle, θ_0. The last two columns are low and high temperature switching times[(c)].

θ_0 (degrees)	Angle (Br-H_1-O) (degrees)	r_1 (Å)	R (Å)	Torsion Angle (H_2-O-H_1-Br) (degrees)	Switching times (ps)	
					50 K	500 K
158.50	146.70	2.03	3.30	171.00	0.13	1.02
149.96(I) [(b)]	114.74	1.79	2.75	12.24	0.05	0.01
148.00	116.74	1.58	2.60	11.54	0.04	0.01
147.97	12.44	3.41	2.00	173.26	Nonreactive	0.18
138.62	22.49	3.79	2.50	97.66	0.12	0.20
138.52(II) [(b)]	126.39	2.26	3.35	9.32	0.11	0.64
113.83	94.46	2.73	3.20	-121.86	0.09	0.04
113.80	105.71	2.47	3.20	-69.13	0.07	0.03
110.15	141.65	1.70	3.00	121.84	0.02	0.01
104.54	52.23	3.88	3.20	-162.85	0.24	0.10
90.04	76.36	1.89	3.00	53.30	0.04	1.05
76.93	50.24	2.59	2.00	60.85	Nonreactive	0.51
69.46	153.89	3.38	2.00	167.97	Nonreactive	0.20
58.01	17.59	4.37	3.00	-106.28	Nonreactive	0.60
55.31	21.04	4.33	3.00	99.06	Nonreactive	0.37
37.08	116.05	2.05	3.00	44.89	0.14	0.21
35.12	140.26	2.24	3.50	89.99	0.16	Nonreactive
34.71(III) [(b)]	124.58	3.23	4.25	-17.83	0.50	1.50
27.71	146.31	1.66	3.00	-81.13	0.07	Nonreactive
21.87	97.50	2.41	2.99	-42.23	0.15	Nonreactive

[(a)] Initial r_2 = 1.47 Å (the HBr bond length) for all trajectories
[(b)] Trajectories corresponding to those in Fig. 3 in the main text.
[(c)] Estimated reaction times where $r_2 = r_1$, see text.

III. ANIMATIONS FROM BOMD CALCULATIONS

Movie S1: Synchronized trajectories for the OH + HBr reaction at low and high temperatures with initial configuration given as (***III***) in the above Table and in Fig 3 in the main text.

REFERENCES

(1) De Oliveira-Filho, A. G. S.; Ornellas, F. R.; Bowman, J. M. Quasiclassical Trajectory Calculations of the Rate Constant of the OH + HBr → Br + H_2O Reaction Using a Full-Dimensional Ab Initio Potential Energy Surface Over the Temperature Range 5 to 500 K. *J. Phys. Chem. Lett.* **2014**, *5*, 706–712.

(2) De Oliveira-Filho, A. G. S.; Ornellas, F. R.; Bowman, J. M. Energy Disposal and Thermal Rate Constants for the OH + HBr and OH + DBr Reactions: Quasiclassical Trajectory Calculations on an Accurate Potential Energy Surface. *J. Phys. Chem. A* **2014**, *118*, 12080–12088.

(3) Clary, D. C.; Stoecklin, T. S.; Wickham, A. G. Rate Constants for Chemical Reactions of Radicals at Low Temperatures. *J. Chem. Soc. Faraday Trans.* **1993**, *89*, 2185.

(4) Clary, D. C.; Nyman, G.; Hernandez, R. Mode Selective Chemistry in the Reactions of OH with HBr and HCl. *J. Chem. Phys.* **1994**, *101*, 3704.

(5) Nizamov, B.; Setser, D. W.; Wang, H.; Peslherbe, G. H.; Hase, W. L. Quasiclassical Trajectory Calculations for the OH(X 2Π) and OD(X 2Π) + HBr Reactions: Energy Partitioning and Rate Constants. *J. Chem. Phys.* **1996**, *105*, 9897.

(6) Liu, J.; Li, Z.; Dai, Z.; Huang, X.; Sun, C. Direct Ab Initio Dynamics Calculations of the Reaction Rates for the Hydrogen Abstraction OH + HBr → H_2O + Br. *J. Phys. Chem. A* **2001**, *105*, 7707–7712.

(7) Ree, J.; Kim, Y. H.; Shin, H. K. Dependence of the Four-Atom Reaction HBr + OH → Br + H_2O on Temperatures between 20 and 2000 K. *J. Phys. Chem. A* **2015**.

(8) Aquilanti, V.; Mundim, K. C.; Elango, M.; Kleijn, S.; Kasai, T. Temperature Dependence of Chemical and Biophysical Rate Processes: Phenomenological Approach to Deviations from Arrhenius Law. *Chem. Phys. Lett.* **2010**, *498*, 209–213.

(9) Aquilanti, V.; Mundim, K. C.; Cavalli, S.; De Fazio, D.; Aguilar, A.; Lucas, J. M. Exact Activation Energies and Phenomenological Description of Quantum Tunneling for Model Potential Energy Surfaces. The F+H2 Reaction at Low Temperature. *Chem. Phys.* **2012**, *398*, 186–191.

(10) Silva, V. H. C.; Aquilanti, V.; de Oliveira, H. C. B.; Mundim, K. C. Uniform Description of Non-Arrhenius Temperature Dependence of Reaction Rates, and a Heuristic Criterion

for Quantum Tunneling vs Classical Non-Extensive Distribution. *Chem. Phys. Lett.* **2013**, *590*, 201–207.

(11) Cavalli, S.; Aquilanti, V.; Mundim, K. C.; De Fazio, D. Theoretical Reaction Kinetics astride the Transition between Moderate and Deep Tunneling Regimes: The F + HD Case. *J. Phys. Chem. A* **2014**, *118*, 6632–6641.

(12) Tsallis, C. *Introduction to Nonextensive Statistical Mechanics: Approaching a Complex World*; Springer: New York, 2009.

(13) Laidler, K. J. A Glossary of Terms Used in Chemical Kinetics, Including Reaction Dynamics. *Pure Appl. Chem.* **1996**, *68*, 149–192.

(14) Perdew, J. P.; Burke, K.; Ernzerhof, M. Generalized Gradient Approximation Made Simple. *Phys. Rev. Lett.* **1996**, *77*, 3865–3868.

(15) Troullier, N.; Martins, J. L. Efficient Pseudopotentials for Plane-Wave Calculations. *Phys. Rev. B* **1991**, *43*, 1993–2006.

(16) Martyna, G. J.; Klein, M. L.; Tuckerman, M. Nosé–Hoover Chains: The Canonical Ensemble via Continuous Dynamics. *J. Chem. Phys.* **1992**, *97*, 2635.

(17) Tuckerman, M. E. On the Quantum Nature of the Shared Proton in Hydrogen Bonds. *Science (80-.).* **1997**, *275*, 817–820.

(18) Durlak, P.; Latajka, Z. Car-Parrinello and Path Integral Molecular Dynamics Study of the Intramolecular Hydrogen Bonds in the Crystals of Benzoylacetone and Dideuterobenzoylacetone. *Phys. Chem. Chem. Phys.* **2014**, *16*, 23026–23037.

(19) Sun, L.; Song, K.; Hase, W. L. A S_N2 Reaction That Avoids Its Deep Potential Energy Minimum. *Science* **2002**, *296*, 875–878.

(20) López, J. G.; Vayner, G.; Lourderaj, U.; Addepalli, S. V; Kato, S.; deJong, W. A.; Windus, T. L.; Hase, W. L. A Direct Dynamics Trajectory Study of F^- + CH(3)OOH Reactive Collisions Reveals a Major Non-IRC Reaction Path. *J. Am. Chem. Soc.* **2007**, *129*, 9976–9985.

PAPER 2:

COUTINHO, N. D., AQUILANTI, V., SILVA, V. H., CAMARGO, A. J., MUNDIM, K. C., & DE OLIVEIRA, H. C. (2016). **Stereodirectional origin of *anti*-arrhenius kinetics for a tetraatomic hydrogen exchange reaction: Born–Oppenheimer molecular dynamics for OH+ HBr**. *The Journal of Physical Chemistry A*,2016, *120*(27), pp. 5408-5417.

The $OH + HBr \longrightarrow H_2O + Br$ is one the most four-atom process studied experimentally. This reaction are of interest of regardin mechanisms for the depletion of ozone form atmosphere, additionally its kinetics has minifested na unusual anti-Arrhenius behavior. Motivation of the study reported in this paper is the investigation of the stereodirectional dynamics of this reaction as the prominent reason for the peculiar kinetics: we started in a previous Letter (J. Phys. Chem. Lett. 2015, 6, 1553-1558) a first-principles Born-Oppenheimer molecular dynamics approach, where the forces acting on the particles are obtained from electronic structure calculations executed in real time. Here, refinements of the method permitted a major increase of the number of trajectories and the consideration of four temperatures 50, 200, 350, and 500 K, for which the sampling of initial conditions allowed us to characterize the stereodynamical effect. The role is documented of the adjustment of the reactants' mutual orientation to encounter the entrance into the "cone of acceptance" for reactivity. The aperture angle of this cone is dictated by a range of directions of approach compatible with the formation of the specific HOH angle of the product water molecule; and consistently the adjustment is progressively less effective the higher the kinetic energy. The extraction of thermal rate constants from this molecular dynamics approach is discussed and the systematic sampling of the canonical ensemble is indicated as needed for quantitative comparison with the kinetic experiments.

My contribution in this study was to perform Born-Oppenheimer molecular dynamics simulations and perform all relevant analyzes, as well as contribute to the discussions and in the paper writing. Acknowledgment to the other authors who contributed to the development of this investigation. To professor Ademir Carmargo for the help in the development of the methodology, to professor Kleber Mundim for the discussions about the non-Arrhenius behavior and by developed to computational code to generate 3D surface used for representation free energy surface, Valter H. Carvalho Silva, Heibbe Cristhian B. de Oliveira and Vincenzo Aquilanti for the results discussions and the paper revision

In addition, a special acknowledgment to the American Chemical Society for the reprinted the paper in my theses. Reprinted with permission from (J. Phys. Chem. A, 2016, 120 (27), pp 5408–5417 DOI: 10.1021/acs.jpca.6b03958).

Title: Stereodirectional Origin of anti-Arrhenius Kinetics for a Tetraatomic Hydrogen Exchange Reaction: Born–Oppenheimer Molecular Dynamics for OH + HBr

Author: Nayara D. Coutinho, Vincenzo Aquilanti, Valter H. C. Silva, et al

Publication: The Journal of Physical Chemistry A

Publisher: American Chemical Society

Date: Jul 1, 2016

PERMISSION/LICENSE IS GRANTED FOR YOUR ORDER AT NO CHARGE

This type of permission/license, instead of the standard Terms & Conditions, is sent to you because no fee is being charged for your order. Please note the following:

- Permission is granted for your request in both print and electronic formats, and translations.
- If figures and/or tables were requested, they may be adapted or used in part.
- Please print this page for your records and send a copy of it to your publisher/graduate school.
- Appropriate credit for the requested material should be given as follows: "Reprinted (adapted) with permission from (COMPLETE REFERENCE CITATION). Copyright (YEAR) American Chemical Society." Insert appropriate information in place of the capitalized words.
- One-time permission is granted only for the use specified in your request. No additional uses are granted (such as derivative works or other editions). For any other uses, please submit a new request.

BACK CLOSE WINDOW

THE JOURNAL OF PHYSICAL CHEMISTRY A

Article

pubs.acs.org/JPCA

Stereodirectional Origin of *anti*-Arrhenius Kinetics for a Tetraatomic Hydrogen Exchange Reaction: Born–Oppenheimer Molecular Dynamics for OH + HBr

Nayara D. Coutinho,[*,†] Vincenzo Aquilanti,[*,‡,§,∥] Valter H. C. Silva,[⊥] Ademir J. Camargo,[⊥] Kleber C. Mundim,[†] and Heibbe C. B. de Oliveira[*,†]

[†]Instituto de Química, Universidade de Brasília, 4478, 70904-970 Brasília, Brazil

[‡]Dipartimento di Chimica, Biologia e Biotecnologie, Università di Perugia, Via Elce di Sotto 8, 06123, Perugia, Italy

[§]Instituto de Física, Universidade Federal da Bahia, 40210 Salvador, Brazil

[∥]Istituto di Struttura della Materia, Consiglio Nazionale delle Ricerche, 00016 Rome, Italy

[⊥]Grupo de Química Teórica e Estrutural de Anápolis, Ciências Exatas e Tecnológicas, Universidade Estadual de Goiás, 0459, 75001-970 Anápolis, GO Brazil

ABSTRACT: Among four-atom processes, the reaction OH + HBr → H_2O + Br is one of the most studied experimentally: its kinetics has manifested an unusual *anti*-Arrhenius behavior, namely, a marked decrease of the rate constant as the temperature increases, which has intrigued theoreticians for a long time. Recently, salient features of the potential energy surface have been characterized and most kinetic aspects can be considered as satisfactorily reproduced by classical trajectory simulations. Motivation of the work reported in this paper is the investigation of the stereodirectional dynamics of this reaction as the prominent reason for the peculiar kinetics: we started in a previous Letter (*J. Phys. Chem. Lett.* **2015**, *6*, 1553−1558) a first-principles Born−Oppenheimer "canonical" molecular dynamics approach. Trajectories are step-by-step generated on a potential energy surface quantum mechanically calculated on-the-fly and are thermostatically equilibrated to correspond to a specific temperature. Here, refinements of the method permitted a major increase of the number of trajectories and the consideration of four temperatures −50, +200, +350, and +500 K, for which the sampling of initial conditions allowed us to characterize the stereodynamical effect. The role is documented of the adjustment of the reactants' mutual orientation to encounter the entrance into the "cone of acceptance" for reactivity. The aperture angle of this cone is dictated by a range of directions of approach compatible with the formation of the specific HOH angle of the product water molecule; and consistently the adjustment is progressively less effective the higher the kinetic energy. Qualitatively, this emerging picture corroborates experiments on this reaction, involving collisions of aligned and oriented molecular beams, and covering a range of energies higher than the thermal ones. The extraction of thermal rate constants from this molecular dynamics approach is discussed and the systematic sampling of the canonical ensemble is indicated as needed for quantitative comparison with the kinetic experiments.

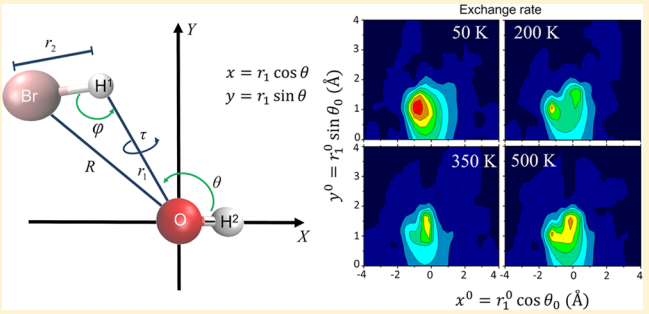

1. INTRODUCTION

1.1. Motivation. The reaction OH + HBr → H_2O + Br plays a special part in reaction kinetics. It belongs to a series of hydrogen transfer processes between the hydroxyl radical and the halogen hydrides, producing water and liberating halogen atoms: these processes are therefore of interest regarding mechanisms for the depletion of ozone from the atmosphere.[1,2] The reaction is also of basic relevance for both experimental and theoretical chemical kinetics: its rate constant in the thermal range decreases as a function of temperature.[3−9] This intriguing feature is in marked contradiction with respect to the generic rule dictating that it should increase, and typically exponentially, according to the established canon of the phenomenological Arrhenius equation.

Therefore, this reaction is considered as a benchmark elementary process that exhibits an *anti*-Arrhenius behavior, possessing a negative apparent activation energy. It is additionally sufficiently simple for being tackled from state-of-the-art quantum electronic structure calculations: extensive classical trajectory simulations[10,11] on a recent accurate global

Special Issue: Piergiorgio Casavecchia and Antonio Lagana Festschrift

Received: April 19, 2016
Revised: May 20, 2016

DOI: 10.1021/acs.jpca.6b03958
J. Phys. Chem. A XXXX, XXX, XXX−XXX

potential energy surface accounted satisfactorily for the peculiar kinetic aspects.

From the point of view of the understanding of the detailed microscopic dynamics of this behavior, an alternative source of important information came from molecular beam scattering experiments with oriented reactants.[12,13] These experiments (see also a review[14]) indicated the key role of the steric effect and provided the motivation for the stereodynamical interpretation of the phenomenon started in the previous Letter.[15] The present paper reports additional extensive numerical experiments to establish a full characterization of this effect. An account follows of improvements permitting us to obtain the salient results, and for their presentation we will have to make frequent references to the previous Letter[15] whenever specific details are needed.

The molecular beam studies with oriented reactants that are available for this reaction were carried out at energies higher than thermal.[12] They have shown that during the process a relevant molecular reorientation occurs and that the effect becomes less pronounced as the collision energy increases, arguably because the reactants have less time to rotate toward the reactive direction of the approach: a consequence is the observation that the reaction cross section decreases as the collision energy increases at a faster than expected rate. These results are consistent with the now accepted view that the reaction proceeds through a negligible barrier.[16,17] This observed negative effect of collision energy could not be explained from previously discussed[15] theoretical approaches, either by the average, long-range mediated dipole−dipole attractive interaction between the reactants or from a specific mediating role of a van-der-Waals intermediate.

Attention toward this reaction interestingly continues: a couple of additional theoretical papers appeared after the preceding Letter was written,[15] one proposing a high-level quantum mechanically generated potential energy surface,[18] another one giving also massive trajectory simulations.[19] None of them considers the stereodynamical aspects previously demonstrated as relevant[12−15] and further elaborated in this paper.

1.2. Plan of the Paper. Motivated by the results from oriented molecular-beam experiments, continuing the presentation of our investigation initiated in the previous Letter,[15] we report in this paper further results on the first-principles stereodynamical approach, which is here extended to provide a wider phenomenology. The strategy that we follow is to use the Born−Oppenheimer molecular dynamics BOMD[20−22] technology to carry out numerical experiments that simulate the reaction in a box, which we consider as our first-principles "nanoreactor" in the spirit, e.g., of ref 23: the reactant molecules introduced in the box explore the potential energy surface at a specified temperature, enforced by a Nosé−Hoover thermalizing bath and therefore representing a "canonical" ensemble.[24] Thermalized sets of these canonical trajectories evolving on a multidimensional potential energy surface quantum mechanically generated on-the-fly, were shown in ref 15 to provide time dependence of free energy landscapes, mapping most visited regions at two temperatures, 50 and 500 K. In this work, we performed our numerical experiments at four temperatures. Illustrations of rearrangements of bonds along trajectories and of the role of specific angles of reactants' mutual approach elucidate the mechanistic change from the low kinetic energy regime (where incident reactants reorient to find the propitious alignment leading to reaction) to high temperature (where speed hinders adjustment of directionality and "roaming" delays reactivity).

Section 2 is devoted to the description of the theoretical methods and of the numerical procedures. Running the trajectories, which are step-to-step thermalized on time-consuming on-the-fly computations of the potential energy surface, is such a demanding procedure that previously[15] it was possible to scrutinize only a few trajectories at different selected initial configurations and to examine comparatively their behavior at two extreme temperatures. A global look emerged on selective sensitivity to the features of the free energy surface when experienced by the reactants at slow or fast relative speed. With respect to, e.g., the visualization as a movie in the Supporting Information to ref 15 showing the synchronized progress of two trajectories with the same initial configurations at the two extreme temperatures, we contribute here to the illustration of these concepts by a much extended investigation involving a systematic sampling made possible by improvements in the computational efficiency, providing a much deeper insight for the understanding of the process.

In section 3, results are presented that document the dependence of the reactivity from the initial orientation. By focusing on the time evolution of trajectories, we illustrate the progress of the reaction as the progressive breaking of the old bond and the concerted formation of the new one. We show how during trajectories molecular reorientation occurs to encounter a mutual approach of reactants favorable for them to proceed to reaction. Besides the demonstration of the crucial role of stereodynamics, additional documentation is also provided on the interesting manifestation of the roaming phenomenon, whereby both the search of the reactive configurations sterically favorable to reaction and the subsequent departure involving vibrational excitation were seen to occur on wandering paths on the potential energy surface not limited to those corresponding to the one of minimum energy.

In the previous Letter,[15] we preliminarily gave some background information on the history of studies of this reaction, in particular viewing at numerous literature data on rate constants and their dependence on temperature, and provided a discussion of the activation energy and *anti*-Arrhenius behavior extending our recent proposal, so far amply tested for the phenomenological description of the *sub*-Arrhenius and *super*-Arrhenius cases.[25−28] A closer scrutiny is possible thanks to the results of this paper, where a perspective avenue leading to the extraction of quantitative information on reaction rate constants from approaches based on molecular dynamics simulations is examined in a remark in section 4, which concludes the paper.

2. THEORETICAL APPROACH AND NUMERICAL PROCEDURES

2.1. Molecular Dynamics Simulations. The aim of disentangling the basic question concerning the peculiar kinetics of this reaction is approached by molecular dynamics simulations. As noted above (see also ref 15), the technique of choice, the Born−Oppenheimer molecular dynamics BOMD,[20−22] is suited to follow the evolution of the reaction and therefore to provide a full explanation of its apparently anomalous features. As a result of the various preceding theoretical and computational investigations, a definite role was attributed to the transient aggregate due to van-der-Waals-like interactions, lying at a lower energy than that of the reactants.

DOI: 10.1021/acs.jpca.6b03958
J. Phys. Chem. A XXXX, XXX, XXX−XXX

This feature is so prominent that it gives this process an unusual reaction path profile[10,11] corresponding to essentially a negative activation barrier. The dynamical relevance of this feature is adequately scrutinized under the microscope of the present canonical trajectory simulations and very relevant appeared to us the additional specific goal to provide a link with the overlooked experimental stereodynamical studies.[12−14]

A previous pioneering investigation[29] of a reactive process where the reactant was the hydroxyl radical, exploited Car−Parrinello dynamics, where motion of the nuclei in the on-the-fly calculated trajectories occurs in the potential generated by the electrons according to classical mechanics. A distinctive feature of the present first-principles Born−Oppenheimer molecular dynamics study is that wave functions are converged at every step, making trajectory calculations much more expensive but arguably more accurate.

Electronic structure calculations are essential in molecular dynamics simulations and the reliability of intermolecular forces depends on the quality of the employed quantum chemistry methods and of the computational effort involved. Because a chemical process involves the adjustment of the electronic structure according to the evolution of the nuclear positions, reaction mechanisms emerge with no need of computationally prohibitive explorations to find reaction pathways. On the contrary, the exploit of the automatic focusing of trajectories on regions actually sampled during the reaction[15] provides information on parts of the multidimensional potential energy surface that demand more accuracy for improving the realistic simulations of the dynamics. Randomly generated initial conditions and procedures for equilibration with respect to a thermal bath (see the following subsection), permit us to efficiently bypass the often severe bottlenecks of computational dynamics, such as both the impact parameter integration to provide total cross sections and their Boltzmann kinetic energy averaging, allowing the direct specification of the temperature: our previous choice[15] was limited to considering two conditions, at the two extremes of the experimentally relevant range, at low 50 K and high 500 K temperatures, and the improvements to be described next allow us to explore a total of four temperatures by a much higher number of trajectories.

2.2. Computational Methods. The main differences—and advantages for present purposes—in comparison with the classical trajectory approach applied previously to this system[10,11] are (i) to avoid potential energy surface fitting, especially when the aim, as in this case, is to examine stereodynamic and roaming features, for which exploration of regions far away from, e.g., the minimum energy profile is crucial and it is insightful allowing the system to originate or visit there, and (ii) to use a "thermostat" to run canonical trajectories corresponding to a given temperature, with no need of fine velocity sampling and Maxwell−Boltzmann averaging.

As in the previous Letter,[15] the results from the BOMD simulations reported in this paper were obtained by utilizing the Car−Parrinello molecular dynamics CPMD 3.17.1 suite of programs, Copyright IBM, 2012. The electronic structure was treated within density functional theory DFT, through the Perdew−Burke−Ernzerhof (PBE)[30] functional. However, the main improvement exploited in this article involves the use of an alternative pseudopotential with respect to the one previously used by Troullier and Martins (MT),[31] which is not norm-conserving. The plane-wave cutoff was previously as large as 70 Ry. To generate a considerably number of trajectories, in the present work our choice was to use the norm-conserving Vanderbilt (VDB) pseudopotential,[32] permitting the reduction of the cutoff at 25 Ry. This was implemented after careful verification that for the same initial configurations for which both pseudopotentials, MT and VDB, were used, the evolutions of the trajectories were remarkably similar. Thus, on account of its lower computational cost, the VDB pseudopotential was chosen for the systematic runs. Having chosen this pseudopotential, we did some tests with other functionals different from PBE to obtain reproducibility with the trajectories calculated in ref 15 at a lower computational cost. The exploration gave no reason not to continue with the same PBE functional that we have used previously.

With the same purpose of obtaining lower computational cost, we increase the step size to 0.1 fs. Also, we ran a total of 2 ps for each trajectory, accounting for a total of 20 000 steps reducing the calculation time by a half. The other parameters of the dynamics, specifically the size of the box and the characteristics of the thermostat, have remained the same as before.[15]

The temperatures of the system were controlled by the Nosé−Hoover thermostat scheme[24] at 50, 200, 350, and 500 K. One HBr molecule and one OH radical were placed inside a cubic cell having a 6 Å side, and periodic boundary conditions were imposed for each trajectory reaching the walls of the cell.

The intermolecular orientation of the two molecules in the initial configurations was not optimized; that is, the starting geometries do not represent local minima of the global potential surface. For those cases in which the reaction did not take place at any of the investigated temperatures, the corresponding trajectories are of potential interest for the study of inelastic and rovibrational energy transfer processes in nonreactive events: they have been stored in view of further analysis of these effects, outside the scope of the present paper.

To follow the evolution of the orbitals along a typical reactive trajectory, we give in section 3.4 an example corresponding to one for which the orientational character is more pronounced. The selected frames account for the region that is most indicative of the reactive process. The molecular orbitals were obtained at the UMP2/6-311G(d) level using the computational G09 package,[33] offering a more robust method than that provided in the first-principles molecular dynamics calculations.

3. RESULTS AND DISCUSSION

3.1. Representation of Stereodirectional Dynamics. Figure 1 illustrates the coordinate choice for this discussion of the reaction. To extract information on the reactivity of the O-end, H-end, and sideways collisions, the Osaka group used an orienting hexapole electrostatic field. Their results[12] showed the relative importance of two reactive sites: it was found that the O-end attack is most favored for this reaction than that for H-end attack and introduced the concept of a "cone of acceptance" for which θ in Figure 1 defines the aperture angle.

In a four-body system, the configuration is fixed by six coordinates, two of them are those utilized here for exhibiting the stereodirectional effect on the molecular dynamics: they are the bond length r_1 and the angle θ. Their values are fixed when the simulations begin and serve to identify the trajectories in the following presentation. Table 1 lists the 80 initial configurations, considered in this work and belonging to the *NVT* ensemble.[24] The initial settings have been selected according to the following criteria: r_1^0 ranging from 1.7 to 3.8 Å with steps of 0.3 Å and θ_0 ranging from 0 to 180° with a 20° increment. All other coordinates were obtained randomly,

DOI: 10.1021/acs.jpca.6b03958
J. Phys. Chem. A XXXX, XXX, XXX−XXX

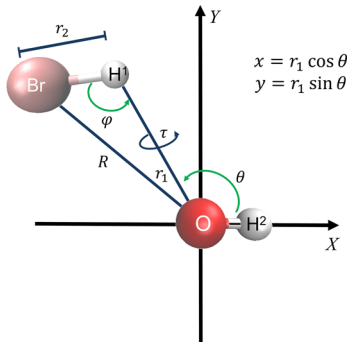

Figure 1. Definitions of geometrical parameters for the configuration of the present four-atom process suited to extract stereodynamical information on the role of the mutual direction between approaching reactants. The origin is on the oxygen atom, and the OH bond, of length r_2, lies in the X axis, whereas Y is the axis perpendicular to X in the $BrOH^2$ plane oriented as in the figure. The initial configurations are identified (Table 1) by a zero affix, namely, by the vector length r_1^0 and the angle θ_0 or by the vectors components x_0 and y_0 on the X and Y axes.

within limits that guaranteed realistic initial configurations of the system. In Table 1 and in the following ones, they are displayed as labels to a matrix with 80 entries, r_1^0 for the eight columns and θ_0 for the ten rows, respectively. In the initial configurations, two other variables are held fixed for all cases, the HBr bond length at 1.47 Å and the OH^2 bond length at 1.0 Å. Two other needed coordinates are chosen randomly among the three φ (deg), τ (deg), and R (Å), one of them being superfluous but used for an internal check. They are listed as entries in Table 1.

An overview of results was illustrated in Figure 2 of previous paper[15] for some reactive trajectories within the reactive box, defined as "canonical"[24] having been associated with specific temperatures. Reconstructed free energy surfaces as sampled by several trajectories were shown at low (50 K) and high (500 K) temperatures.

At low temperature, trajectories experience the free energy landscape probing the small basin due to the reactants' intermolecular attraction according to the now established minimum energy path profile for this exothermic reaction.[10,11,15] The profile features van-der-Waals-like complexes in the reactant and product channels, and a transition-state-like barrier energetically lower than the entrance state.

As the temperature increases, reactive trajectories are found to typically wander around before encountering their relatively narrow road toward product formation and are relatively insensitive to the details of the reaction profile.

The coordinate s appropriate to simply describe the evolution of the reactive event is the difference between lengths being broken and formed bonds, respectively ($s = r_2 - r_1$). The *exchange rate* for the reaction is conveniently defined as the inverse of the "switching" time, i.e., when $r_1 = r_2$ or $s = 0$. The correlation between the initial geometry of the propensity to reaction is illustrated in Figure 2 and in Tables 2–5. In the

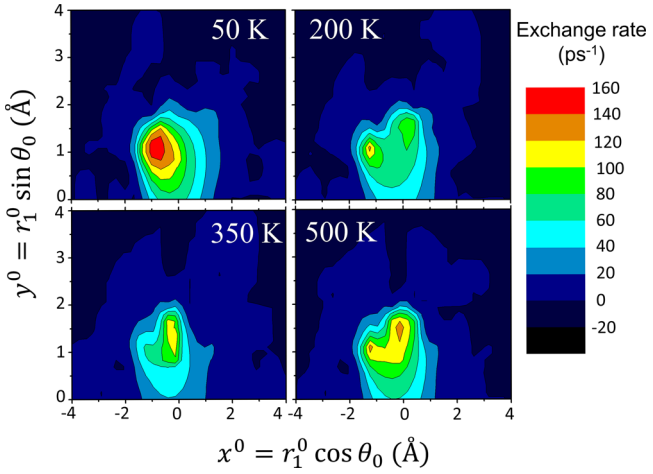

Figure 2. Contour plots of reactivity data, the latter estimated on the assumption that the velocity of reaction can be correlated to the so-called "switching time", namely, to the moment when $r_1 = r_2$. Its inverse (see text), is defined as "exchange rates" and can be extracted from the entries of Tables 2–5.

tables the exchange rate is given as a function of r_1^0 and θ_0 and in Figure 2 in the plane of the Cartesian components of the r_1 vector, $x_0 = r_1^0 \cos\theta_0$ and $y_0 = r_1^0 \sin\theta_0$. For a temperature, e.g., of 50 K the reactivity is seen as largest for both x_0 and y_0 in the 0–2 Å range, manifesting stereodynamical propensity for θ_0 angles in the 90–180° range. For values of x_0 larger than 1.7 Å the reactivity is very low. As the system temperature increases, the dependence of reactivity on the stereodirectionality is lower and other initial conditions can lead to the final product, as can be seen in the corresponding panels at 200, 350, and 500 K and

Table 1. Initial Values of the Coordinates for All Trajectories, Arranged as a Function of the Stereodynamical Angle, θ_0, and the Distance r_1 of Figure 1[a]

	r_1^0 (Å)							
θ_0 (deg)	1.7	2.0	2.3	2.6	2.9	3.2	3.5	3.8
0	60, 142, **1.60**	158, 129, **3.4**	115, 127, **3.21**	60, 132, **2.26**	117, 124,**3.80**	173, 123, **4.66**	60, 124, **3.04**	157, 115, **5.19**
20	144, −20, **3.02**	127, 66, **3.12**	78, −28, **2.46**	60, 132, **2.26**	107, 0, **3.62**	169, 82, **4.65**	144, −20, **4.77**	127, 66,**4.84**
40	129, 169, **2.86**	102, −100, **2.71**	138, −14, **3.53**	111, 39, **3.42**	60, −79, **2.51**	132, −168, **4.33**	129, 169, **4.57**	102, −100,**4.34**
60	92, 97, **2.29**	117, 52, **2.97**	134, 21,**3.49**	151, −90, **3.95**	163, 128, **4.33**	158, −60, **4.59**	177, −148,**4.97**	117, 52, **4.65**
80	177, −148, **3.17**	167, 114, **3.45**	179, 47,**3.77**	168, 120, **4.05**	60, 113, **2.51**	60, 28, **2.77**	177, −148, **4.97**	167, 114,**5.24**
100	175, −151, **3.17**	126,-5, **3.11**	145, 157, **3.60**	60, −146, **2.26**	60, −168, **2.51**	128, −158, **4.26**	175, −151,**4.97**	126, −5, **4.82**
120	145, −107,**3.02**	162, 20,**3.43**	60, −26,**2.02**	60, 95,**2.26**	60, −111, **2.51**	60, −21, **2.77**	145, −107, **4.78**	162, 20, **5.22**
140	145, −147, **3.03**	121, 97, **3.03**	117, −130, **3.25**	95, 20,**3.10**	120, 61, **3.86**	122, 163, **4.18**	145, −147, **4.78**	121, 97, **4.72**
160	173, −125, **3.16**	179, 172, **3.47**	141, 170, **3.56**	169, 130, **4.05**	60, 97, **2.51**	113, −109, **4.01**	173, −125,**4.96**	179, 172,**5.27**
180	60, −76, **1.60**	65, −82, **1.92**	124, 89, **3.35**	78, −93, **2.71**	138, −110, **4.12**	160, 171, **4.61**	60, −99,**3.04**	65, −100,**3.45**

[a]The initial values for φ (degrees), τ (degrees), and R (Å), are the entries of the table in this order.

DOI: 10.1021/acs.jpca.6b03958
J. Phys. Chem. A XXXX, XXX, XXX−XXX

Table 2. Exchange Rates (ps^{-1}, See Text) for Reactive Trajectories for 50 K[a]

θ_0 (deg)	r_1^0 (Å) 1.7	2	2.3	2.6	2.9	3.2	3.5	3.8
0	0	0	0	0	0	0	0	0
20	13.25	10.02	0	0	0	0	0	0
40	22.62	12.42	9.09	3.35	0	0	0	0
60	31.75	30.77	10.87	5.08	0	0	0	0
80	36.10	0	0	0	0	0	0	0
100	46.30	29.50	7.59	0	0	0	0	0
120	120.48	12.64	0	0	0	1.86	0	0
140	138.89	42.92	19.88	0	5.29	0	0	0
160	23.53	0	0	0	0	0	0	0
180	0	0	13.74	0	0	0	3.90	0

[a]Zero entries corresponding to non-reactive trajectories.

in Tables 3−5. A new maximum peak appears in the 0−1 Å range for x_0 and 1−2 Å range for y_0, corresponding to angles between 40° and 80°. For high temperatures the reactivity of the system is less sensitive to the system initial conditions, and the memory of the initial configuration appears to be lost during the reactive process, arguably because of the manifestation of the roaming effect, to be discussed next.

3.2. Delayed Reactivity and Vibrational Roaming of Product Water. The information from Tables 2−5 focused on "switching" times along trajectories, identified as the moment when $r_1 = r_2$: they convey the approximate view of the event, as involving the sudden breaking of the reactant HBr molecule and the synchronous formation of the H_2O product. A more articulate view emerges when, as in Figure 3, we choose to represent the evolution in time of the reaction as the detailed breaking of the old bond r_1 and the formation of the new one r_2 (see also the video in Supporting Information in ref 15). The main visual impression from a scrutiny of the ample phenomenology of Figure 3 is the evident delayed reactivity for trajectories which often appear to wander in search of proper paths. In general, the effect appears to disfavor the high-temperature situations, where additionally more pronounced is the emergence of "roaming" in vibrational modes in search of propitious outcomes. Also crucially affecting the delay is the initial stretching of r_1.

A discussion of the "roaming" phenomenon is now in order. It has been amply documented as occurring in photodissociation experiments as the emergency of routes to molecular fragmentation channels[34,35] that circumvent transition-state reaction paths. The presence of these alternative pathways can be inferred by the properties of the translational and internal distribution of the product fragments. Because they involve regions far from the neighborhoods of saddle points along minimum energy paths and lead to avenues to reaction beyond the venerable transition state approach,[14,36] they are challenging to theories of chemical kinetics and demand explorations by on-the-flight dynamics, such as the one presented in this work.

Experimental fingerprints of roaming are slow, delayed photodissociation products, as inferred by late arrival of products in time-of-flight measurements. Detailed investigations[34] on the threshold for the opening of the breakdown in three fragments and molecular dynamics simulations pointed out the role of nonadiabatic transitions at a conical intersection between ground state and excited potential energy surfaces.[34]

The origin of roaming as a rearrangement between weakly bound reactants is connected to high-lying regions of the ground state potential energy surfaces[37,38] and indicated in refs 35, 39, and 40. Typically, they involve molecular configurations far from the transition state geometry and are propitiated by pronounced bond elongations, such as when emerging from nonadiabatic paths involving conical intersections. From Figure 3, we observe analogously that in our case "roaming" is favored by starting trajectories at elongated r_1^0.

3.3. Angle of Approach and Excitation of Bending in the Departing Water. In this section, the important role of the stereodynamical angle of approach θ_0 in influencing the reaction is discussed in detail with reference to Figure 4.

Figure 4 shows that when the dynamics is started with those values of θ_0 close to that leading to the formation of the bond angle of water ($\theta_w \sim 104°$), the system finds an easier way to products, and possible reorientation facilitating the process is hindered as the temperature increases. The specific value of the s coordinate, indicated as $s^{\ddagger}$, marks at each temperature the estimated averaged configuration in terms of new and old bond differences, characterizing the moment in the dynamics when the water molecule can be considered as effectively formed. These values are in general higher than the previously considered values of s corresponding to $r_1 = r_2$, which were used in the preceding estimates of the exchange rates. They decrease from about 1.7 Å at 50 K to 1.4 Å at 500 K. In the next section, these values will be correlated to reaction times for each temperature and will provide further information on the kinetic rate constants.

Table 3. Exchange Rates (ps^{-1}, See Text) for Reactive Trajectories for 200 K[a]

θ_0 (deg)	r_1^0 (Å) 1.7	2	2.3	2.6	2.9	3.2	3.5	3.8
0	5.95	0	1.10	0	0	0	0	0
20	0	0	0	0	0	0	0	0
40	27.03	0	12.35	2.23	0	4.24	0	0
60	22.22	26.32	13.70	7.09	0	0	0	3.34
80	116.28	1.13	0	0	0	0	0	0
100	71.43	19.23	5.03	0	0	0	0	0
120	24.39	0	6.10	0	0	1.15	0	0
140	142.86	47.6	21.28	4.55	10.99	0	0	0
160	25.64	0	0	0	0	0	0	0
180	0	0	19.05	0	0	0	8.00	0

[a]Zero entries corresponding to nonreactive trajectories.

DOI: 10.1021/acs.jpca.6b03958
J. Phys. Chem. A XXXX, XXX, XXX−XXX

Table 4. Exchange Rates (ps^{-1}, See Text) for Reactive Trajectories for 350 K[a]

	r_1^0(Å)							
θ_0 (deg)	1.7	2	2.3	2.6	2.9	3.2	3.5	3.8
0	7.52	0	0	0.75	0	0	1.11	0
20	0	1.07	6.33	0	0	0	0	0
40	26.32	2.27	0	0	5.26	0	0	0
60	0.79	9.17	8.13	9.09	0	0	0	3.04
80	16.67	0	0	0	0.79	0.64	0	0
100	142.86	22.22	9.17	0	0	0	0	0
120	37.04	21.74	8.62	0	6.14	4.65	0	0
140	66.67	45.45	17.24	0	9.17	0	0	0
160	25.00	0	0	0	4.35	0	0	0
180	7.30	1.00	19.61	0.59	0	0	6.67	3.25

[a]Zero entries corresponding to nonreactive trajectories.

Table 5. Exchange Rates (ps^{-1}, See Text) for Reactive Trajectories for 500 K[a]

	r_1^0 (Å)							
θ_0 (deg)	1.7	2	2.3	2.6	2.9	3.2	3.5	3.8
0	1.78	2.80	1.57	3.62	0	0	0	0
20	1.96	0	1.23	0	0	0	0	0
40	22.73	2.71	0	1.58	0	0	0	1.33
60	0.96	2.32	1.45	12.82	0	0	0	0
80	111.11	0	0	2.98	2.22	3.31	0	0
100	142.86	1.36	0	0.76	1.10	0	0	0
120	40.00	22.73	8.93	3.36	2.37	5.46	0	0
140	142.86	43.48	17.24	3.51	5.29	0	0	1.29
160	21.28	0	0	0	5.24	0	0	0
180	7.75	8.93	19.61	0.91	0	0	7.41	0

[a]Zero entries corresponding to nonreactive trajectories.

In Figure 4, the trajectories that are visualized are conveniently listed following the initial value of the stereodynamically relevant angle, θ_0, which represents the direction of the approach of the H atom to OH. Because the process evolves as the atom departs from HBr and is effectively terminated when it sticks to OH forming a bond angle typical of that of the bending angle for water, the propitious orientation is crucial. We note again the "roaming" effect in the search for a favorable approaching angle for reactivity and also note that such an effect is more evident at the higher temperature considered, 350 and 500 K. Additionally, it has to be noted how the final energy appears to dispose as excitation in the bending mode of the product water, as is visually clear to a much greater extent again for the higher temperatures (see ref 38 for experimental comparisons for an analogous study case). The ranges of values spanned by the θ angle around 104° as the water molecule departs can be taken as a visualization of the disposal of the energy disposal into the bending mode of the molecular product.

3.4. Molecular Orbital Evolution. The orientation dependence for Br formation in the reaction of oriented OH radical with HBr molecule can be understood with the spatial distribution of the highest occupied molecular orbital (HOMO) of the reactants as previously discussed in refs 12 and 13. To investigate the hydrogen rearrangement in the OH + HBr reaction, Figure 5 describes the time evolution of the HOMO orbital. Frames are shown for the trajectory corresponding to the initial configuration (120°, 3.2 Å), according to the nomenclature of Table 1. In the initial stage of the reaction, from 0 to 388 fs, the HOMO can be described as a π nonbonding between the OH and HBr molecules. However, it is possible to recognize that these orbitals are able to interact and to foster a hydrogen atom abstraction from the HBr molecule to the OH radical. From 388 to 504 fs, the HOMO orbital favors the oxygen attack by direct interaction with the hydrogen atom of the HBr molecule. A correlation between the HOMO localized at the oxygen atom and the acceptable angle in the reaction for direct abstraction of the hydrogen atom from the HBr molecule supports the role of the frontier orbital in the stereodirectional propensity character of the reaction,[12,13] in accordance with the early stage of the time evolution of the HOMO presented in Figure 5 and with the effect of initial trajectory configurations presented in Figure 4.

At 524 fs, a transition state-like configuration is assisted by a σ bonding orbital in the formation of a bond $H^1\cdots O$ due to the contributions of the π nonbonding orbital. In the hydrogen abstraction process, from 524 to 533 fs, the HOMO cooperatively evolves around the $Br\cdots H^1\cdots O$ moiety and separates with the formation of the H_2O molecule. In the final stage, at 582 fs, the products recover the π nonbonding character.

4. FINAL REMARKS

The molecular-dynamics work reported here has been devoted mostly to the stereodirectional aspects featuring as most relevant in the unusual kinetics of this reaction. In general, the extraction of quantitative information on rate constants from molecular dynamics simulations is an important issue but a very difficult one to be tackled.

On the contrary, quantum mechanical benchmark rate constants have been so far satisfactorily obtained only for

DOI: 10.1021/acs.jpca.6b03958
J. Phys. Chem. A XXXX, XXX, XXX−XXX

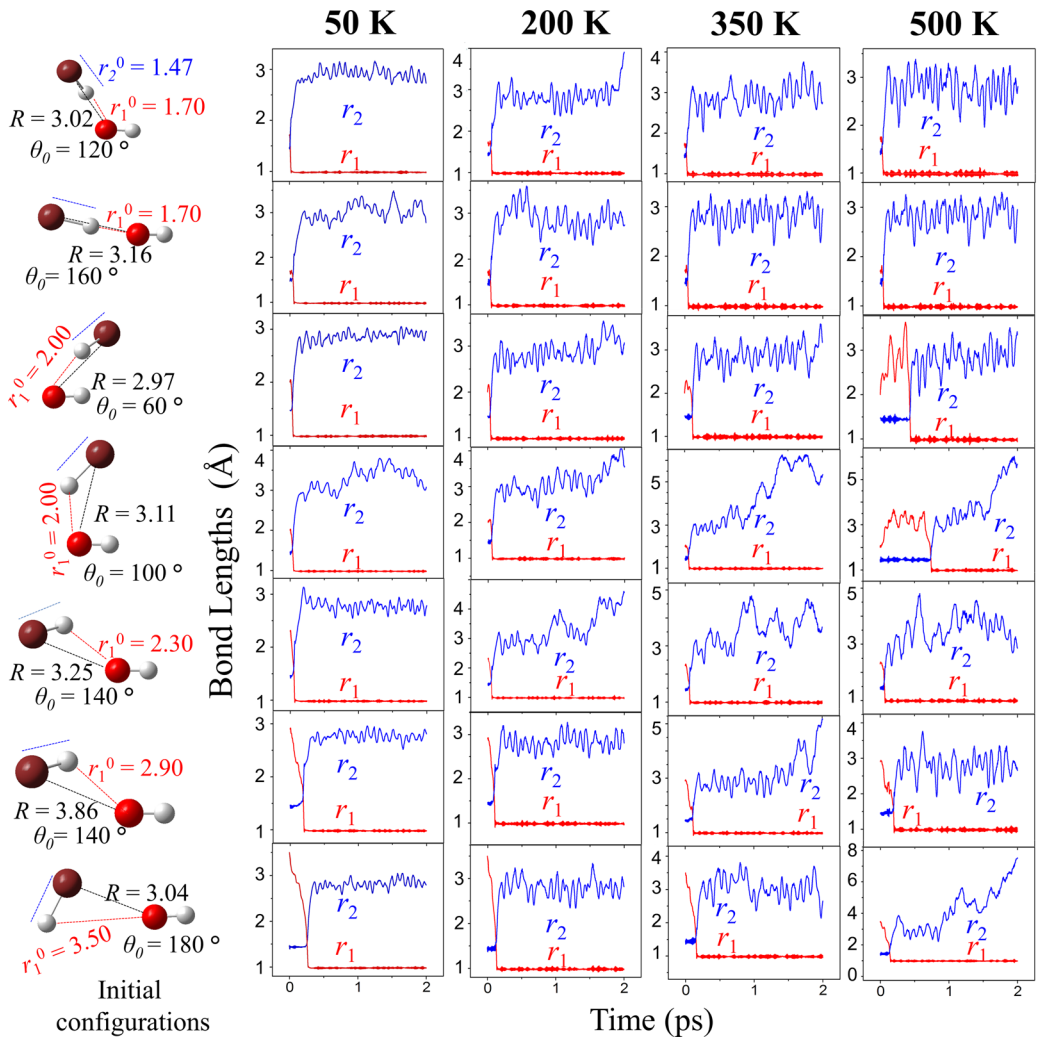

Figure 3. Exemplary "canonical" trajectories at four temperatures for seven initial configurations, chosen among those 16 trajectories that were found reactive with the same initial conditions for all four temperatures. Configurations are fixed by assigning six geometrical parameters according to the list given in Table 1; the relevant initial bond lengths and the stereodynamically relevant bond lengths reported as a function of time are the lengths of the bond that is broken r_1 and of the bond that is formed r_2: the former is in all case set at the 1.47 Å of the reactant HBr molecule; the latter is seen tending fast after hydrogen exchange to the asymptotic value ca. 1 Å, the length of the OH bond of water.

specific three-atom processes, involving great theoretical and computational efforts, and evolving along a series of steps the first of which is the construction or availability of an accurate potential energy surface. In *ab initio* "exact" quantum dynamics, many further other steps are needed to go all the way from the interaction to rate constants. One must proceed through state-to-state coupled-channel Schrödinger dynamics, giving scattering matrices (a major step), and then sum over all involved angular momenta, obtaining differential and integral cross sections on a large number of the reactants' kinetic energy values. The integral cross sections have to be obtained in a fine enough grid to finally generate temperature-dependent rate constants by computationally demanding averaging on the Maxwell–Boltzmann distribution of the reactants' velocities. As a paradigmatic case, only in the past few years this has been achieved for the triatomic system F + H_2 → HF + H, and the predictions[41] have been verified experimentally, in particular from thermal down to the very low-temperature reactivity range where tunneling is dominant.[42] For the related isotopic variant F + HD, see refs 28 and 42.

The present system involves only four atoms, yet its kinetics is unusual and attractive to theorists as archetypal of four-center reactions. As a quantum-mechanical time-independent four-body problem, (i) computation and fitting of multidimensional PES of high accuracy is demanding (six effective degrees of freedom), (ii) exact quantum close coupling state-to-state dynamics is prohibitively expensive, and (iii) even for model PES, benchmark cross sections are difficult to obtain and rate constants out-of-reach (time-dependent techniques typically need calibration against time-independent benchmarks). However, comparison of results for the present four-atom reaction with three-atom processes bearing features in common with this one is interesting: for the reaction OH + HBr, see remarks in ref 10; for the H + HBr reaction ref 43 reports experimental and computational evidence of reactive trajectories far from the minimum energy path, a signature for "roaming" in the same spirit as our discussion of Figure 3.

There is ample current activity investigating whether advances in molecular dynamics simulations can provide quantitatively reliable rate constants. Recent refs 44 and 45 indicate that only order-of-magnitude estimates can be

DOI: 10.1021/acs.jpca.6b03958
J. Phys. Chem. A XXXX, XXX, XXX−XXX

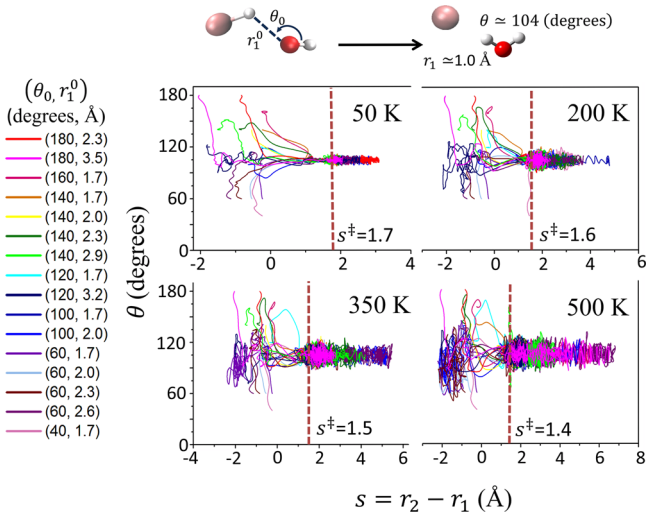

Figure 4. Evolution at four temperatures of the stereodynamical angle of approach θ Figure 1 for "canonical" trajectories versus the reaction coordinate $s = r_2 - r_1$, conveniently defined as the difference between the lengths of the bond that is broken r_1 and of the bond that is formed r_2. The total of 16 trajectories are those that are found to lead to reaction for all four temperatures considered in the simulations: the trajectories are distinguished by different colors as listed in the right panel and arranged in decreasing order of θ_0, the initial values for the θ angle; the other value characterizing the trajectory is that of r_1^0; the other parameters defining the initial configurations can be extracted by the corresponding entries in Table 1. Indicated by arrows is the value of $s^{\ddagger}$, identified by averaging for all trajectories of a given temperature the values of the reaction coordinate $s = r_2 - r_1$ for which a water molecule can be considered as formed.

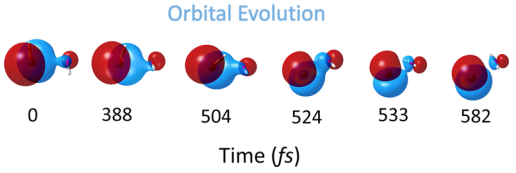

Figure 5. Time evolution of the HOMO-β orbital along the trajectory with initial values: r_1^0 = 3.2 Å, θ_0 = 120° (other coordinates specifying the initial configuration can be read as entries in Table 1) at T = 50 K calculated at the UMP2/6-311G* level. This is a trajectory for which the orientational adaptation of orbitals is particularly pronounced. The red and blue contours distinguish the spatial distributions wave functions with different signs. The OH reactant is represented on the right-hand-side of the structure of each frame and the H_2O formation is progressively visualized.

currently obtained. Typically, rates are overestimated and accuracy deteriorates enormously with temperature. Uncertainties are often associated with those in the accurate characterization of transition state features, crucial in applications of TST-type approaches to calculations of rates. Additionally, inherent difficulties of possible direct evaluations from molecular dynamics simulation originate from those regarding the statistical validity of samplings of the system phase space. The latter of course increases enormously with temperature as far as both energy and angular momentum are concerned.

A different approach to estimate rate constants was briefly suggested in the preceding Letter.[15] Here we describe some possible refinements proposed on the basis of a much more detailed information made available from this work and we discuss them with reference to Figure 6 and Table 6.

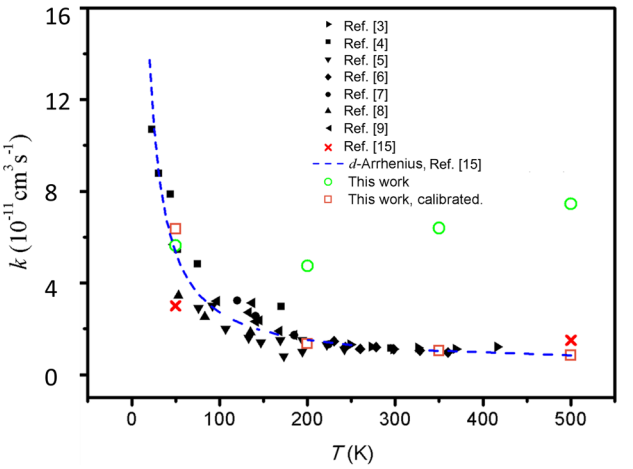

Figure 6. Reaction rate constants as a function of temperature. We also present the theoretical estimates from ref 15 (crosses) and this work (circles and squares, see text and Table 6). They are compared with temperature dependence for a selection of available experimental rate constant from refs 3−9 and the fit by the d-Arrhenius formula, where the addition of the parameter d accounts for deviations from linearity of the Arrhenius plot. (For details and parameter values see ref 15.)

Table 6. Transition Times (ps) and Rate Constants (10^{-11} cm^3 s^{-1}) at Different Temperatures (K)

T	$t^{\ddagger}$	k	k_{exp}	$k'_{calibrated} = k/0.018T$
50	1.15	5.63	5.52	6.35
200	1.54	4.74	1.52	1.34
350	1.52	6.39	1.03	1.03
500	1.48	7.45	0.84	0.84

In our numerical experiments, we place one molecule of OH and one molecule of HBr in a cubic box of 6 Å in size, amounting to a concentration $[C] \sim 5 \times 10^{21}$ molecules cm^{-3} for each reactant. Previously,[15] from the decay times of the order of 1 ps at 50 K and 2 ps at 500 K, we estimated bimolecular rates on order of 3×10^{-11} and 1.5×10^{-11} cm^3 s^{-1} respectively, in a range consistent with experimental values (see crosses in Figure 6, displaying also experimental comparison). Previously,[15] we found it insightful to give a view of the general trend introducing a fit of a relevant selection of the kinetic data extending to this *anti*-Arrhenius case the d-Arrhenius formula employed successfully to cases where curvatures in Arrhenius plots were found:[25−28] in Figure 6 data and fit are plotted, together with the so extracted rate constants at the values of the temperatures needed for comparison with those of this work, denoted k_{exp} and given in Table 6. The availability of considerable more information from the present results and especially the visualization from Figure 4 and its discussion of the delayed reactivity leading to emergency from of a water molecule, permit us to explore an alternative approach based on the rate of formation of water rather than on the rate of disappearance of reactants. Specifically, for an evaluation of the reaction rate constant we now start from the observation that, being the bimolecular process OH + HBr of the second order, the general formula for the rate constant can be written

$$k = \frac{d[H_2O]}{dt}([OH][HBr])^{-1}$$

DOI: 10.1021/acs.jpca.6b03958
J. Phys. Chem. A XXXX, XXX, XXX−XXX

as the ratio of the rate of formation of water and the product of the initial concentrations of the two reactants (this has been estimated above as $[C] \sim 5 \times 10^{21}$ molecules cm^{-3} for both [OH] and [HBr]). The formation of water is "observed" in our first-principles nanoreactor as the appearance of one product molecule in the volume of the box, i.e., [C] times the fraction f of reactive versus total trajectories and emerging at the "transition time", $t^{\ddagger}$:

$$\frac{d[H_2O]}{dt} = \frac{f[C]}{t^{\ddagger}}$$

In this illustrative estimate, the fractional number of reactive trajectories f can be extracted from Tables 2−5 and the resulting values of $t^{\ddagger}$ for each temperature can be obtained from Table 6. Because the transition time is meant to represent the average time that elapses for the chemical reaction to take place in the nanoreactor, for its present evaluation we searched for the moments along trajectories when the evolution coordinate s corresponded to the emergency of water as a product. Average values of s for each temperature are denoted $s^{\ddagger}$ and highlighted in the plots in Figure 4 providing the correlation between the angle θ and s.

As documented in other cases, such as the recent ones already considered above,[44,45] the rate constant k so obtained (Table 6) is larger than k_{exp}, and the more so the higher the temperature. As discussed above, one crucial reason is arguably the fact that our choice of initial conditions (reactants in a small box with close encounters) increases chances of reactive versus total collisions, especially at high temperature. This points out the general need of how to "calibrate" a first-principles nanoreactor, where the statistically satisfactory sampling of the phase space of the canonical ensemble can only be attempted at very low temperatures. A way, as in this case, is offered when experimental data are available. We note that the ratio k/k_{exp} scales as ca. $0.02T$, i.e., linearly with temperature. If the factor, 0.018, obtained by averaging over the four temperatures, is used to calibrate the present nanoreactor, a recalculation of rate constants gives the results as the entries of the last column in Table 6 and as the squares in Figure 6. The results are indicative of an at least semiquantitative route to the extraction of rate constants from first-principles molecular dynamics experiments.

AUTHOR INFORMATION

Corresponding Authors

*N. D. Coutinho. Phone: +55 61 3107-3899. Fax: +55 61 3273-4149. E-mail: nayaradcoutinho@gmail.com.
*V. Aquilanti. E-mail: vincenzoaquilanti@yahoo.it.
*H. C. B. de Oliveira. E-mail: heibbe@unb.br.

Notes

The authors declare no competing financial interest.

ACKNOWLEDGMENTS

The authors acknowledge grants from Brazilian CAPES, FAPEG, CNPQ, and FINATEC. V. Aquilanti thanks CAPES for the appointment as Professor Visitante Especial at Instituto de Fisica, Universidade Federal da Bahia, Salvador (Brazil), and the Italian Ministry for Education, University and Research, MIUR, for financial support: ⟨*SIR* 2014 (*RBSI*14*U* 3 VF)⟩.

REFERENCES

(1) Read, K. A.; Mahajan, A. S.; Carpenter, L. J.; Evans, M. J.; Faria, B. V. E.; Heard, D. E.; Hopkins, J. R.; Lee, J. D.; Möller, S. J.; Lewis, A. C.; et al. Extensive Halogen-Mediated Ozone Destruction over the Tropical Atlantic Ocean. *Nature* **2008**, *453*, 1232−1235.
(2) Saiz-Lopez, A.; von Glasow, R. Reactive Halogen Chemistry in the Troposphere. *Chem. Soc. Rev.* **2012**, *41*, 6448−6472.
(3) Ravishankara, A. R.; Wine, P. H.; Wells, J. R. The OH + HBr Reaction Revisited. *J. Chem. Phys.* **1985**, *83*, 447−448.
(4) Sims, I. R.; Smith, I. W. M.; Clary, D. C.; Bocherel, P.; Rowe, B. R. Ultra-Low Temperature Kinetics of Neutral-Neutral Reactions - New Experimental and Theoretical Results For OH + HBr Between 295 and 23 K. *J. Chem. Phys.* **1994**, *101*, 1748−1751.
(5) Atkinson, D. B.; Jaramillo, V. I.; Smith, M. A. Low-Temperature Kinetic Behavior of the Bimolecular Reaction OH + HBr (76−242 K). *J. Phys. Chem. A* **1997**, *101*, 3356−3359.
(6) Bedjanian, Y.; Riffault, V.; Le Bras, G.; Poulet, G. Kinetic Study of the Reactions of OH and OD with HBr and DBr. *J. Photochem. Photobiol., A* **1999**, *128*, 15−25.
(7) Jaramillo, V. I.; Smith, M. A. Temperature-Dependent Kinetic Isotope Effects in the Gas-Phase Reaction: OH + HBr. *J. Phys. Chem. A* **2001**, *105*, 5854−5859.
(8) Mullen, C.; Smith, M. A. Temperature Dependence and Kinetic Isotope Effects for the OH + HBr Reaction and H/D Isotopic Variants at Low Temperatures (53−135 K) Measured Using a Pulsed Supersonic Laval Nozzle Flow Reactor. *J. Phys. Chem. A* **2005**, *109*, 3893−3902.
(9) Jaramillo, V. I.; Gougeon, S.; Le Picard, S. D.; Canosa, A.; Smith, M. A.; Rowe, B. R. A Consensus View of the Temperature Dependence of the Gas Phase Reaction: OH + HBr → H_2O + Br. *Int. J. Chem. Kinet.* **2002**, *34*, 339−344.
(10) de Oliveira-Filho, A. G. S.; Ornellas, F. R.; Bowman, J. M. Quasiclassical Trajectory Calculations of the Rate Constant of the OH + HBr → Br + H_2O Reaction Using a Full-Dimensional Ab Initio Potential Energy Surface Over the Temperature Range 5 to 500 K. *J. Phys. Chem. Lett.* **2014**, *5*, 706−712.
(11) de Oliveira-Filho, A. G. S.; Ornellas, F. R.; Bowman, J. M. Energy Disposal and Thermal Rate Constants for the OH + HBr and OH + DBr Reactions: Quasiclassical Trajectory Calculations on an Accurate Potential Energy Surface. *J. Phys. Chem. A* **2014**, *118*, 12080−12088.
(12) Tsai, P.-Y.; Che, D.-C.; Nakamura, M.; Lin, K.-C.; Kasai, T. Orientation Dependence in the Four-Atom Reaction of OH + HBr Using the Single-State Oriented OH Radical Beam. *Phys. Chem. Chem. Phys.* **2010**, *12*, 2532−2534.
(13) Tsai, P.-Y.; Che, D.-C.; Nakamura, M.; Lin, K.-C.; Kasai, T. Orientation Dependence for Br Formation in the Reaction of Oriented OH Radical with HBr Molecule. *Phys. Chem. Chem. Phys.* **2011**, *13*, 1419−1423.
(14) Kasai, T.; Che, D.-C.; Okada, M.; Tsai, P.-Y.; Lin, K.-C.; Palazzetti, F.; Aquilanti, V. Directions of Chemical Change: Experimental Characterization of the Stereodynamics of Photodissociation and Reactive Processes. *Phys. Chem. Chem. Phys.* **2014**, *16*, 9776−9790.
(15) Coutinho, N. D.; Silva, V. H. C.; de Oliveira, H. C. B.; Camargo, A. J.; Mundim, K. C.; Aquilanti, V. Stereodynamical Origin of Anti-Arrhenius Kinetics: Negative Activation Energy and Roaming for a Four-Atom Reaction. *J. Phys. Chem. Lett.* **2015**, *6*, 1553−1558.
(16) Che, D.-C.; Matsuo, T.; Yano, Y.; Bonnet, L.; Kasai, T. Negative Collision Energy Dependence of Br Formation in the OH + HBr Reaction. *Phys. Chem. Chem. Phys.* **2008**, *10*, 1419−1423.
(17) Che, D.-C.; Doi, A.; Yamamoto, Y.; Okuno, Y.; Kasai, T. Collision Energy Dependence for the Br Formation in the Reaction of OD + HBr. *Phys. Scr.* **2009**, *80*, 048110.
(18) Zhang, M.; Hao, Y.; Guo, Y.; Xie, Y.; Schaefer, H. F. Anchoring the Potential Energy Surface for the Br + H_2O → HBr + OH Reaction. *Theor. Chem. Acc.* **2014**, *133*, 1513.

DOI: 10.1021/acs.jpca.6b03958
J. Phys. Chem. A XXXX, XXX, XXX−XXX

(19) Ree, J.; Kim, Y. H.; Shin, H. K. Dependence of the Four-Atom Reaction HBr + OH → Br + H_2O on Temperatures between 20 and 2000 K. *J. Phys. Chem. A* **2015**, *119*, 3147−3160.
(20) Marx, D.; Hutter, J. Ab Initio Molecular Dynamics: Theory and Implementation. *Mod. methods algorithms quantum Chem.* **2000**, *1*, 301−449.
(21) Paranjothy, M.; Sun, R.; Zhuang, Y.; Hase, W. L. Direct Chemical Dynamics Simulations: Coupling of Classical and Quasiclassical Trajectories with Electronic Structure Theory. *WIRE Comput. Mol. Sci.* **2013**, *3*, 296−316.
(22) Marx, D.; Hutter, J. *Ab Initio Molecular Dynamics: Basic Theory and Advanced Methods*; Cambridge University Press: Cambridge, U.K., 2009.
(23) Wang, L.-P.; Titov, A.; McGibbon, R.; Liu, F.; Pande, V. S.; Martínez, T. J. Discovering Chemistry with an Ab Initio Nanoreactor. *Nat. Chem.* **2014**, *6*, 1044−1048.
(24) Martyna, G. J.; Klein, M. L.; Tuckerman, M. Nose−Hoover Chains: The Canonical Ensemble via Continuous Dynamics. *J. Chem. Phys.* **1992**, *97*, 2635−2643.
(25) Aquilanti, V.; Mundim, K. C.; Elango, M.; Kleijn, S.; Kasai, T. Temperature Dependence of Chemical and Biophysical Rate Processes: Phenomenological Approach to Deviations from Arrhenius Law. *Chem. Phys. Lett.* **2010**, *498*, 209−213.
(26) Aquilanti, V.; Mundim, K. C.; Cavalli, S.; De Fazio, D.; Aguilar, A.; Lucas, J. M. Exact Activation Energies and Phenomenological Description of Quantum Tunneling for Model Potential Energy Surfaces. The F+H2 Reaction at Low Temperature. *Chem. Phys.* **2012**, *398*, 186−191.
(27) Silva, V. H. C.; Aquilanti, V.; de Oliveira, H. C. B.; Mundim, K. C. Uniform Description of Non-Arrhenius Temperature Dependence of Reaction Rates, and a Heuristic Criterion for Quantum Tunneling vs Classical Non-Extensive Distribution. *Chem. Phys. Lett.* **2013**, *590*, 201−207.
(28) Cavalli, S.; Aquilanti, V.; Mundim, K. C.; De Fazio, D. Theoretical Reaction Kinetics astride the Transition between Moderate and Deep Tunneling Regimes: The F + HD Case. *J. Phys. Chem. A* **2014**, *118*, 6632−6641.
(29) Frank, I.; Parrinello, M.; Klamt, A. Insight into Chemical Reactions from First-Principles Simulations: The Mechanism of the Gas-Phase Reaction of OH Radicals with Ketones. *J. Phys. Chem. A* **1998**, *102*, 3614−3617.
(30) Perdew, J. P.; Burke, K.; Ernzerhof, M. Generalized Gradient Approximation Made Simple. *Phys. Rev. Lett.* **1996**, *77*, 3865−3868.
(31) Troullier, N.; Martins, J. L. Efficient Pseudopotentials for Plane-Wave Calculations. *Phys. Rev. B: Condens. Matter Mater. Phys.* **1991**, *43*, 1993−2006.
(32) Vanderbilt, D. Soft Self-Consistent Pseudopotentials in a Generalized Eigenvalue Formalism. *Phys. Rev. B: Condens. Matter Mater. Phys.* **1990**, *41*, 7892−7895.
(33) Frisch, M. J.; Trucks, G. W.; Schlegel, H. B.; Scuseria, G. E.; Robb, M. A.; Cheeseman, J. R.; Scalmani, G.; Barone, V.; Mennucci, B.; Petersson, G. A.; et al. *Gaussian 09*, Revision D.01; Gaussian Inc: Wallingford, CT, 2009.
(34) Tsai, P.-Y.; Hung, K.-C.; Li, H.-K.; Lin, K.-C. Photodissociation of Propionaldehyde at 248 Nm: Roaming Pathway as an Increasingly Important Role in Large Aliphatic Aldehydes. *J. Phys. Chem. Lett.* **2014**, *5*, 190−195.
(35) Nakamura, M.; Tsai, P.-Y.; Kasai, T.; Lin, K.-C.; Palazzetti, F.; Lombardi, A.; Aquilanti, V. Dynamical, Spectroscopic and Computational Imaging of Bond Breaking in Photodissociation: Roaming and Role of Conical Intersections. *Faraday Discuss.* **2015**, *177*, 77−98.
(36) Bowman, J. M. Roaming. *Mol. Phys.* **2014**, *112*, 2516−2528.
(37) Hause, M. L.; Herath, N.; Zhu, R.; Lin, M. C.; Suits, A. G. Roaming-Mediated Isomerization in the Photodissociation of Nitrobenzene. *Nat. Chem.* **2011**, *3*, 932−937.
(38) Herath, N.; Suits, A. G. Roaming Radical Reactions. *J. Phys. Chem. Lett.* **2011**, *2*, 642−647.
(39) Tsai, P.-Y.; Chao, M.-H.; Kasai, T.; Lin, K.-C.; Lombardi, A.; Palazzetti, F.; Aquilanti, V. Roads Leading to Roam. Role of Triple Fragmentation and of Conical Intersections in Photochemical Reactions: Experiments and Theory on Methyl Formate. *Phys. Chem. Chem. Phys.* **2014**, *16*, 2854−2865.
(40) Lombardi, A.; Palazzetti, F.; Aquilanti, V.; Li, H.-K.; Tsai, P.-Y.; Kasai, T.; Lin, K.-C. Rovibrationally Excited Molecules on the Verge of a Triple Breakdown: Molecular and Roaming Mechanisms in the Photodecomposition of Methyl Formate. *J. Phys. Chem. A* **2016**, DOI: 10.1021/acs.jpca.6b00723.
(41) Tizniti, M.; Le Picard, S. D.; Lique, F.; Berteloite, C.; Canosa, A.; Alexander, M. H.; Sims, I. R. The Rate of the F + H_2 Reaction at Very Low Temperatures. *Nat. Chem.* **2014**, *6*, 141−145.
(42) De Fazio, D.; Aquilanti, V.; Cavalli, S.; Aguilar, A.; Lucas, J. M. Exact Quantum Calculations of the Kinetic Isotope Effect: Cross Sections and Rate Constants for the F + HD Reaction and Role of Tunneling. *J. Chem. Phys.* **2006**, *125*, 133109.
(43) Pomerantz, A. E.; Camden, J. P.; Chiou, A. S.; Ausfelder, F.; Chawla, N.; Hase, W. L.; Zare, R. N. Reaction Products with Internal Energy beyond the Kinematic Limit Result from Trajectories far from the Minimum Energy Path: An Example from H + HBr → H_2 + Br. *J. Am. Chem. Soc.* **2005**, *127*, 16368−16369.
(44) Döntgen, M.; Przybylski-Freund, M.-D.; Kröger, L. C.; Kopp, W. A.; Ismail, A. E.; Leonhard, K. Automated Discovery of Reaction Pathways, Rate Constants, and Transition States Using Reactive Molecular Dynamics Simulations. *J. Chem. Theory Comput.* **2015**, *11*, 2517−2524.
(45) Fleming, K. L.; Tiwary, P.; Pfaendtner, J. New Approach for Investigating Reaction Dynamics and Rates with Ab Initio Calculations. *J. Phys. Chem. A* **2016**, *120*, 299−305.

DOI: 10.1021/acs.jpca.6b03958
J. Phys. Chem. A XXXX, XXX, XXX−XXX

PAPER 3:

COUTINHO, ND, CARVALHO-SILVA, VH, de OLIVEIRA, HCB, AQUILANTI, V. (2016). **The HI + OH ⟶ H_2O + I Reaction by First-Principles Molecular Dynamics: Stereodirectional and *anti*-Arrhenius Kinetics**. *Lecture Notes in Computer Science. In International Conference on Computational Science and Its Applications.* 2017, 10408 pp. 297–313.

Exemplary of four-atom processes, the reaction between OH and HI to give H_2O and I manifests an unusual *anti*-Arrhenius behavior, namely a marked decrease of the rate constants as the temperature increases, and this has intrigued theoreticians for a long time. Motivation of the study reported in this paper is the continuation of the investigation of the stereodirectional dynamics of these reaction as the prominent reason for the peculiar kinetics, started in previous papers for OH + HBr reaction (J. Phys. Chem. Lett. 2015, 6, 1553-1558J. Phys. Chem. A, 2016, 120, 5408–5417).

A first-principles Born-Oppenheimer 'canonical' molecular dynamics approach involves trajectories step-by-step generated on a potential energy surface quantum mechanically calculated on-the-fly, and thermostatically equilibrated in order to correspond to a specific temperature. Previous refinements of the method permitted a high number of trajectories at 50, 200, 350 and 500 K, for which the sampling of initial conditions allowed us to characterize the stereodynamical effect. The visualizations of the trajectories as a function of the coordinates that correlate the broken and formed bonds during the reaction and the approach angles showed that there is a mechanism change as a function of temperature. The aperture angle of this cone is dictated by a range of directions of approach compatible with the formation of the specific HOH angle of the product water molecule; and consistently the adjustment is progressively less effective at higher the kinetic energy. Thermal rate constants from this molecular dynamics approach are discussed: provided that the systematic sampling of the canonical ensemble is adequate as in this case, quantitative comparison with the kinetic experiments is obtained.

My contribution in this study was to perform Born-Oppenheimer molecular dynamics simulations and perform all relevant analyzes, as well as contribute to the discussions and in the paper writing. Acknowledgment to the other authors who contributed to the development of this investigation. Thank you professor Valter H. Carvalho Silva, Heibbe Cristhian B. de Oliveira and Vincenzo Aquilanti for the results discussions and the paper revision.

In addition, a special thanks to Springer for the reprinted the paper in my theses. Reprinted with permission from (Lecture Notes in Computer Science, In International Conference on Computational Science and Its Applications. 2017, 10408, 297–313).

Title: The $$ {\mathbf{HI}}\,\varvec{ + }\, {\mathbf{OH}}\, \to \, {\mathbf{H}}_{{\mathbf{2}}} {\mathbf{O}}\, + \, {\mathbf{I}} $$HI+OH→H2O+I Reaction by First-Principles Molecular Dynamics: Stereodirectional and anti-Arrhenius Kinetics

Author: Nayara D. Coutinho, Valter H. Carvalho-Silva, Heibbe C. B. de Oliveira et al

Publication: Springer eBook

Publisher: Springer Nature

Date: Jan 1, 2017

Order Completed

Thank you for your order.

This Agreement between Universidade de Brasília -- Nayara Coutinho ("You") and Springer Nature ("Springer Nature") consists of your license details and the terms and conditions provided by Springer Nature and Copyright Clearance Center.

Your confirmation email will contain your order number for future reference.

printable details

License Number	4334840201083
License date	Apr 23, 2018
Licensed Content Publisher	Springer Nature
Licensed Content Publication	Springer eBook
Licensed Content Title	The $$ {\mathbf{HI}}\,\varvec{ + }\,{\mathbf{OH}}\, \to \,{\mathbf{H}}_{{\mathbf{2}}} {\mathbf{O}}\, + \,{\mathbf{I}} $$HI+OH→H2O+I Reaction by First-Principles Molecular Dynamics: Stereodirectional and anti-Arrhenius Kinetics
Licensed Content Author	Nayara D. Coutinho, Valter H. Carvalho-Silva, Heibbe C. B. de Oliveira et al
Licensed Content Date	Jan 1, 2017
Type of Use	Thesis/Dissertation
Requestor type	academic/university or research institute
Format	print and electronic
Portion	full article/chapter
Will you be translating?	no
Circulation/distribution	1,001 to 2,000
Author of this Springer Nature content	yes
Title	The HI þ OH ! H2O þ I Reaction by First-Principles Molecular Dynamics: Stereodirectional and anti-Arrhenius Kinetics
Instructor name	Heibbe Cristhian Benedito de Oliveira
Institution name	Universidade de Brasília
Expected presentation date	Apr 2018
Attachment	
Requestor Location	Universidade de Brasília Asa Norte - Brasília-DF

	Brasília, Distrito Federal 70910-900 Brazil Attn: Universidade de Brasília
Billing Type	Invoice
Billing address	Universidade de Brasília Asa Norte - Brasília-DF Brasília, Brazil 70910-900 Attn: Universidade de Brasília
Total	0.00 USD

ORDER MORE CLOSE WINDOW

The HI + OH → H_2O + I Reaction by First-Principles Molecular Dynamics: Stereodirectional and *anti*-Arrhenius Kinetics

Nayara D. Coutinho[1(✉)], Valter H. Carvalho-Silva[2], Heibbe C.B. de Oliveira[1], and Vincenzo Aquilanti[3,4]

[1] Laboratório de Estrutura Eletrônica e Dinâmica Molecular (LEEDMOL), Institute of Chemistry, University of Brasília, Campus Darcy Ribeiro, Brasília, Brazil
nayaradcoutinho@gmail.com
[2] Grupo de Química Teórica e Estrutural de Anápolis, Ciências Exatas e Tecnológicas, Universidade Estadual de Goiás, CP 459, Anápolis, GO 75001-970, Brazil
[3] Dipartimento di Chimica, Biologia e Biotecnologie, Università di Perugia, Via Elce di Sotto 8, 06123 Perugia, Italy
[4] Istituto di Struttura della Materia, Consiglio Nazionale delle Ricerche, 00185 Rome, Italy

Abstract. Exemplary of four-atom processes, the series of reactions between OH and HX to give $H_2O + X$ (here X is a halogen atom) is one of the most studied theoretically and experimentally: the kinetics for X = Br and I manifests an unusual *anti*-Arrhenius behavior, namely a marked decrease of the rate constants as the temperature increases, and this has intrigued theoreticians for a long time. Motivation of the work reported in this paper is the continuation of the investigation of the stereodirectional dynamics of these reaction as the prominent reason for the peculiar kinetics, started in previous papers on X = Br. A first-principles Born-Oppenheimer 'canonical' molecular dynamics approach involves trajectories step-by-step generated on a potential energy surface quantum mechanically calculated on-the-fly, and thermostatically equilibrated in order to correspond to a specific temperature. Previous refinements of the method permitted a high number of trajectories at 50, 200, 350 and 500 K, for which the sampling of initial conditions allowed us to characterize the stereodynamical effect. It was confirmed also for X = I that the adjustment of the reactants' mutual orientation in order to encounter the entrance into the 'cone of acceptance' is crucial for reactivity. The aperture angle of this cone is dictated by a range of directions of approach compatible with the formation of the specific HOH angle of the product water molecule; and consistently the adjustment is progressively less effective at higher the kinetic energy. Thermal rate constants from this molecular dynamics approach are discussed: provided that the systematic sampling of the canonical ensemble is adequate as in this case, quantitative comparison with the kinetic experiments is obtained.

O. Gervasi et al. (Eds.): ICCSA 2017, Part V, LNCS 10408, pp. 297–313, 2017.
DOI: 10.1007/978-3-319-62404-4_22

1 Introduction

Reactive halogen species (Cl, Br and I) play a crucial role in the atmospheric chemistry by disturbing the natural equilibrium processes that create and destroy ozone in the stratosphere. For example, depletion of ozone through the reaction with halogen atoms occurs through efficient catalytic cycles. These atoms react with ozone molecules to yield halogen monoxide (XO) and oxygen (O_2) molecules [1, 2].

In particular, the $OH + HX \rightarrow H_2O + X(X = C1, Br\,and\,I)$ reactions have been extensively studied because they are major providers for the halogens in the atmosphere. Additionally, these four-body reactions are also of basic relevance for both experimental and theoretical chemical kinetics. The rate constants for most rate processes depend on absolute temperature according to the Arrhenius law: however, for reactions of OH with hydrogen halides, when extended to low temperatures, deviations are observed: the kinetics data available for the reaction with HCl [3, 4] show a strong concave curvature for low temperatures, a phenomenon described as *sub*-Arrhenius behavior, while reactions with HBr [5–11] and HI [12–16] are considered as a typical of processes that exhibit negative temperature dependence of the reaction rate (*anti*-Arrhenius behavior).

In our previous works [17, 18] and as described in Sect. 2, we have approached the study of the *anti*-Arrhenius mechanism of the OH + HBr reaction using first-principles Born-Oppenheimer molecular dynamics. Here, in order to understand the peculiar kinetics of the systems involving hydroxyl radical and hydrogen halides and to continue the previous discussion about *non*-Arrhenius behavior [19–24], we focus on the $OH + HI \rightarrow H_2O + I$ reaction. Work is in progress regarding the Cl case, presenting different behavior to be examined accordingly.

The experimental kinetic data for OH + HI are limited: just a few values are available for rate constants in a narrow range of temperatures [12–16]: under these conditions, the rate constants show a negative temperature dependence. These results are discussed in Sect. 3.

As a contribution to the understanding of the detailed microscopic dynamics of the OH + HI reaction, Moise and collaborators using crossed molecular beam experiments to measure relative state-to-state cross section and steric asymmetries and a comparison was made with the previously studied systems OH-HCl and OH-HBr [25]. They provide an insight on the relevance of the potential energy surface landscape of these molecular systems in the reactive process. From a theoretical perspective, starting in 2010 [26], the direct and reverse reactions have been of interest since some time regarding the potential energy profile of the I + H_2O reaction and showing that the relative energy of products is lower than that of the transition state. Furthermore, quantitative rate constants where determined for the reactions involving iodine-containing species using the canonical transition state theory with a simple Wigner tunneling correction. Recently, the stationary points, zero-point vibrational energies and vibrational frequencies for the I + H_2O potential energy surface have been predicted at high-level *ab initio* CCSD(T) method, with the spin–orbit coupling corrections [27]. However, all previous works neglect the understanding of the *anti*-Arrhenius behavior.

Here, the strategy that we follow to assess to *anti*-Arrhenius mechanism is to use the Born-Oppenheimer molecular dynamics [28–30] technology to carry out numerical experiments that simulate the reaction in a box, which we consider as our first-principles "nanoreactor" [31]: the reactant molecules introduced in the box explore the potential energy surface at a specified temperature, enforced by a Nosé-Hoover thermalizing bath and therefore representing a 'canonical' ensemble [32]. Although computations of the potential energy surface on-the-fly are time-consuming, we can scrutinize trajectories at different configurations and will examine comparatively their behavior at four descriptive temperatures. We show how during trajectories molecular reorientation occurs in order to encounter a mutual approach of reactants favorable for them to proceed to reaction. Besides the demonstration of the crucial role of stereodynamics, additional documentation is also provided on the interesting manifestation of the roaming phenomenon, whereby both the search of the reactive configurations sterically favorable to reaction and the subsequent departure involving vibrational excitation, were seen to occur on wandering paths on the potential energy surface not limited to those corresponding to the one of minimum energy. A closer scrutiny is possible thanks to the results of this paper, where a perspective avenue leading to the extraction of quantitative information on reaction rate constants emerges from the analysis of molecular dynamics simulations.

2 Theoretical and Numerical Procedures and Results

2.1 Molecular Dynamics Simulations

The aim of disentangling the basic question concerning the peculiar kinetics of this reaction is approached by molecular dynamics simulations. As noted above (see also Ref. [17]) the technique of choice, the Born-Oppenheimer molecular dynamics (BOMD) [28–30], is suited to follow the evolution of the reaction and therefore to provide a description of its apparently anomalous features. As a result of the various preceding theoretical and computational investigations, a definite role was attributed to the transient aggregate due to van-der-Waals – like interactions, lying at a lower energy than that of the reactants. This feature is so prominent to give to this process an unusual reaction path profile [33, 34] corresponding to essentially a negative activation barrier. The dynamical relevance of this feature is adequately scrutinized under the microscope of the present canonical trajectory simulations. In the HBr case very relevant appeared to us the additional specific goal to provide a link with the available but overlooked experimental stereodynamical studies [35–37].

A previous pioneering investigation [38] of a reactive process where the reactant was the hydroxyl radical, exploited Car-Parrinello molecular dynamics, where motion of the nuclei in the on-the-fly calculated trajectories occurs in the potential generated by the electrons according to classical mechanics. A distinctive feature of the present first-principles Born-Oppenheimer molecular dynamics study is that quantum chemical wavefunctions are converged at every step, making trajectory calculations much more expensive but arguably more accurate.

Electronic structure calculations are essential in molecular dynamics simulations and the reliability of intermolecular forces depends on the quality of the employed quantum chemistry methods and of the dedicated computational effort. Since a reactive process involves the adjustment of the electronic structure according to the evolution of the nuclear positions, reaction mechanisms emerge with no need of computationally prohibitive explorations to find reaction pathways. On the contrary, the exploit of the automatic focusing of trajectories on regions actually sampled during the reaction provides information on parts of the multidimensional potential energy surface which demand more accuracy for improving the realistic simulations of the dynamics. Randomly generated initial conditions and procedures for equilibration with respect to a thermal bath (see the following subsection), permit to efficiently bypass the often severe bottlenecks of computational dynamics, such as both the impact parameter integration to provide total cross sections, and their Boltzmann kinetic energy averaging, allowing the direct specification of the temperature: our previous choice [17] was limited to consider two temperatures only, at the two extremes of the experimentally relevant range, at low (50 K) and high (500 K) temperatures, and the improvements to be described next allow us to explore a total of four temperature by a much higher number of trajectories in both Ref. [18] and in this work.

2.2 Computational Methods

The results from BOMD simulations reported in this paper were obtained utilizing the Car-Parrinello-Molecular-Dynamics CPMD 3.17.1 suite of programs, Copyright IBM, 2012. The electronic structure calculations employed was density functional theory DFT, through the Perdew-Burke-Ernzerhof [39] functional. The plane-wave cutoff was equal to 25 Ry, and the core electrons were described using the Vanderbilt pseudopotential [40]. We used a step size to 0.1 fs and run a total of 2 ps for each trajectory.

The temperatures of the system were controlled by the Nosé-Hoover Thermostats (NVT) scheme [32] at 50, 200, 350 and 500 K. One HI molecule and one OH radical were placed inside a cubic cell having a 6 Å side and periodic boundary conditions were imposed for each trajectory reaching the walls of the cell. The intermolecular orientation of the two molecules in the initial configurations was not optimized; that is, the starting geometries do not represent local minima of the global potential surface.

2.3 Representation of Stereodirectional Dynamics

Figure 1 (upper panel) illustrates the coordinate choice for this discussion of the $OH + HI \rightarrow H_2O + I$ reaction. In a four-body system, the configuration is fixed by six coordinates, two of them are those utilized here for exhibiting the stereodirectional effect on the molecular dynamics: they are the bond length r_1 and the angle θ. Their values are fixed when starting the simulations and serve to identify the trajectories in the following presentation. In order to compare with result for the OH + HBr reaction presents in our previous paper [18], we used the same 60 initial configurations with characteristic values listed in Table 1. The initial settings have been selected according

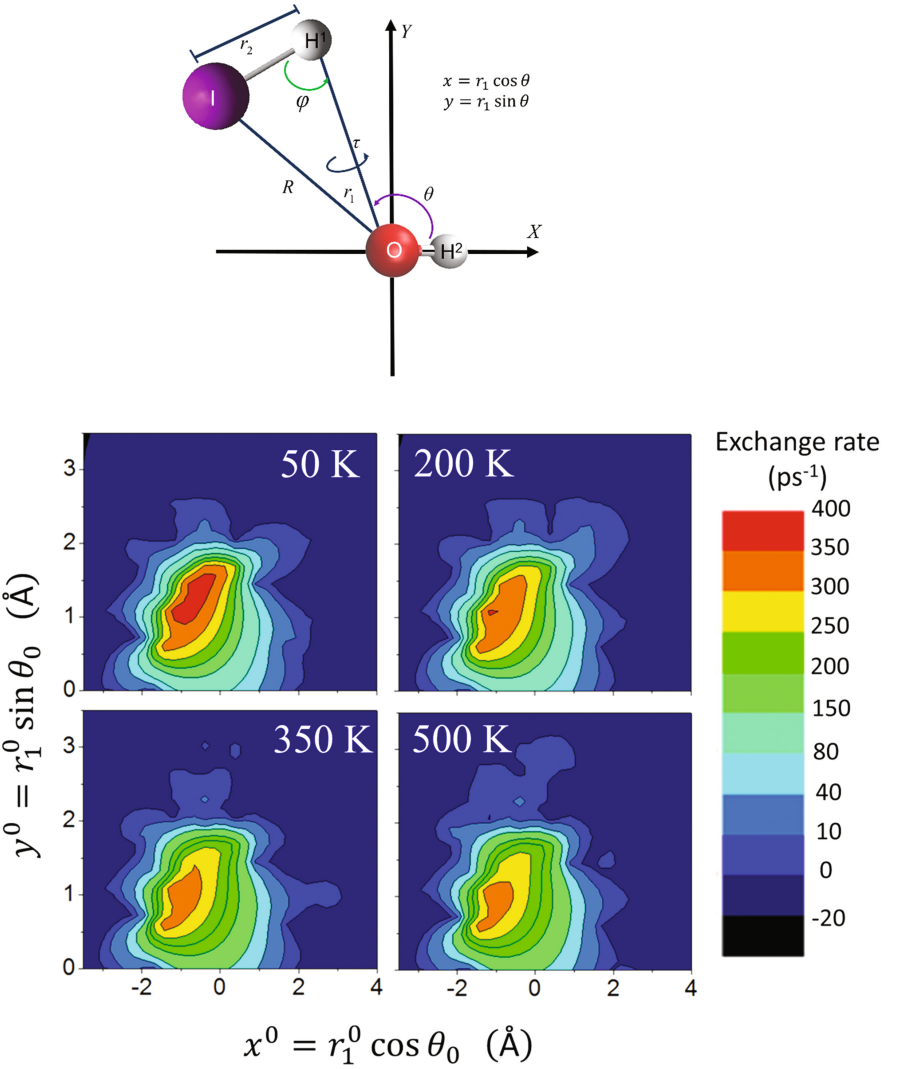

Fig. 1. Upper panel: definitions of geometrical parameters for the configuration of the present four-atom process suited to extract stereodynamical information on the role of the mutual direction between approaching reactants. The origin is on the oxygen atom, the OH bond, of length r_2, lies in the X axis, while Y is the axis perpendicular to X in the IOH^2 plane oriented as in the figure. The initial configurations are identified (Table 1) by a zero affix, namely by the vector length r_1^0 and the angle θ_0 or by the vectors components x_0 and y_0 on the X and Y axes. Lower panel: contour plots of reactivity data, the latter estimated on the assumption that the velocity of reaction can be correlated to the so-called 'switching time', namely to the moment when $r_1 = r_2$. Its inverse (see text), is defined as 'exchange rates', and can be extracted from the entries of Table 2.

to the following criteria: r_1^0 ranging from 1.7 to 3.2 Å with steps of 0.3 Å and θ_0 ranging from 0 to 180° with a 20° increment; all other coordinates were obtained randomly, within limits that guaranteed realistic initial configurations of the system. In Table 1 and in the following ones, they are displayed as labels to a matrix with 60 entries, r_1^0 for the six columns and θ_0 for the ten rows, respectively. In the initial configurations, two other variables are held fixed for all cases, the HI bond length at 1.61 Å and the OH^2 bond length at 1.0 Å. Two other needed coordinates are chosen randomly among the three φ (degrees), $\boldsymbol{\tau}$(degrees) and R(Å), one of them being superfluous but used for internal check.

As the temperature increases, reactive trajectories are found to typically wander around before encountering their relatively narrow road towards product formation and are relatively insensitive to the details of the reaction profile.

The coordinate s appropriate to simply describe the evolution of the reactive event is the difference between lengths of bonds being broken and formed, respectively ($s = r_2 - r_1$, see Fig. 1). The "exchange rate" for the reaction is conveniently defined as the inverse of the "switching" time, defined by the time when either $r_1 = r_2$ or $s = 0$. The correlation between the initial geometry of the propensity to reaction is illustrated in Fig. 1 (lower panel) and in Tables 2, 3, 4 and 5. In the tables, the exchange rate is

Table 1. Initial values of the coordinates for all trajectories for the $OH + HI \rightarrow H_2O + I$ reaction, arranged as a function of the stereodynamical angle, θ_0, and the distance r_1^0 of Fig. 1 (upper panel). The initial values for φ (degrees), τ(degrees) and $\boldsymbol{R}$(Å), are the entries of the table in this order

θ_0 (degrees)	r_1^0 (Å)					
	1.7	2.0	2.3	2.6	2.9	3.2
0	60, *142*, **1.66**	158, *129*, **3.54**	115, *127*, **3.32**	60, *132*, **2.27**	117, *124*,**3.90**	173, *123*, **4.80**
20	144, *−20*, **3.15**	127, *66*, **3.24**	78, *−28*, **2.52**	60, *132*, **2.27**	107, *0*, ***3.71***	169, *82*, **4.79**
40	129, *169*, **2.99**	102, *−100*, **2.81**	138, *−14*, **3.66**	111, 39, **3.52**	60, *−79*, **2.52**	132, *−168*, **4.44**
60	92, *97*, **2.39**	117, *52*, **3.08**	134, *21*, **3.61**	151, *−90*, **4,08**	163, *128*, **4.47**	158, *−60*, **4.73**
80	177, *−148*, **3.31**	167, *114*, **3.59**	179, *47*, **3.91**	168, *120*, **4.19**	60, *113*, **2.52**	60, *28*, **2.77**
100	175, *−151*, **3.31**	126, *−5*, **3.23**	145, *157*, **3.73**	60, *−146*, **2.27**	60, *−168*, **2.52**	128, *−158*, **4.37**
120	145, *−107*, **3.16**	162, *20*, **3.57**	60, *−26*, **2.04**	60, *95*, **2.27**	60, *-111*, **2.52**	60, *−21*, **2.77**
140	145, *−147*, **3.16**	121, *97*, **3.14**	117, *−130*, **3.36**	95, *20*, **3.18**	120, *61*, **3.96**	122, *163*, **4.29**
160	173, *−125*, **3.30**	179, *172*, **3.61**	141, *170*, **3.69**	169, *130*, **4.05**	60, *97*, **2.52**	113, *−109*, **4.11**
180	60, *−76*, **1.66**	65, *−82*, **1.97**	*124, 89*, ***3.47***	78, *−93*, **2.76**	138, *−110*, **4.24**	160, *171*, **4.75**

Table 2. Exchange rates (ps^{-1}, see Text) for reactive trajectories at 50 K. Zero entries correspond to non-reactive trajectories.

θ_0 (degrees)	r_1^0 (Å)					
	1.7	2.0	2.3	2.6	2.9	3.2
0	0	0	0	0	0	0
20	0	13.48	0	0	0	0
40	28.49	0	0	0	0	0
60	0	46.95	17.89	0	0	0
80	312.50	0	0	0	0	0
100	357.14	32.79	15.48	0	0	0
120	370.37	90.91	0	0	0	0
140	384.62	56.50	28.01	0	7.35	0
160	344.83	9.96	0	0	0	0
180	0	0	17.42	0	0	0

Table 3. Exchange rates (ps^{-1}, see Text) for reactive trajectories at 200 K. Zero entries correspond to non-reactive trajectories.

θ_0 (degrees)	r_1^0 (Å)					
	1.7	2.0	2.3	2.6	2.9	3.2
0	0	0	0	0	0	0
20	0	0	0	0	0	0
40	29.24	0	0	0	0	0
60	0	42.55	17.33	13.33	0	0
80	256.41	3.75	0	0	0	0
100	294.12	24.69	16.16	0	0	0
120	322.58	121.95	0	0	0	0
140	370.37	56.50	29.15	0	10.49	0
160	357.14	17.45	0	0	0	0
180	0	0	22.47	0	0	0

given as a function of r_1^0 and θ_0 and in Fig. 2 in the plane of the Cartesian components of the r_1 vector, $x_0 = r_1^0 \cos\theta_0$ and $y_0 = r_1^0 \sin\theta_0$. For a temperature, e.g. of 50 K the reactivity is seen as largest for x_0 equal to −2 to 0.5 Å range and y_0 equal to 0.5 to 1.5 Å range, manifesting stereodynamical propensity for θ_0 angles in the 80–160º range and for r_1^0 less than 2.3 Å. For values of x_0 larger than 2.3 Å, the reactivity is very low. As the system temperature increases, the dependence of reactivity on the stereodirectionality is lower and other initial conditions can lead to the final product, as can be seen in the corresponding panels at 350 and 500 K and in Tables 3, 4 and 5. For high temperatures the reactivity of the system is less sensitive to the system initial conditions, and the memory of the initial configuration appears to be partially lost during the reactive process, arguably because of the manifestation of the roaming effect, to be discussed next.

Table 4. Exchange rates (ps^{-1}, see Text) for reactive trajectories at 350 K. Zero entries correspond to non-reactive trajectories.

θ_0 (degrees)	r_1^0 (Å)					
	1.7	2.0	2.3	2.6	2.9	3.2
0	0	0	0	0	0	0
20	0	0	0	0	5.63	0
40	28.01	0	0	0	0	0
60	0	29.76	0	0	0	0
80	232.56	0	0	0	0	0
100	263.16	0	15.85	0	0	0
120	294.12	126.58	0	0.75	0	0
140	357.14	54.64	27.62	0	13.81	0
160	357.14	16.13	0	4.36	0	0
180	0	0	23.75	0	0	0

Table 5. Exchange rates (ps^{-1}, see text) for reactive trajectories at 500 K. Zero entries correspond to non-reactive trajectories.

θ_0 (degrees)	r_1^0 (Å)					
	1.7	2.0	2.3	2.6	2.9	3.2
0	0	0	1.52	0	0	0
20	0	0	0	0	0	0
40	26.25	0	3.20	0	0	0
60	0	18.80	0.85	0	0	0
80	217.39	0	0	0	0.71	0.71
100	250	0	17.54	0	0	0
120	270.27	129.87	0	3.45	1.83	0
140	357.14	52.91	23.36	0	14.45	0
160	357.14	0	0.52	0	0	0
180	0	0	24.27	0	0	0

2.4 Delayed Reactivity and Vibrational Roaming of Product Water

The information from Tables 2, 3, 4 and 5 focused on "switching" times along trajectories, identified as the moment when $r_1 = r_2$: they convey the approximate view of the event, as involving the sudden breaking of the reactant HI molecule and the synchronous formation of the H_2O product. Remarkable is the delayed reactivity for trajectories for high temperatures and for high initial stretching of r_1: additionally, this effect appears from emergence of "roaming" in vibrational modes in search of propitious outcomes.

The "roaming" phenomenon has been amply documented as occurring in photodissociation experiments as the emergency of routes to molecular fragmentation channels [41, 42] that circumvent transition-state reaction paths. The presence of these alternative pathways can be inferred by the properties of the translational and internal distribution of the product fragments. Since they involve regions far from the

neighborhoods of saddle points along minimum energy paths and lead to avenues to reaction beyond the venerable transition state approach [37, 43–45], they are challenging to theories of chemical kinetics and demand explorations by on-the-fly dynamics, such as the one presented in this work.

Experimental fingerprints of roaming are slow, delayed photodissociation products, as inferred by late arrival of products in time-of-flight measurements. Detailed investigations [41] on the threshold for the opening of the breakdown in three fragments and molecular dynamics simulations pointed out the role of non-adiabatic transitions at a conical intersection between ground state and excited potential energy surfaces [41].

The origin of roaming as a rearrangement between weakly bound reactants is connected to high-lying regions of the ground state potential energy surfaces [46, 47] and indicated in Refs. [42, 48, 49]. Typically, they involve molecular configurations far from the transition state geometry and are propitiated by pronounced bond elongations, such as manifested when emerging from nonadiabatic paths involving conical intersections. From Tables 2, 3, 4 and 5, we observe analogously that in our case "roaming" is favored by starting trajectories at elongated r_1^0.

2.5 Angle of Approach and Excitation of Bending in the Departing Water

In this section, the important role of the stereodynamical angle of approach θ_0 in influencing the reaction is discussed in detail with reference to Fig. 2. The figure shows that when the dynamics is started with those values of θ_0 close to that leading to the formation of the bond angle of water $(\theta_w \sim 104^\circ)$, the system finds an easier way to products, and possible reorientation facilitating the process is hindered as the temperature increases. The specific value of the s coordinate, indicated as $s^\ddagger$, marks at each temperature the estimated averaged configuration in terms of new and old bond differences, characterizing the moment in the dynamics when the water molecule can be considered as effectively formed. These values are in general higher than the previously considered values of s corresponding to $r_1 = r_{2,}$ which were used in the preceding estimates of the exchange rates. They decrease from about 1.9 Å at 50 K to 1.6 Å at 500 K. In the following, these values will be correlated to reaction times for each temperature, and will provide further information on the kinetic rate constants (Sect. 3).

In Fig. 2, the trajectories that are visualized are conveniently listed following the initial value of the stereodynamically relevant angle, θ_0, which represents the direction of the approach of the H atom to OH (Fig. 1). Since the process evolves as the H-atom departs from HI and is effectively terminated when it sticks to OH forming a bond angle typical to that of the bending angle for water, the propitious orientation is crucial. It has to be noted here not only again the "roaming" effect as the search of a favorable approaching angle for reactivity, but also that such an effect results more evident at the higher temperature considered, 350 e 500 K. Additionally, it has to be noted how the final energy appears to be disposed of as excitation in the bending mode of the product water, as it is visually clear to a much greater extent again for the higher temperatures (see Ref. [47] for experimental comparisons for an analogous study case). The ranges of values span by the θ angle around 104° as the water molecule departs can be taken as a visualization of the disposal of the energy into the bending mode of the molecular product.

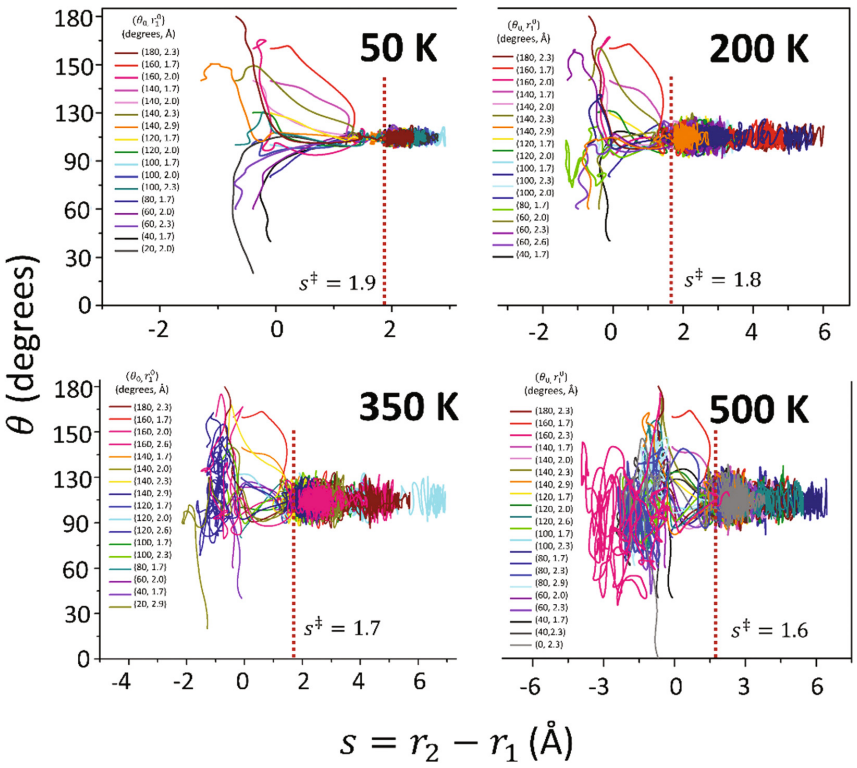

Fig. 2. Evolution at four temperatures of the stereodynamical angle of approach θ (Fig. 1) for "canonical" trajectories versus the reaction coordinate $s = r_2 - r_1$, conveniently defined as the difference between the lengths of the bond which is broken r_1 and of the bond which is formed r_2. The number of reactive trajectories changes with temperature. The trajectories are distinguished by different colors as listed in the right panel and arranged in decreasing order of θ_0, the initial values for the θ angle; the other value characterizing the trajectory is that of r_1^0; the other parameters defining the initial configurations can be extracted by the corresponding entries in Table 1. Indicated by vertical dashed lines is the value of $s^{\ddagger}$, identified by averaging for all trajectories of a given temperature the values of the reaction coordinate $s = r_2 - r_1$ for which a water molecule can be considered as formed.

3 Rate Constants and Comparison with Experiments

The molecular dynamics investigation reported here has been devoted mostly to the elucidation of the stereodirectional aspects featuring as most relevant in the unusual kinetics of this reaction. In general, the extraction of quantitative information on rate

constants from molecular dynamics simulations is an important issue but a very difficult to be tackled.

On the other hand, quantum mechanical benchmark rate constants [50–52] have been so far satisfactorily obtained only for specific three-atom processes, involving great theoretical and computational efforts, and evolving along a series of steps, the first one being the construction or availability of an accurate potential energy surface. In *ab initio* "exact" quantum dynamics, many further other steps are needed to go all the way from the interaction to rate constants. One must proceed through state-to-state coupled-channel Schrödinger dynamics giving scattering matrices (a major step), and then sum over all involved angular momenta, obtaining differential and integral cross sections on a large number of the reactants' kinetic energy values. The integral cross sections have to be obtained in a fine enough grid to finally generate temperature dependent rate constants by computationally demanding averaging on the Maxwell-Boltzmann distribution of the reactants' velocities. As a paradigmatic case, only in the last few years this has been achieved for the triatomic system F + H_2 → HF + H, and the predictions [53] have been verified experimentally, in particular from thermal down to the very low temperature reactivity range where tunneling is dominant [54]. For the related isotopic variant F + HD, see Refs. [21, 54].

The present system involves only four atoms, yet its kinetics is unusual and attractive to theorists as archetypal of four-center reactions. As a quantum-mechanical time-independent four-body problem: (i) computation and fitting of multidimensional PES of high accuracy is demanding (six effective degrees of freedom); (ii) exact quantum close coupling state-to-state dynamics is prohibitively expensive, and (iii) even for model PES, benchmark cross sections are difficult to obtain and rate constants out-of-reach (time-dependent techniques typically need calibration against time-independent benchmarks). However, comparison of results for the present four-atom reaction with three-atom processes bearing features in common with this one is interesting: for the reaction OH + HBr, see remarks in Ref. [33]; for the H + HBr reaction, Ref. [55] reports experimental and computational evidence of reactive trajectories far from the minimum energy path, a signature for 'roaming' in the same spirit as our discussion of Fig. 2.

There is ample current activity investigating whether advances in molecular dynamics simulations can provide quantitatively reliable rate constants. Recent Refs. [55–59] indicate that only order-of-magnitude estimates can be currently obtained. Typically, rates are overestimated and accuracy deteriorates considerably with temperature. Uncertainties are often dominated by those in the accurate characterization of transition state features, crucial in applications of TST-type approaches to calculations of rates. Additionally, inherent difficulties of possible direct evaluations from molecular dynamics simulation originate from those regarding the statistical validity of samplings of the system phase space. The latter of course increases enormously with temperature as far as both energy and angular momentum are concerned.

A different approach to estimate rate constants was briefly suggested in the preceding Letter [17] and later expanded in the subsequent work [18] on the basis of a much more detailed information available. The availability of considerably more information from the present results and especially the visualization from Fig. 2 and its discussion of the delayed reactivity leading to emergency of a water molecule, confirm

the alternative approach based on the rate of formation of water rather than on the rate of disappearance of reactants. Specifically, for an evaluation of the reaction rate constants we now start from the observation that, being the bimolecular process OH + HI of the second order, the general formula for the rate constant can be written

$$k = \frac{\mathrm{d}[\mathrm{H_2O}]}{\mathrm{d}t}\left([\mathrm{OH}][\mathrm{HI}]\right)^{-1}$$

as the ratio of the rate of formation of water and the product of the initial concentrations of the two reactants. In our numerical experiments, we place one molecule of OH and one molecule of HI in a cubic box of 6 Å in size, amounting to a concentration $[\mathrm{C}] \sim 5 \times 10^{21}$ molecules.cm^{-3} for each reactant. The formation of water is "observed" in our first-principles nanoreactor as the appearance of one product molecule in the volume of the box, *i.e.* [C] times the fraction f of reactive *versus* total trajectories and emerging at the 'transition time', $t^{\ddagger}$:

$$\frac{\mathrm{d}[\mathrm{H_2O}]}{\mathrm{d}t} = \frac{f[\mathrm{C}]}{t^{\ddagger}}$$

The fractional number of reactive trajectories f and the resulting values of the transition time $t^{\ddagger}$ for each temperature can be extracted from Tables 2, 3, 4 and 5. Since the transition time is meant to represent the average time that elapses for the chemical reaction to take place in the nanoreactor, for its present evaluation we searched for the moments along trajectories when the evolution coordinate s corresponded to the emergency of water as a product. Average values of s for each temperature are denoted $s^{\ddagger}$ and highlighted in the plots in Fig. 2 providing the correlation between the angle θ and s.

As documented in other cases, such as the recent ones already considered above [56, 57], and as the HBr system, the rate constant k so obtained were larger than experimental rate constant and the more so the higher the temperature. As discussed there [18], one crucial reason is arguably the fact that the choice of initial conditions (reactants in a small box with close encounters) increases chances of reactive *versus* total collisions, especially at high temperature. This points out at the general need of calibrating a first-principles nanoreactor against experimental results. Fig. 3 shows that this is not necessary in the present case, due high reactivity between OH and HI compared with HCl and HBr. Indeed, this results is indicative of an at least semi-quantitative route to the extraction of rate constants from first-principles molecular dynamics numerical experiments. The better agreement obtained in this case of larger reactivity can be taken as an indication that calibration may be more needed the rarer are the reactive encounters.

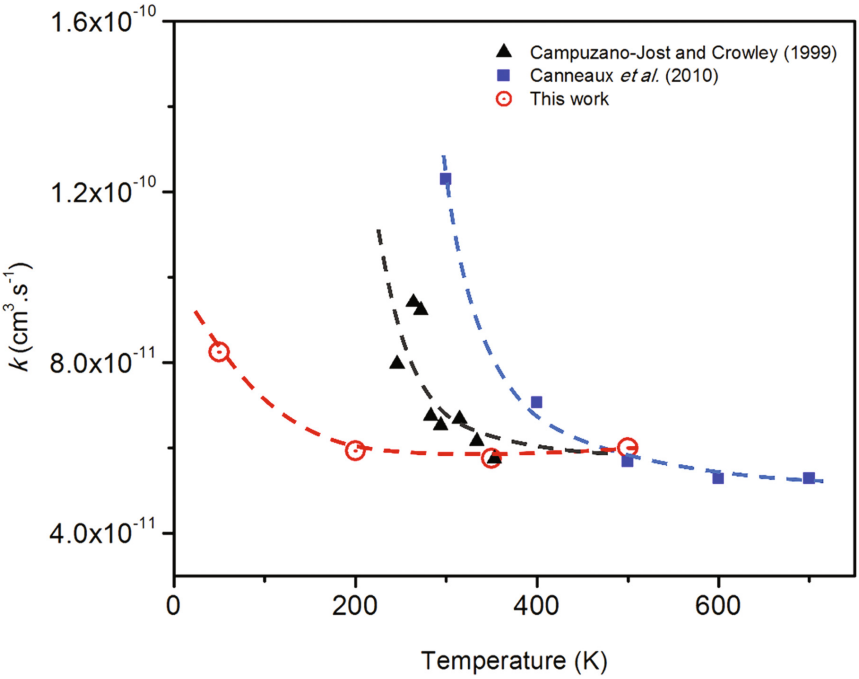

Fig. 3. Reaction rate constants as a function of temperature. We present the estimated rate constant obtained from Born-Oppenheimer molecular dynamics (red circles, see text and Table 6). They are reported together with experimental rate constants from reference [16], and the theoretical values obtained by Canneaux *et al.* [26]. Curves are drawn as aid to the eyes of readers. (Color figure online)

Table 6. Transition times (ps) and rate constants (10^{-11}cm^3.s^{-1}) at different temperatures (Kelvin).

T	$t^{\ddagger}$	k
50	0.74	8.25
200	1.09	5.93
350	1.06	5.75
500	1.26	6.00

Acknowledgments. The authors acknowledge grants from Brazilian CAPES, FAPEG, FAPDF, CNPQ and FINATEC. V. H. Carvalho-Silva thanks PrP/UEG for research funding through PROBIP and PRO-PROJETOS programs.

References

1. Read, K.A., Mahajan, A.S., Carpenter, L.J., Evans, M.J., Faria, B.V.E., Heard, D.E., Hopkins, J.R., Lee, J.D., Moller, S.J., Lewis, A.C., Mendes, L., McQuaid, J.B., Oetjen, H., Saiz-Lopez, A., Pilling, M.J., Plane, J.M.C.: Extensive halogen-mediated ozone destruction over the tropical Atlantic Ocean. Nature **453**, 1232–1235 (2008)
2. Saiz-Lopez, A., von Glasow, R.: Reactive halogen chemistry in the troposphere. Chem. Soc. Rev. **41**, 6448–6472 (2012)
3. Zuo, J., Zhao, B., Guo, H., Xie, D.: A global coupled cluster potential energy surface for HCl + OH ↔ Cl + H_2O. Phys. Chem. Chem. Phys. **120**, 3433–3440 (2016)
4. Zuo, J., Zhao, B., Guo, H., Xie, D.: A global coupled cluster potential energy surface for HCl + OH ↔ Cl + H_2O. Phys. Chem. Chem. Phys. **19**, 9770–9777 (2017)
5. Ravishankara, A.R., Wine, P.H., Wells, J.R.: The OH + HBr reaction revisited. J. Chem. Phys. **83**, 447–448 (1985)
6. Sims, I.R., Smith, I.W.M., Clary, D.C., Bocherel, P., Rowe, B.R.: Ultra-low temperature kinetics of neutral-neutral reactions - new experimental and theoretical results for OH + HBr between 295 K and 23 K. J. Chem. Phys. **101**, 1748–1751 (1994)
7. Atkinson, D.B., Jaramillo, V.I., Smith, M.A.: Low-temperature kinetic behavior of the bimolecular reaction OH + HBr (76−242 K). J. Phys. Chem. A **101**, 3356–3359 (1997)
8. Bedjanian, Y., Riffault, V., Le Bras, G., Poulet, G.: Kinetic study of the reactions of OH and OD with HBr and DBr. J. Photochem. Photobiol. A Chem. **128**, 15–25 (1999)
9. Jaramillo, V.I., Smith, M.A.: Temperature-dependent kinetic isotope effects in the gas-phase reaction: OH + HBr. J. Phys. Chem. A **105**, 5854–5859 (2001)
10. Mullen, C., Smith, M.A.: Temperature dependence and kinetic isotope effects for the OH + HBr reaction and H/D isotopic variants at low temperatures (53–135 K) measured using a pulsed supersonic Laval nozzle flow reactor. J. Phys. Chem. A **109**, 3893–3902 (2005)
11. Jaramillo, V.I., Gougeon, S., Le Picard, S.D., Canosa, A., Smith, M.A., Rowe, B.R.: A consensus view of the temperature dependence of the gas phase reaction: OH + HBr → H_2O + Br. Int. J. Chem. Kinet. **34**, 339–344 (2002)
12. Takacs, G.A., Glass, G.P.: Reactions of hydroxyl radicals with some hydrogen halides. J. Phys. Chem. **77**, 1948–1951 (1973)
13. Leod, H. M., Balestra, C., Jourdain, J.L., Laverdet, G., Le Bras, G.: Kinetic study of the reaction OH + HI by laser photolysis-resonance fluorescence. Int. J. Chem. Kinet. **22**, 1167–1176 (1990)
14. Lancar, I.T., Mellouki, A., Poulet, G.: Kinetics of the reactions of hydrogen iodide with hydroxyl and nitrate radicals. Chem. Phys. Lett. **177**, 554–558 (1991)
15. Butkovskaya, N.I., Setser, D.W.: Dynamics of OH and OD radical reactions with HI and GeH4 studied by infrared chemiluminescence of the H_2O and HDO products. J. Chem. Phys. **106**, 5028–5042 (1997)
16. Campuzano-Jost, P., Crowley, J.N.: Kinetics of the reaction of OH with HI between 246 and 353 K. J. Phys. Chem. A **103**, 2712–2719 (1999)
17. Coutinho, N.D., Silva, V.H.C., de Oliveira, H.C.B., Camargo, A.J., Mundim, K.C., Aquilanti, V.: Stereodynamical origin of anti-arrhenius kinetics: negative activation energy and roaming for a four-atom reaction. J. Phys. Chem. Lett. **6**, 1553–1558 (2015)
18. Coutinho, N.D., Aquilanti, V., Silva, V.H.C., Camargo, A.J., Mundim, K.C., de Oliveira, H. C.B.: Stereodirectional origin of anti-arrhenius kinetics for a tetraatomic Hydrogen exchange reaction: Born-Oppenheimer molecular dynamics for OH + HBr. J. Phys. Chem. A **120**, 5408–5417 (2016)

19. Silva, V.H.C., Aquilanti, V., de Oliveira, H.C.B., Mundim, K.C.: Uniform description of non-Arrhenius temperature dependence of reaction rates, and a heuristic criterion for quantum tunneling vs classical non-extensive distribution. Chem. Phys. Lett. **590**, 201–207 (2013)
20. Carvalho-Silva, V.H., Aquilanti, V., de Oliveira, H.C.B., Mundim, K.C.: Deformed transition-state theory: deviation from arrhenius behavior and application to bimolecular hydrogen transfer reaction rates in the tunneling regime. J. Comput. Chem. **38**, 178–188 (2017)
21. Cavalli, S., Aquilanti, V., Mundim, K.C., De Fazio, D.: Theoretical reaction kinetics astride the transition between moderate and deep tunneling regimes: the F + HD case. J. Phys. Chem. A **118**, 6632–6641 (2014)
22. Aquilanti, V., Mundim, K.C., Elango, M., Kleijn, S., Kasai, T.: Temperature dependence of chemical and biophysical rate processes: phenomenological approach to deviations from Arrhenius law. Chem. Phys. Lett. **498**, 209–213 (2010)
23. Aquilanti, V., Mundim, K.C., Cavalli, S., De Fazio, D., Aguilar, A., Lucas, J.M.: Exact activation energies and phenomenological description of quantum tunneling for model potential energy surfaces. The F + H_2 reaction at low temperature. Chem. Phys. **398**, 186–191 (2012)
24. Aquilanti, V., Coutinho, N.D., Carvalho-Silva, V.H.: Kinetics of low-temperature transitions and reaction rate theory from non-equilibrium distributions. Philos. Trans. R. Soc. London A **375**, 20160204 (2017)
25. Moise, A., Parker, D.H., Ter Meulen, J.J.: State-to-state inelastic scattering of OH by HI: A comparison with OH-HCI and OH-HBr. J. Chem. Phys. **126**, 124302 (2007)
26. Canneaux, S., Xerri, B., Louis, F., Cantrel, L.: Theoretical study of the gas-phase reactions of Iodine atoms (2P3/2) with H_2, H_2O, HI, and OH. J. Phys. Chem. A **114**, 9270–9288 (2010)
27. Hao, Y., Gu, J., Guo, Y., Zhang, M., Xie, Y., Schaefer III, H.F.: Spin-orbit corrected potential energy surface features for the I (2P3/2) + H_2O → HI + OH forward and reverse reactions. Phys. Chem. Chem. Phys. **16**, 2641–2646 (2014)
28. Marx, D., Hutter, J.: Ab initio molecular dynamics: theory and implementation. Mod. Methods Algorithms Quantum Chem. **1**, 301–449 (2000)
29. Paranjothy, M., Sun, R., Zhuang, Y., Hase, W.L.: Direct chemical dynamics simulations: coupling of classical and quasiclassical trajectories with electronic structure theory. WIRE Comput. Mol. Sci. **3**, 296–316 (2013)
30. Marx, D., Hutter, J.: Ab Initio Molecular Dynamics: Basic Theory and Advanced Methods. Cambridge University Press, Cambridge (2009)
31. Wang, L.-P., Titov, A., McGibbon, R., Liu, F., Pande, V.S., Martínez, T.J.: Discovering chemistry with an ab initio nanoreactor. Nat. Chem. **6**, 1044–1048 (2014)
32. Martyna, G.J., Klein, M.L., Tuckerman, M.: Nose-Hoover chains: the canonical ensemble via continuous dynamics. J. Chem. Phys. **97**, 2635–2643 (1992)
33. de Oliveira-Filho, A.G.S., Ornellas, F.R., Bowman, J.M.: Quasiclassical trajectory calculations of the rate constant of the OH + HBr → Br + H_2O reaction using a full-dimensional Ab initio potential energy surface over the temperature range 5 to 500 K. J. Phys. Chem. Lett. **5**, 706–712 (2014)
34. de Oliveira-Filho, A.G.S., Ornellas, F.R., Bowman, J.M.: Energy disposal and thermal rate constants for the OH + HBr and OH + DBr reactions: quasiclassical trajectory calculations on an accurate potential energy surface. J. Phys. Chem. A **118**, 12080–12088 (2014)
35. Tsai, P.-Y., Che, D.-C., Nakamura, M., Lin, K.-C., Kasai, T.: Orientation dependence in the four-atom reaction of OH + HBr using the single-state oriented OH radical beam. Phys. Chem. Chem. Phys. **12**, 2532–2534 (2010)

36. Tsai, P.-Y., Che, D.-C., Nakamura, M., Lin, K.-C., Kasai, T.: Orientation dependence for Br formation in the reaction of oriented OH radical with HBr molecule. Phys. Chem. Chem. Phys. **13**, 1419–1423 (2011)
37. Kasai, T., Che, D.-C., Okada, M., Tsai, P.-Y., Lin, K.-C., Palazzetti, F., Aquilanti, V.: Directions of chemical change: experimental characterization of the stereodynamics of photodissociation and reactive processes. Phys. Chem. Chem. Phys. **16**, 9776–9790 (2014)
38. Frank, I., Parrinello, M., Klamt, A.: Insight into chemical reactions from first-principles simulations: the mechanism of the gas-phase reaction of OH radicals with Ketones. J. Phys. Chem. A **102**, 3614–3617 (1998)
39. Perdew, J.P., Burke, K., Ernzerhof, M.: Generalized gradient approximation made simple. Phys. Rev. Lett. **77**, 3865–3868 (1996)
40. Vanderbilt, D.: Soft self-consistent pseudopotentials in a generalized eigenvalue formalism. Phys. Rev. B **41**, 7892–7895 (1990)
41. Tsai, P.-Y., Hung, K.-C., Li, H.-K., Lin, K.-C.: Photodissociation of Propionaldehyde at 248 nm: roaming pathway as an increasingly important role in large Aliphatic Aldehydes. J. Phys. Chem. Lett. **5**, 190–195 (2014)
42. Nakamura, M., Tsai, P.-Y., Kasai, T., Lin, K.-C., Palazzetti, F., Lombardi, A., Aquilanti, V.: Dynamical, spectroscopic and computational imaging of bond breaking in photodissociation: roaming and role of conical intersections. Faraday Discuss. **177**, 77–98 (2015)
43. Bowman, J.M.: Roaming. Mol. Phys. **112**, 2516–2528 (2014)
44. Spezia, R., Martínez-Nuñez, E., Vazquez, S., Hase, W.L.: Theoretical and computational studies of non-equilibrium and non-statistical dynamics in the gas phase, in the condensed phase and at interfaces. Philos. Trans. R. Soc. London A Math. Phys. Eng. Sci. **375**, 20170035 (2017)
45. Ma, X., Hase, W.L.: Perspective: chemical dynamics simulations of non-statistical reaction dynamics. Philos. Trans. R. Soc. London A Math. Phys. Eng. Sci. **375**, 20160204 (2017)
46. Hause, M.L., Herath, N., Zhu, R., Lin, M.C., Suits, A.G.: Roaming-mediated isomerization in the photodissociation of nitrobenzene. Nat. Chem. **3**, 932–937 (2011)
47. Herath, N., Suits, A.G.: Roaming radical reactions. J. Phys. Chem. Lett. **2**, 642–647 (2011)
48. Tsai, P.-Y., Chao, M.-H., Kasai, T., Lin, K.-C., Lombardi, A., Palazzetti, F., Aquilanti, V.: Roads leading to roam. Role of triple fragmentation and of conical intersections in photochemical reactions: experiments and theory on methyl formate. Phys. Chem. Chem. Phys. **16**, 2854–2865 (2014)
49. Lombardi, A., Palazzetti, F., Aquilanti, V., Li, H.-K., Tsai, P.-Y., Kasai, T., Lin, K.-C.: Rovibrationally excited molecules on the verge of a triple breakdown: molecular and roaming mechanisms in the photodecomposition of methyl formate. J. Phys. Chem. A **120**, 5155–5162 (2016)
50. Bonnet, L.: On the dynamical foundations of transition state theory: a semiclassical analysis. Ann. Phys. (N.Y.) **314**, 99–118 (2004)
51. Rayez, J.-C., Bonnet, L., Larrégaray, P., Perrier, A.: Transition state theory: a reaction dynamics tool applied to gas-surface reactions. Mol. Sci. **3**, A0029-1–A0029-10 (2009)
52. Bonnet, L., Rayez, J.-C.: Dynamical derivation of Eyring equation and the second-order kinetic law. Int. J. Quantum Chem. **110**, 2355–2359 (2010)
53. Tizniti, M., Le Picard, S.D., Lique, F., Berteloite, C., Canosa, A., Alexander, M.H., Sims, I. R.: The rate of the F + H_2 reaction at very low temperatures. Nat. Chem. **6**, 141–145 (2014)
54. De Fazio, D., Aquilanti, V., Cavalli, S., Aguilar, A., Lucas, J.M.: Exact quantum calculations of the kinetic isotope effect: cross sections and rate constants for the F + HD reaction and role of tunneling. J. Chem. Phys. **125**, 133109 (2006)

55. Pomerantz, A.E., Camden, J.P., Chiou, A.S., Ausfelder, F., Chawla, N., Hase, W.L., Zare, R. N.: Reaction products with internal energy beyond the kinematic limit result from trajectories far from the minimum energy path: an example from H + HBr → H_2 + Br. J. Am. Chem. Soc. **127**, 16368–16369 (2005)
56. Döntgen, M., Przybylski-Freund, M.-D., Kröger, L.C., Kopp, W.A., Ismail, A.E., Leonhard, K.: Automated discovery of reaction pathways, rate constants, and transition states using reactive molecular dynamics simulations. J. Chem. Theor. Comput. **11**, 2517–2524 (2015)
57. Fleming, K.L., Tiwary, P., Pfaendtner, J.: New approach for investigating reaction dynamics and rates with Ab initio calculations. J. Phys. Chem. A **120**, 299–305 (2016)
58. Fu, C.D., Oliveira, L.F.L., Pfaendtner, J.: Assessing generic collective variables for determining reaction rates in metadynamics simulations. J. Chem. Theor. Comput. **13**, 968–973 (2017)
59. Piccini, G., McCarty, J., Valsson, O., Parrinello, M.: Variational flooding study of a SN2 reaction. J. Phys. Chem. A **8**, 580–583 (2017)

PAPER 4:

COUTINHO, ND, SILVA, SANCHES-NETO, FO, CARVALHO-SILVA, VH, de OLIVEIRA, HCB, RIBEIRO-JUNIOR, AQUILANTI, V. **Kinetics of the $OH + HCl \longrightarrow H_2O + Cl$ reaction: rate determining roles of stereodynamic and of quantum tunnelling.** Submitted.

Among the processes involving four atoms, the reaction between the radical hydroxyl and the hydrogen chloride is one of the most studied both experimentally and theoretically. Here inspired by our previous studies on the OH + HBr and OH + HI reactions, which manifest an *anti*-Arrhenius behavior that was explained by a stereodynamic effect, we expand the strategy to understand the transition to *sub*-Arrhenius behaviour after simple halogen replacement. As in previous cases, we perform a blend of first-principle on-the-fly BornOppenheimer molecular dynamics thermalized at four temperatures (0,50, 200, 350 and 500 K) and high-level TransitionState-Theory modified to account quantum tunnelling conditions. The theoretical rate constants calculated with Bell tunnelling corrections are found to be in good agreement with extensive experimental data available for this reaction in the ample temperature range from 200 to 2000 K using an insightful approach more direct than previous treatments. Additionally, the Born-Oppenheimer molecular dynamics simulations showed that the role of molecular orientation process in promoting this reaction is minor than in the previous cases and with respect to that of quantum mechanical penetration through the of energy barrier along the reaction path on the potential energy surface. The discussion of these results provides clarification of the occurrence of the different non-Arrhenius mechanisms involved in the series of reactions.

My contribution in this study was to perform Born-Oppenheimer molecular dynamics simulation and perform all relevant analyzes, as well as to contribute to the discussions and writing of the paper. Thank you very much to the other authors who contributed to the development of this investigation. Thank you to Flavio Olimpo Sanches Neto by theoretical calculations of the rate constant, to professor Valter H. Carvalho Silva, Heibbe Cristhian B. de Oliveira and Vincenzo Aquilanti for the results discussions and the paper revision.

PAPER

Kinetics of the $OH + HCl \longrightarrow H_2O + Cl$ reaction: rate determining roles of stereodynamics and of quantum tunnelling

Nayara Dantas Coutinho,*[a] Flávio Olimpo Sanches-Neto [b], Valter Henrique Carvalho-Silva , [c] Heibbe Cristhian Benedito de Oliveira, [a] Luciano. A. Ribeiro[c] and V. Aquilanti [d,e]

The $OH + HCl \longrightarrow H_2O + Cl$ reaction is one of the most studied four-body systems, extensively investigated by both experimental and theoretical approaches. Here, as a continuation of our previous work on the OH + HBr and OH + HI reactions, which manifest an anti-Arrhenius behaviour that was explained by stereodynamic and roaming effects, we extend the strategy in order to understand the transition to the sub-Arrhenius behaviour occurring for the HCl case. As previously, we perform first-principles on-the-fly Born-Oppenheimer molecular dynamics, thermalized at four temperatures (0,50, 200, 350 and 500 K), but this time we also apply a high-level Transition-State-Theory, modified to account for tunnelling conditions. We find that the theoretical rate constants calculated with Bell tunnelling corrections are in good agreement with extensive experimental data available for this reaction in the ample temperature range from 200 to 2000 K using an insightful approach more direct than previous treatments. Therefore for the HCl case, (i) – the Born-Oppenheimer molecular dynamics simulations show that the roles of molecular orientation in promoting this reaction and of roaming in finding the favourable path are minor than in the HBr and HI cases, and (ii) – dominating is the effect of quantum mechanical penetration through the energy barrier along the reaction path on the potential energy surface. The discussion of these results provides clarification of the origin on different non-Arrhenius mechanisms observed along this series of reactions.

Introduction

Experimental and theoretical background. The $OH + HCl \longrightarrow H_2O + Cl$ reaction plays an important role in atmospheric chemistry: for example, it belongs to a class of processes producing halogen atoms, responsible for disturbing the natural equilibrium established by creation and destruction of ozone. From a fundamental view point, this elementary reaction is of basic relevance for both experimental and theoretical chemical kinetics. At variance with Arrhenius law, the experimental rate constants for this reaction[1–10], when extended to low temperatures, show a strong concave curvature in the Arrhenius plot, a phenomenon designated as sub-Arrhenius behaviour[11,12]. There is general consensus in the literature that often processes exhibiting sub-Arrhenius behaviour are those intrinsically dominated by the quantum tunnelling effect of penetration of an energy barrier along the reaction path on the potential energy surface[13,14]. Further information on the OH + HCl reaction regards the observation of a large primary kinetic isotope effect[10].

From a theoretical perspective, much effort has been dedicated to obtain the potential energy surface (PES) and to calculate the rate constants for this reaction. Recently, the Schaefer group obtained a potential energy profile of the OH + HCl reaction by the CCSD(T) method with correlation consistent basis sets through cc-pVQZ, showing energy, geometry and frequencies for five stationary points along the reaction path[15]. The Guo group calculated a full-dimensional global PES generated by fitting ca. 25,000 multi-reference configuration interaction points using a permutation invariant polynomial method[16]. Later, they calculated thermal rate constants for a wide range of temperature using the ring-polymer molecular dynamics and observed deviation from Arrhenius behaviour for the available experimental data at low temperatures[17].

In order to improve the accuracy of their full-dimensional global PES, the Guo group fitted a new set of ab initio points obtained by (UCCSD(T)-F12b/AVTZ) and calculated the rate constants by canonical variational transition state theory. The authors found a barrier for forward reaction lower than that of the previous PES[16] obtaining for the rate constants a better agreement with experimental values, at least for high temperatures; however for low temperatures the disagreement was still significant[18]. More recently, the Guo Group19 presented a study using ring polymer molecular dynamics (RPMD) for both the OH + HCl reaction and its deuterated analogue OH + DCl . The calculated RPMD rate constants are in good agreement with experimental data confirming the accuracy of the potential energy surface. An additional recent information on the reaction between OH and HCl is the investigation of the catalytic effect of NH3 and HCOOH: both

sub-Arrhenius and anti-Arrhenius plots were found for rate constants, depending of the reactive channel analysed[20].

Using the quasi-classical trajectory method, the Guo group showed that for the OH + HCl reaction, the vibrational excitation of the HCl reactant greatly increases the reactivity, while the OH vibrational acts essentially as a spectator[21]. This result was indicated as contradicting the Polanyi's rule, which suggests that the translational energy is more efficient than vibrational energy in enhancing an early barrier reaction: the authors elucidated this violation by a sudden vector projection model, which attributes the promotional effect of the HCl vibration mode to its strong coupling with the reaction coordinate at the transition state[21–23].

The present approach. Relevant from our view point are the quasi-classical trajectory calculations by Bonnet *et al.*[24,] who demonstrated unexpected reaction pathways involving strong reorientation of the reagents, and showed that the most important channels were far from the minimum energy reaction path. They propose a dynamical extension of the notion of cone of acceptance to rationalize the stereodynamic effects.[24] These effects largely ignored previously are central to our appreciation of the understanding of the microscopic reaction dynamics.

An alternative source of important information comes from molecular beam scattering experiments with oriented reactants[25], however limited to the non-reactive case: Cireasa and collaborators[26] report stereodynamical features in the inelastic collisions between OH and HCl molecule, showing that H-end attack is favoured for the inelastic collision system. They define a "steric asymmetry factor" and found it negative, in contrast with the analogous four-body reaction, OH + HBr, for which the O-end attack is more favourable by a factor three over that at the H-end[27,28].

In our previous work[29–31], we have approached the study of the steroselective mechanism of the OH + HBr and OH + HI reactions using first-principles Born-Oppenheimer molecular dynamics. We have shown how molecular reorientation occurs in order that the reactants encounter a mutual angle of approach favourable for them to proceed to reaction. Therefore, the demonstration of the crucial role of stereodynamics, additional documentation was also provided on the interesting manifestation of the roaming phenomenon, regarding both the wandering of the reactants in the search of the reactive configurations sterically favourable to reaction and also the involvement of vibrational excitation of products in their subsequent departure.

Here, the strategy that we follow to tackle the sub-Arrhenius mechanism and to explain the combined role of stereodynamic and quantum mechanical tunnelling effects employed both (i) the Born-Oppenheimer molecular dynamics technology, whereby numerical experiments are carried out, simulating the reaction in a box, where the reactants explore the potential energy surface at a specified temperature (enforced by a Nosé-Hoover thermalizing bath), and (ii) a high-level Transition-State-Theory upon which a careful treatment is implemented to describe the deep tunnelling characteristics of this process. Accordingly, the following treatment is divided in two parts, dealing first with stereodynamics and second with quantum tunnelling dominated rates. A final section is devoted to additional and concluding remarks.

I Part One: stereodynamics

I-1 On-the-fly Molecular Dynamics

The first-principles Born-Oppenheimer Molecular Dynamics (BOMD) simulations were carried out using the Car-Parrinello MD 3.17.1 package.[32] The reaction was modelled as occurring in periodically repeated cubic cells each of side-length 6 Å, where one HCl molecule and one OH radical are added and let react. The electronic structure was treated within the generalized gradient approximation to density functional theory (DFT), through the Perdew-Burke-Ernzerhofn (PBE) exchange-correlation functional.[33] Vanderbilt ultrasoft pseudopotentials were employed to represent core-valence electron interactions[34]. A plane-wave basis set was used to expand the valence electronic wave function with an energy cutoff of 25 Ry. The equations of motion were integrated using the Verlet scheme with a time step of 4 au (0.121 fs) and a total time of 2 ps. The temperatures of the system were controlled by the Nosé-Hoover Thermostat scheme[35] at 50, 200, 350 and 500 K. At each temperature, 60 trajectories were simulated with different initial configurations, as detailed next.

I-2 Representation of Stereodirectional dynamics

Fig. 1 illustrates our choice of coordinates for this discussion of the $OH + HCl \longrightarrow H_2O + Cl$ reaction. Two of the six coordinates needed for specifying a four-body configuration are utilized here for exhibiting the stereodirectional effect on the molecular dynamics: they are the bond length r_1 and the angle θ . Their values are fixed at the start of the simulations and serve to identify the trajectories in the following presentation. We used the 60 initial configurations with characterizing values listed in Table I.

The initial settings have been selected according to the following criteria: r_1^0 ranging from 1.7 to 3.2 Å with steps of 0.3 Å and θ_0 ranging from 0 to 180° with a 20° increment; all other coordinates were obtained randomly, within limits that guaranteed realistic initial configurations of the system. In the initial configurations, two other variables are held fixed for all cases, the HCl bond length at 1.27 Å and the OH2 bond length at 1.0 Å. Two of the other needed coordinates are chosen randomly among the three parameters: ϕ (degrees), τ(degrees) and R(Å): since a four-body configuration is represented by six parameters, one of them is superfluous but is convenient for internal check. The difference among this Table and the corresponding ones for the HBr and HI[29–31] cases are essentially due to the differences in the bond lengths of the hydrogen halides.

Table 1 Initial values of the coordinates for all trajectories, arranged as a function of the stereodynamical angle, θ_0, and the distance r_1^0. The initial values for ϕ (degrees), τ (degrees), and R (Å), are the entries of the table in this order.

r_1^0(Å)					
1.7	2.0	2.3	2.6	2.9	3.2
60, *145*, **1.53**	158, *129*, **3.21**	115, *127*, **3.06**	60, *130*, **2.25**	117, *124*,**3.66**	173, *123*, **4.46**
144, *-20*, **2.83**	127, *66*, **2.95**	78, *-28*, **2.38**	60, *132*, **2.25**	107, *0*, ***3.49***	169, *82*, **4.45**
129, *169*, **2.69**	102, *-100*, **2.58**	138, *-14*, **3.35**	111, 39, **3.28**	60, *-79*, **2.52**	132, *-168*, **4.16**
92, *97*, **2.16**	117, *52*, **2.81**	134, *21*,**3.31**	151, *-90*, **3.76**	163, *128*, **4.13**	158, *-60*, **4.40**
177, *-149*, **2.97**	167, *114*, **3.25**	179, *47*, **3.57**	168, *120*, **3.85**	60, *113*, **2.52**	60, *28*, **2.79**
175, *-151*, **2.97**	126, *-5*, **2.94**	145, *157*, **3.42**	60, *-146*, **2.25**	60, *-168*, **2.52**	128, *-158*, **4.10**
145, *-107*,**2.84**	162, *20*,**3.23**	60, *-26*, **2.00**	60, *95*,**2.25**	60, *-111*, **2.52**	60, *-21*, **2.79**
145, *-147*, **2.84**	121, *97*, **2.87**	117, *-130*, **3.10**	95, *20*, **2.99**	120, *61*, **3.71**	122, *163*, **4.03**
173, *-125*, **2.96**	179, *172*, **3.27**	141, *170*, **3.38**	169, *130*, **3.85**	60, *97*, **2.52**	113, *-109*, **3.88**
60, *-76*, **1.53**	65, *-83*, **1.87**	*124, 89,* ***3.19***	78, *-93*, **2.65**	138, *-102*, **4.94**	160, *171*, **4.42**

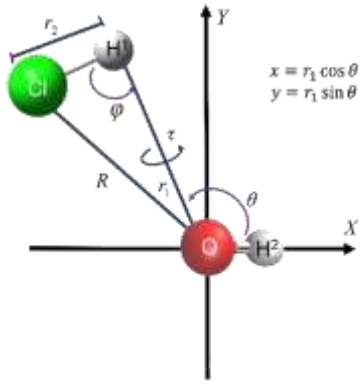

Fig. 1. Definitions of geometrical parameters for the configuration of the present four-atom process suited to extract stereodynamical information from the role of the mutual direction between approaching reactants. The origin is on the oxygen atom, and the OH bond, of length r_2 , lies in the X axis, whereas Y is the axis perpendicular to X in the ClOH[2] plane oriented as in the figure. The initial configurations are identified (Table 1) by a zero affix, namely, by the vector length r_1^0 and the angle θ_0 or by the vectors components x_0 and y_0 on the X and Y axes.

The monitoring of reactive trajectories was made by the coordinate s, defined as the difference between the length of the bond that is broken and the length of the bond that is formed, i.e, $s = r_2 - r_1$. Negative values of s correspond to the configuration of reagents, positive values to those of the products. As a characteristic signature of the completion of the reactive event we can consider the moment that reaction occurs by $s = 0$ denoted by us as the "switching" time. The exchange rate for the reaction is conveniently defined as the inverse of the "switching" time.

The correlation between the initial configuration and the propensity to reaction is illustrated in Fig. 2 and in Tables II-V at the simulated temperatures. In the tables, the exchange rates are given as functions of r_1^0 and θ_0 and in Fig. 2 in the plane of the Cartesian components of the r_1 vector, $x_0 = r_1^0 \cos\theta_0$ and $y_0 = r_1^0 \sin\theta_0$. The number of reactive events change with temperature: at 50 K it was observed that 31 trajectories lead to products, while at 200, 350 and 500 K the number of reactive events was almost the same, 45, 44 and 43, respectively. The peak of reactivity is seen for x_0 between -1 and 1 Å and for y_0 in the 1-2 Å range, manifesting propensity to react for θ_0 angles in the 60-120° range. However, the dependence of reactivity on the stereodirectionality is markedly lower than observed for HBr and HI. The memory of the initial configuration appears to be lost during the reactive process, arguably because of the manifestation of roaming effect. This effect was previously documented for the OH + HBr and OH + HI reactions: for those cases, the roaming effect was less pronounced than here[29,30].

Table 2 Exchange rates (ps-1, see Text) for reactive trajectories for 50 K. Zero entries correspond to non-reactive trajectories.

θ_0 (degrees)	r_1^0(Å)					
	1.7	2.0	2.3	2.6	2.9	3.2
0	0	1.98	0	0	0	0
20	12.41	9.51	3.57	0	0	0
40	18.02	7.81	9.73	8.57	0.55	2.85
60	16.03	23.47	12.14	4.63	0	0
80	108.70	5.51	0	0	0.94	4.27
100	0	28.41	6.72	0	0	0
120	129.87	17.30	3.61	0	0	0
140	52.63	32.68	18.76	0	6.13	0
160	28.49	7.96	0	0	0	0
180	0	0	10.20	9.26	0	0

The origin of roaming as a rearrangement between weakly bound reactants is connected to high-lying regions of the ground state potential energy surfaces[36,37] and indicated in Refs.[38–40]. Typically, these regions involve molecular configurations far from the transition state geometry and are propitiated by pronounced bond elongations, such as manifested when on the way to reaction systems are emerging from nonadiabatic paths involving conical intersections. From Tables II-V, we observe analogously that in our case "roaming" is favoured by starting trajectories at elongated r_1^0.

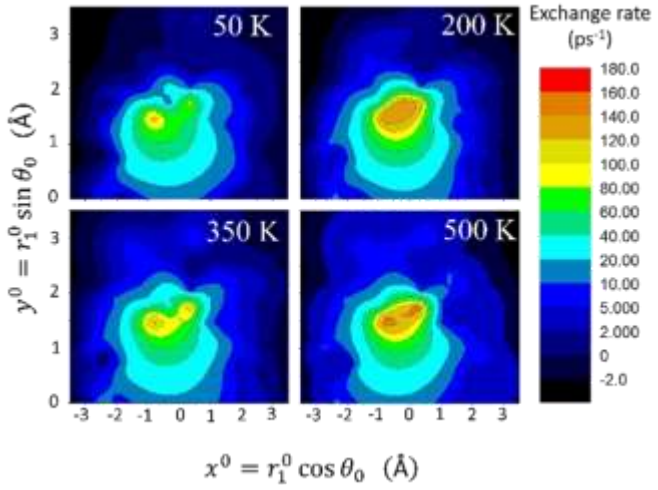

Fig. 2. Contour plots of reactivity data, the latter estimated on the assumption that the velocity of reaction can be correlated to the "switching time", namely, to the moment when $r_1 = r_2$. Its inverse (see text), is defined as "exchange rates" and can be extracted from entries of Tables II- V.

Fig. 3 shows the evolution of the stereodynamical angle, θ, versus the reaction coordinate s. We selected a total of 24 trajectories which best represent the important role of the stereodynamical angle in the reactive process. It can be seen that when the simulation is started with those values of θ_0 close to that leading to the formation of the bond angle of water ($\theta_w \sim 104°$), the system finds an easier way to products. However, there are trajectories that experience difficulty in finding the favourable approaching angle for reactivity, evidencing again the "roaming" effect. Additionally, it has to be noted how the final energy appears to dispose as excitation in the bending mode of the product water, as is visually clear to a much greater extent again for the higher temperatures (see Ref.37 for experimental comparisons for an analogous case study).

The specific value of the s coordinate, indicated as $s^{\ddagger}$, marks at each temperature the estimated averaged configuration in terms of new and old bond differences, characterizing the moment in the dynamics when the water molecule can be considered as effectively formed. These values are in general higher than the previously considered values of s corresponding to $r_1 = r_2$, which were used in the preceding estimates of the exchange rates. In the next section, these values will be correlated to reaction times for each temperature, and will provide further information on the kinetic rate to be later compared with experimental and transition state theoretical ones with tunnelling corrections.

I-3 Born-Oppenheimer molecular dynamics rate constants

In general, the extraction of quantitative information on rate constants from molecular dynamics simulations is an important issue but a very difficult one to be tackled. A direct approach to estimate rate constants was suggested and tested in the previous works[30,31] and is based on the rate of formation of a product, water in this case; being the bimolecular process OH + HCl of the second order, the general formula for the rate constants can be written:

$$k = \frac{\mathrm{d}[\mathrm{H_2O}]}{\mathrm{d}t}([\mathrm{OH}][\mathrm{HCl}])^{-1}$$

as the ratio of the rate of formation of water and the product of the initial concentrations of the two reactants. In our numerical experiments, the concentration for each reactant is [C] ~ $5\text{x}10^{21}$ molecules.cm^{-3}. The formation of water is "observed" in our first-principles nanoreactor as the appearance of one product molecule in the volume of the box, *i.e*. [C] times the fraction f of reactive *versus* total trajectories and emerging at the 'transition time', $t^{\ddagger}$:

$$\frac{\mathrm{d}[\mathrm{H_2O}]}{\mathrm{d}t} = \frac{f[\mathrm{C}]}{t^{\ddagger}}$$

These quantities can be estimated from tables II-V and Figure 3, generating rate constant information to be compared to the experiments and theoretical ones discussed in the next part.

II PART TWO: RATE CONSTANTS AND TUNNEL

II -1 Stationary Electronic Structure Calculations

The electronic structure properties of reactants, of products and of the transition state were calculated at MP2/6-311++G(d,p) and MP2/aug-cc-pVTZ (for deuterated case) level of theory. For the stationary points analytic harmonic frequency

Table 3 Exchange rates (ps-1, see Text) for reactive trajectories for 200 K. Zero entries correspond to non-reactive trajectories.

θ_0 (degrees)	r_1^0(Å)					
	1.7	2.0	2.3	2.6	2.9	3.2
0	7.01	1.95	3.63	1.51	0	0
20	6.29	1.42	5.59	2.51	0	0
40	20.24	3.58	13.74	1.49	2.72	2.70
60	13.33	22.88	15.20	7.44	0	0
80	136.99	6.98	0	0	1.39	2.54
100	147.06	39.06	8.59	1.62	5.16	0
120	149.25	22.12	10.32	7.72	5.72	2.72
140	53.48	36.63	21.69	11.56	7.81	0
160	27.10	13.02	0	0	12.27	0
180	1.65	1.87	15.58	9.32	0	0

calculations were performed: the absence or the existence of one imaginary frequency characterize each of the optimized structure either as a local minimum or as a transition state, respectively. The zero-point vibrational energy contributions were considered in the calculations of the barrier.

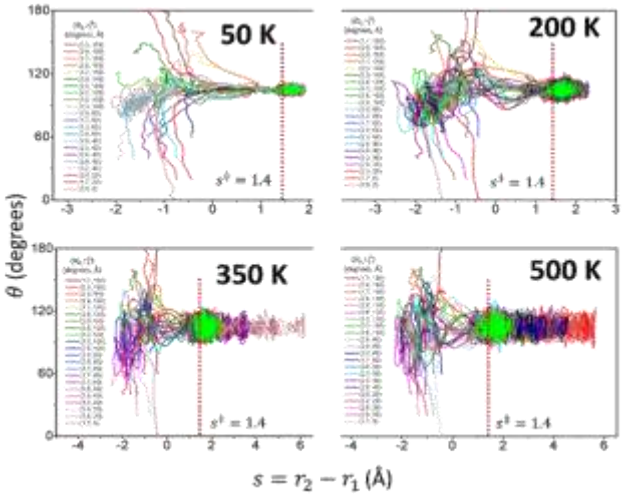

Fig. 3. Evolution at four temperatures of the stereodynamical angle of approach θ (Fig.1) for "canonical" trajectories versus the reaction coordinate $s = r_2 - r_1$, conveniently defined as the difference between the lengths of the bond which is broken r_1 and of the bond which is formed r_2. The number of reactive trajectories changes with temperature. The trajectories are distinguished by different colors as listed in the right panel and arranged in decreasing order of θ_0, the initial values for the θ angle; the other value characterizing the trajectory is that of r_1^0; the other parameters defining the initial configurations can be extracted by the corresponding entries in Table 1. Indicated by arrows is the value of $s^{\ddagger}$, identified by averaging for all trajectories of a given temperature the values of the reaction coordinate $s = r_2 - r_1$ for which a water molecule can be considered as formed

II-2 Theoretical Rate Constants

The Transition State Theory is arguably the most popular procedure to study the kinetics of chemical reactions from the theoretical point of view. The general idea of the theory lies in considering activated complexes in "quasi-equilibrium" with reactants. The rate of transformation is, then, obtained by a mix of considerations of thermodynamics, of kinetic theory and of statistical mechanics. For a general bimolecular reaction such as $R_1 + R_2 \longrightarrow TS^{\dagger} \longrightarrow$ Products, it is necessary to compute the partition functions Q_1, Q_2 and $Q^{\dagger}$ of reactants 1 and 2 and of the transition state, respectively. At absolute temperature T, the rate constant is given by:

$$k^{TST} = \frac{k_B T}{h}\frac{Q^{\dagger}}{Q_1 Q_2}\exp\left(-\frac{E_0}{k_B T}\right), \quad (1)$$

where k_B is Boltzmann's constant; h is Planck's constant; and E_0 is the effective height of the energy barrier, here given by:

$$E_0 = V + \varepsilon_{ZPE} \quad (2)$$

where ε_{ZPE} is the harmonic zero-point energies and V is the potential energy barrier height.

The analysis of Ref. [41] indicates that the tunnelling regimes can be characterized according to the crossover temperature parameter ($T_c = h\nu^{\dagger}/2\pi k_B$) as: classical ($T > 4T_c$), negligible($4T_c > T > 2T_c$), moderate ($2T_c < T < T_c$) and deep ($T < T_c$). We first apply the deformed-transition-state theory (d-TST - k_d^{TST})14 formula:

$$k_d^{TST} = \frac{k_B T}{h}\frac{Q^{\dagger}}{Q_1 Q_2}\left(1 - d\frac{E_0}{k_B T}\right)^{1/d}, \qquad d = -\frac{1}{3}\left(\frac{h\nu^{\dagger}}{2E_0}\right)^2 \quad (3)$$

that covers uniformly the range from classical to moderate tunnelling regimes but is inadequate for deep tunnelling. In (3), $\nu^{\dagger}$ is the imaginary frequency for crossing the barrier and d is the "deformation parameter". To cover the moderate-to-deep tunnelling transition, we apply both the Bell-1935 and the Bell-1958 corrections[41].

$$k_d^{TST} = \frac{k_B T}{h}\frac{Q^{\dagger}}{Q_1 Q_2}\left(1 - d\frac{E_0}{k_B T}\right)^{1/d}, \qquad d = -\frac{1}{3}\left(\frac{h\nu^{\dagger}}{2E_0}\right)^2 \quad (3)$$

$$\kappa_{Bell\ 1935} = \frac{\left[\frac{E_0}{\hbar\nu^{\dagger}} - \frac{E_0}{k_B T}\exp\left(\frac{E_0}{k_B T} - \frac{E_0}{\hbar\nu^{\dagger}}\right)\right]}{\frac{E_0}{\hbar\nu^{\dagger}} - \frac{E_0}{k_B T}} \quad (4)$$

Table 4 Exchange rates (ps-1, see Text) for reactive trajectories for 350 K. Zero entries correspond to non-reactive trajectories.

θ_0 (degrees)	r_1^0(Å)					
	1.7	2.0	2.3	2.6	2.9	3.2
0	7.58	0	3.85	7.18	0	0
20	6.48	1.56	5.76	3.99	0	0
40	20.28	4.84	7.63	4.26	2.18	4.32
60	7.28	18.83	14.64	8.32	0	0
80	142.86	3.07	0	0	8.94	4.68
100	27.17	37.59	11.95	3.45	5.19	0
120	149.25	24.10	12.11	5.23	6.76	6.50
140	44.05	35.97	22.78	10.94	9.68	0
160	26.81	10.03	0	0	14.41	0
180	7.42	2.77	16.89	12.52	0	0

$$\kappa_{Bell\ 1958} = \frac{\left(\frac{\hbar\nu^{\dagger}}{2k_B T}\right)}{\sin\left(\frac{\hbar\nu^{\dagger}}{2k_B T}\right)} - \frac{E_0 \exp\left(\frac{E_0}{k_B T} - \frac{E_0}{\hbar\nu^{\dagger}}\right)}{\left(\frac{E_0 k_B T}{\hbar\nu^{\dagger}} - E_0\right)} \qquad (5)$$

that, although non-uniform across the transition between negligible and moderate tunnel regimes were found to behave smoothly enough to adequately perform practically astride the whole range.

More details about this treatment can be found in Ref. [14]. A code to compute the kinetic rate constants with tunnelling corrections has been developed in script-shell language and is available in ESI.

II-3 Rate constants and comparison with experiments

The rate constants for reaction between the hydroxyl radical and hydrogen chloride are only slightly independent of temperature in the range 138-300 K, although, as temperature increases a positive temperature dependence is observed. This strong concave curvature detected in the Arrhenius plot (*sub*-Arrhenius behaviour) is the most convincing evidence of the role of deep quantum tunnelling for this reaction. Procedures to account for the tunnelling effect consist in incorporating corrections to the rate constants obtained by the TST approach sketched in the previous section: As we mentioned, our choice is to employ the *deformed*-Transition State Theory (*d*-TST) and both the Bell-1935 and Bell-1958 formulas to calculate the kinetic rate constants for the OH + HCl reaction in a wide range of temperatures (200 – 2000 K) at the MP2/6-311++G(d,p) calculation level. The geometries, energies and frequencies necessary to compute the rate constants are available in Supplementary Information.

A comparison between the calculated rate constants with experiments and previous theoretical works is shown in Fig. 4. No major differences were found using either the Bell-1935 or Bell-1958 formulas: also, it can be seen that both formulations, involving minimal effort with respect to much more elaborated treatments, can estimate with satisfactory agreement the rate constants of the reaction for the whole wide range of investigated temperatures. On the other hand, as expected, the *d*-TST does not describe the range of experimental data for low temperature, where tunnelling effects become more dominant, because its validity is limited to weak tunnelling[14,42]. In the lower panel in Fig. 4, we also show rate constants for the isotope substituted reaction, OH + DCl , obtained with the Bell and d -TST formulas at MP2/aug-cc-pVTZ level of calculation. Our results are in reasonable agreement with previous experimental and theoretical values[19].

ADDITIONAL REMARKS AND CONCLUSIONS

Rates from on-the-fly dynamics. Estimates of rate constants from Born-Oppenheimer molecular dynamics simulations were obtained as in Sec. I-3 of this paper. The fractional number of reactive trajectories f are extracted from Tables II-V and the resulting values of the transition time $t^{\ddagger}$ for each temperature from Fig. 3, as follows.

Since the transition time $t^{\ddagger}$ is meant to represent the average time that elapses for the chemical reaction to take place in our computational "nanoreactor", for its present evaluation we searched for the moments along trajectories (as depicted in Fig. 3) when the evolution coordinate s corresponded to the emergency of water as a product. Average values of s for each temperature are denoted $s^{\ddagger}$ and highlighted in the plots in Fig. 3. For all temperatures the value of $s^{\ddagger}$ was found to be around 1.4 Å; and of $t^{\ddagger}$ are available in Supplementary Information.

As documented in the HBr case, the rate constants k obtained from Born-Oppenheim molecular dynamics turned out larger than the experimental rate constant ones. As discussed there[30], one crucial reason is arguably the fact that the choice of initial conditions (reactants in a small box with close encounters) increases chances of reactive *versus* total collisions and the reaction process may be occurring in a shorter time than it would in real conditions. This points out at the general need to calibrating a first-principles nanoreactor against experimental results. A way, as in this case, is offered when experimental data are available. We note that the ratio k_{exp}/k scales as ca. 2.43x10^{-4}T, *i.e.,* linearly with temperature. If the factor, 2.43x10^{-4}, obtained by averaging over the three available temperatures (200, 350 and 500 K), is used to calibrate performances of the present nanoreactor, a recalculation of rate constants gives the results as presented in the upper panel of Fig. 4. Compared to our previous works, the better agreement with experimental data was obtained for the case where reactivity is larger, namely OH + HI[31], where no calibration correction was needed. This result can be taken as

Table 5 Exchange rates (ps-1, see Text) for reactive trajectories for 500 K. Zero entries correspond to non-reactive trajectories.

θ_0 (degrees)	r_1^0(Å)					
	1.7	2.0	2.3	2.6	2.9	3.2
0	0	0	4.63	3.98	3.37	0
20	6.49	3.48	6.97	9.38	0	0
40	19.53	4.65	6.56	2.17	6.44	0
60	4.99	4.62	12.41	12.29	0	0
80	151.52	6.82	0	0	10.27	5.70
100	109.89	32.15	11.49	6.55	5.30	0
120	149.25	24.88	12.92	6.29	6.04	7.94
140	44.84	34.84	22.78	10.73	10.41	0
160	27.10	0	0	0	15.41	0
180	9.42	3.43	17.21	2.93	0	0

an indication that calibration may be more demanding the lower the reactivity of the system, requiring wider exploration of phase space.

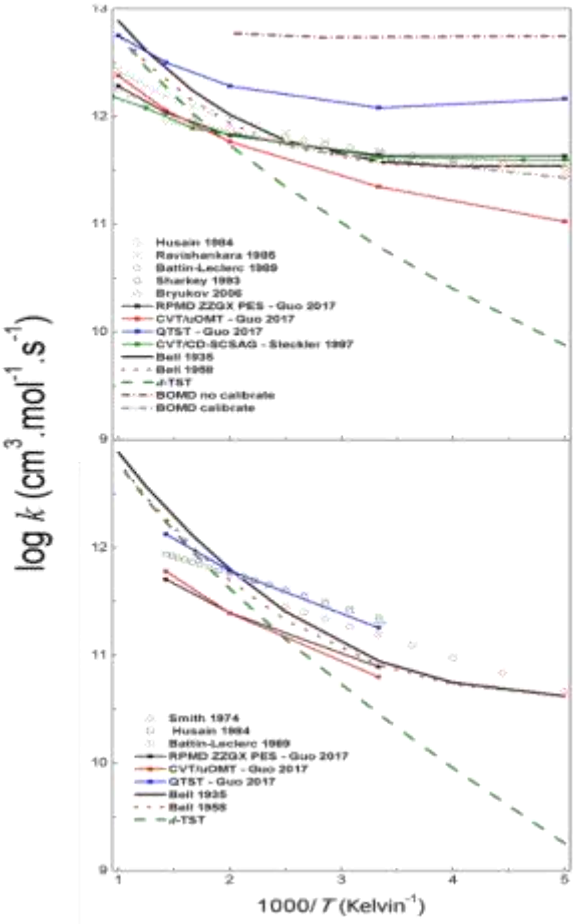

Fig.4. Reaction rate constants as a function of temperature for the $\mathrm{OH} + \mathrm{HCl} \longrightarrow \mathrm{H_2O} + \mathrm{Cl}$ (upper panel) and $\mathrm{OH} + \mathrm{DCl} \longrightarrow \mathrm{HOD} + \mathrm{Cl}$ (low panel). We present the estimated rate constant obtained from Born-Oppenheimer molecular dynamics (see text and Table 6). For comparison theoretical and experimental results are included in both panels.

Potential energy profiles for the OH-hydrogen halide series. To document and discuss the transition from anti-Arrhenius to sub-Arrhenius behaviours, here we put into perspective the reaction of OH with the series of halogen hydrides. Fig. 5, top panel, shows a schematic view of the potential energy surface profile for the four cases: it is reconstructed from data in Ref. [43], where the main focus was actually on the inverse reactions. The reaction among hydroxyl radical with hydrogen iodine, hydrogen bromide and hydrogen chloride are highly exothermic, with ΔH^0 equal a -47.9, -31.7 and -16.1 Kcal/mol44, respectively, while the reaction with hydrogen fluoride is endothermic (ΔH^0 =17.6 kcal/mol)44. These differences reflect the fact that the energy of dissociation of HF is much larger than that for the other hydrogen halides and decreases moving to the heavier halogens. The PES for the four reactions show an entrance complex, a barrier and an exit complex in the exit channel: their energies change substantially along the series from HF to HI. The transition-state barrier has positive energy values for HF and the HCl cases, while for the other two reactions the transition state is energetically lower than the reactants (apparent negative activation energy).

The anisotropic forces generated by electrostatic and dispersion interactions between reactants promote the formation of the wells in the entrance channels in the PES. However, differently from the entrance channel complex (HO---HX), the origin of stability of the exit channel complex (X---H2O) cannot be explained by electrostatic or dispersion interactions, since neither the geometry nor the energy encodes with this type of interactions. Ref. [45] showed strong evidence that the interactions between halogens and water has a covalent origin due to two-center-electron bond formed between the unpaired electron of the halogen atom and a lone pair of H_2O.

Rates for the OH-hydrogen halides series. The low panel of Fig. 5 shows the comparison of the rate constants of the reactions of OH with HCl, HBr and HI (for the endothermic OH + HF reaction there are no kinetic data available). As can be seen, among the three reactions, the HI reactant is found to exhibit the highest reactivity in the range of available temperature and HCl the lowest. Additionality, the reaction between HCl and OH has a sub-Arrhenius behaviour, while the other two cases have an anti-Arrhenius behaviour.

The reactivity of the chemical reactions is controlled by the relative orientation of the reagents and by the height of the barrier to reaction. More specifically, for the OH + HCl reaction, the Born-Oppenheimer molecular dynamics simulations show that the orientation process play a minor role, so that the increase of the temperature favours the reactive process, while below the cross-over temperature, it is observed that reactivity remains flat as the temperature decreases, a signature of the tunnelling effect. At low temperature, the anisotropy of long-range interaction forces provides the orientation of reactants favouring the formation of the OH---HCl complex. It could have been expected that the complex formation delayed the reactive process: however, this complex carries an excess of internal energy, that may be used to overcome the reaction barrier, increasing thus the tunnelling efficiency, and consequently, the probability of effective collisions. As the temperature increases, the number of reactive process that visit the entrance complex decreases: accordingly, at high temperature, this system is much less sensitive than the HBr and HI cases to the reaction profile along the potential energy surface.

For the reactions showing an *anti*-Arrhenius behaviour (the HBr and HI cases), stereodynamics plays an important role for reactivity. We have shown in previous work[29,30] that at low temperature in both these cases the reactants reorient to find the propitious alignment leading to reaction: along this orientation process, an entrance channel complex is formed, requiring an adjustment progressively less effective the higher the kinetic energy.

The reactions of OH with HF and H_2. The orientation effect manifesting as stereodynamical and roaming features, is of interest for the reactions between OH radical and the hydrogen halides: however, the role along the series differs, since it competes with the kinetic energy of reactants, which is highly influenced by the profile of the PES. The reaction between OH and HF is very endothermic and high barrier, considering

probable is the relevance of non-adiabatic processes and the reactivity is so low that there is a lack of reliable kinetic experimental values[46,47].

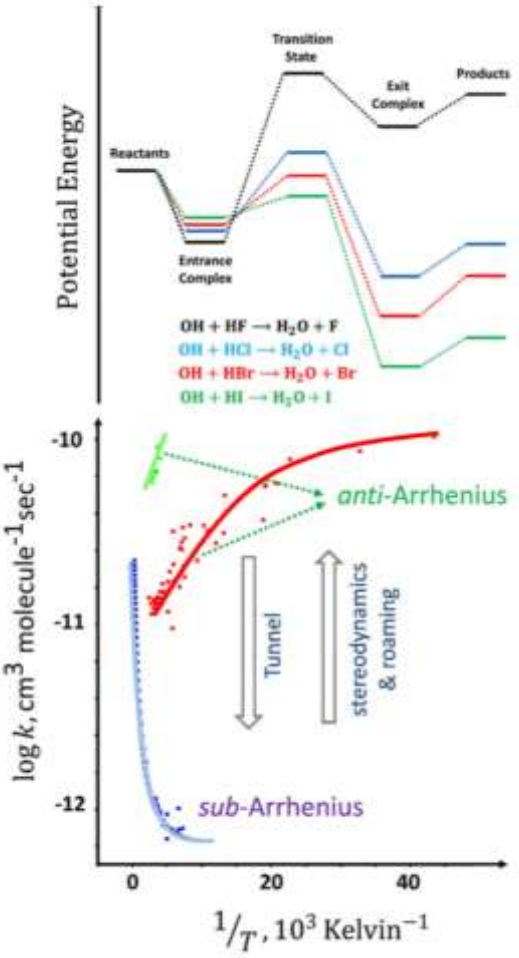

Fig. 5. Pictorial view of comparing schematically the stationary points on the potential energy surfaces for the $OH + HX \longrightarrow H_2O + X$ (X= Halogen), adapted from Ref. [43]. The influence of tunnelling effect increases from HI to HF and that of sterodynamics increases in the opposite direction (see opposite arrows in the upper panel). In the lower panel, experimental available rate constants44 are presented: they witness, the transition from anti-Arrhenius (HI and HBr) to sub-Arrhenius behaviour. To our knowledge, there are no experimental values for the OH + HF reaction.

Therefore, additional strategies may be invoked to describe this case. However, the understanding obtained with the analogous reactions strongly suggests a sub-Arrhenius behaviour under moderate quantum tunnelling. Situation is similar to the reaction of OH and H_2, much studied experimentally and theoretically because of its simplicity: in a sense, it can be included in this series of OH + HX reaction when X=H. As expected, we have verified using present techniques together with path integral formulations that tunneling is the only mechanism for low temperature reactivity. In view of the so low number of electrons involved, we were able to observe that addition of water molecules enhances reactivity[48].

Conflicts of interest

In accordance with our policy on Conflicts of interest please ensure that a conflicts of interest statement is included in your manuscript here. Please note that this statement is required for all submitted manuscripts. If no conflicts exist, please state that "There are no conflicts to declare".

Acknowledgements

The authors are grateful for the support given by CAPES and CNPq. Valter H. Carvalho-Silva thanks FAPDF for research funding programs. Research developed with support of the High Performance Computing Center at the Universidade Estadual de Goias (UEG).

Notes and references

1 1 I. W. M. Smith and R. Zellner, *J. Chem. Soc. Faraday Trans.*, 1973, **8**, 1045–1056.
2 2 M. S. Zahniser and F. Kaufman, *Chem. Phys. Lett.*, 1974, **27**, 507–510.
3 3 L. F. Keyser, *J. Phys. Chem.*, 1984, **88**, 4750–4758.
4 4 M. Molina, L. Molina and C. Smith, *Int. J. Chem. Kinet.*, 1984, **16**, 1151–1160.
5 5 D. Husain, J. M. C. Plane and N. K. H. Slater, *J. Chem. Soc. Faraday Trans. 2*, 1981, **77**, 1949–1962.
6 6 A. R. Ravishankara, P. H. Wine, J. R. Wells and R. L. Thompson, *Chem. Phys. Lett.*, 1985, **17**, 1281–1297.
7 7 I. W. M. Smith and M. D. Williams, *J. Chem. Soc. Faraday Trans. 2 Mol. Chem. Phys.*, 1986, **82**, 1043–1055.
8 8 P. Sharkey and I. W. M. Smith, *J. Chem. Soc. Faraday Trans.*, 1993, **89**, 631–637.
9 9 F. Battin-Leclerc, I. K. Kim, R. K. Talukdar, R. W. Portmann, A. R. Ravishankara, R. Steckler and D. Brown, *J. Phys. Chem. A*, 1999, **103**, 3237–3244.
10 10 M. G. Bryukov, B. Dellinger and V. D. Knyazev, *J. Phys. Chem. A*, 2006, **110**, 936–943.
11 11 V. Aquilanti, K. C. Mundim, S. Cavalli, D. De Fazio, A. Aguilar and J. M. Lucas, *Chem. Phys.*, 2012, **398**, 186–191.
12 12 S. Cavalli, V. Aquilanti, K. C. Mundim and D. De Fazio, *J. Phys. Chem. A*, 2014, **118**, 6632–6641.
13 13 V. H. C. Silva, V. Aquilanti, H. C. B. De Oliveira and K. C. Mundim, *Chem. Phys. Lett.*, 2013, **590**, 201–207.
14 14 V. H. Carvalho-Silva, V. Aquilanti, H. C. B. de Oliveira and K. C. Mundim, *J. Comput. Chem.*, 2017, **38**, 178–188.
15 15 Y. Guo, M. Zhang, Y. Xie and H. F. Schaefer, *J. Chem. Phys.*, 2013, **139**, 10–14.
16 16 J. Li, R. Dawes and H. Guo, *J. Chem. Phys.*, 2013, **139**, 74302.
17 17 J. Zuo, Y. Li, H. Guo and D. Xie, *J. Phys. Chem. A*, 2016, **120**, 3433–3440.
18 18 J. Zuo, B. Zhao, H. Guo and D. Xie, *Phys. Chem. Chem. Phys.*, 2017, **15**, 9770–9777.
19 19 J. Zuo, C. Xie, H. Guo and D. Xie, *J. Phys. Chem. Lett.*, 2017, **8**, 3392–3397.
20 20 S. Mallick, S. Sarkar, B. Bandyopadhyay and P. Kumar, *J. Phys. Chem. A*, 2018, **122**, 350–363.
21 21 J. Li, J. C. Corchado, J. Espinosa-Garcia and H. Guo, *J. Chem. Phys.*, 2015, **142**, 84314.
22 22 H. Song and H. Guo, *J. Phys. Chem. A*, 2015, **119**, 826–831.
23 23 H. Guo; and K. Liu, *Chem. Sci.*, 2016, **7**, 3992–4003.

24 24 L. Bonnet, P. Larrégaray, B. Duguay, J.-C. Rayes, D.-C. Che and T. Kasai, *Chem. Soc. Japan*, 2007, **80**, 707–710.
25 25 H. Pan, K. Liu, A. Caracciolo and P. Casavecchia, *Chem. Soc. Rev.*, 2017, **46**, 7517–7547.
26 26 R. Cireasa, M. C. van Beek, A. Moise and J. J. ter Meulen, *J. Chem. Phys.*, 2005, **122**, 74319.
27 27 P.-Y. Tsai, D.-C. Che, M. Nakamura, K.-C. Lin and T. Kasai, *Phys. Chem. Chem. Phys.*, 2011, **13**, 1419–1423.
28 28 P.-Y. Tsai, D.-C. Che, M. Nakamura, K.-C. Lin and T. Kasai, *Phys. Chem. Chem. Phys.*, 2010, **12**, 2532–2534.
29 29 N. D. Coutinho, V. H. C. Silva, H. C. B. de Oliveira, A. J. Camargo, K. C. Mundim and V. Aquilanti, *J. Phys. Chem. Lett.*, 2015, **6**, 1553–1558.
30 30 N. D. Coutinho, V. Aquilanti, V. H. C. Silva, A. J. Camargo, K. C. Mundim and H. C. B. De Oliveira, *J. Phys. Chem. A*, 2016, **120**, 5408–5417.
31 31 N. D. Coutinho, V. H. Carvalho-Silva, H. C. B. de Oliveira and V. Aquilanti, *The HI + OH → H_2O + I reaction by first-principles molecular dynamics: Stereodirectional and anti-Arrhenius kinetics*, 2017, vol. 10408 LNCS.
32 32 CPMD version 3.17.1, 2012.
33 33 J. P. Perdew, K. Burke and M. Ernzerhof, *Phys. Rev. Lett.*, 1997, **78**, 1396.
34 34 D. Vanderbilt, *Phys. Rev. B*, 1990, **41**, 7892–7895.
35 35 G. J. Martyna, M. L. Klein and M. Tuckerman, *J. Chem. Phys.*, 1992, **97**, 2635–2643.
36 36 M. L. Hause, N. Herath, R. Zhu, M. C. Lin and A. G. Suits, *Nat. Chem.*, 2011, **3**, 932–7.
37 37 N. Herath and A. G. Suits, *J. Phys. Chem. Lett.*, 2011, **2**, 642–647.
38 38 P.-Y. Tsai, M.-H. Chao, T. Kasai, K.-C. Lin, A. Lombardi, F. Palazzetti and V. Aquilanti, *Phys. Chem. Chem. Phys.*, 2014, **16**, 2854–65.
39 39 A. Lombardi, F. Palazzetti, V. Aquilanti, H.-K. Li, P.-Y. Tsai, T. Kasai and K.-C. Lin, *J. Phys. Chem. A*, 2016, **120**, 5155–5162.
40 40 M. Nakamura, P.-Y. Tsai, T. Kasai, K.-C. Lin, F. Palazzetti, A. Lombardi and V. Aquilanti, *Faraday Discuss.*, 2015, **177**, 77–98.
41 41 R. P. Bell, *The Tunnel Effect in Chemistry*, Champman and Hall, London, 1980.
42 42 F. O. Sanches-Neto, N. D. Coutinho and V. H. Carvalho-Silva, *Phys. Chem. Chem. Phys.*, 2017, **19**, 24467–24477.
43 43 Y. Hao, J. Gu, Y. Guo, M. Zhang, Y. Xie and H. F. Schaefer III, *Phys. Chem. Chem. Phys.*, 2014, **16**, 2641- 2646.
44 44 NIST Chemistry Web Book.
45 45 J. Li, Y. Li and H. Guo, *J. Chem. Phys.*, 2013, **138**, 2013–2016.
46 46 J. Li, B. Jiang and H. Guo, *Chem. Sci.*, 2013, **4**, 629–632.
47 47 R. Otto, J. Ma, A. W. Ray, J. S. Daluz, J. Li, H. Guo and R. E. Continetti, *Science*, 2014, **343**, 396–399.
48 48 N. D. Coutinho, V. Aquilanti, F. O. Sanches-Neto and V. H. Carvalho-Silva, *in Press*.

4 CONCLUSIONS

In retrospect, the reactions between the hydroxyl radical and hydrogen halide are among the most studied elementary reactions, both from an experimental and theoretical point of view. The rate constants for these reactions evidence a *non*-Arrhenius behavior. While the reaction with HCl is characterized by *sub*-Arrhenius behavior, the reactions with HBr and HI are prototypes of reactions with *anti*-Arrhenius behavior and therefore have apparent negative activation energy. Here, the strategy that we followed to tackle the non-Arrhenius mechanism and to explain the combined role of stereodynamic and quantum mechanical tunnelling effects employed both the Born-Oppenheimer molecular dynamics technology, whereby numerical experiments are carried out, simulating the reaction in a box, in which the reactants explore the potential energy surface at a specified temperature (enforced by a Nosé-Hoover thermalizing bath), and a high-level Transition-State-Theory upon which a careful treatment is implemented to describe the deep tunneling characteristics of this process.

Firstly, using Born-Oppenheimer molecular dynamics, this study was able to provide an interpretation of the negative temperature dependence of the rate constant for the OH + HBr and OH + HI reactions, confirming the suggestion obtained experimentally that this phenomenon has stereodynamic origin, which until now has been neglected by theoretical studies. For the OH + HBr reaction, the analysis of simulations showed that for low temperature, the reactants reorient to find the propitious alignment leading to reaction; however, this adjustment is progressively less effective for higher temperatures. The wandering paths observed mainly for high temperature, evidence the "roaming" effect, which becomes more preponderant for higher r_1^0 (lengths of the bond that is formed) values. This process of orientation could be better understood by the analysis of the evolution of the frontier molecular orbital, HOMO, where it showed that there is a correlation between the location of the HOMO orbital and the determination of the cone of acceptance. In addition, the rate constants were phenomenologically described using *d*-Arrhenius. The Free Energy of the system in function of the temperatures of 50 and 500 K was reconstructed. This study has been able to show that the free energy profile for the temperature of 50 K represents the minimum energy path for this reaction, and that at 500 K the paths are not sensitive to this energy profile. Additionally, we propose a new methodology to extract the thermal rate constants from molecular dynamics. After calibration of the nanoreactor, the calculated rate constants were in good agreement with experimental data, at least for low temperatures.

Using the same methodology, we obtained similar conclusions for the OH + HI reaction. However, we observed that there were a smaller number of reactive trajectories and that the time required for the mutual reactant orientations for the hydrogen exchange was less than for the OH + HBr reaction. These findings suggest that the stereodynamic effect is more pronounced for the OH + HI reaction. Furthermore, the rate constants calculated from Born-Oppenheimer molecular dynamics are in excellent agreement with experimental data. And for this case calibration was not necessary.

Furthermore, the OH + HBr and OH + HI reactions are processed with a null barrier. Generally, reactions have energetic features with no threshold, leading to a lower rate constant at high temperatures. It is a matter of general knowledge that the reactivity of chemical reactions depends not only on the reaction barrier height, but also on the relative orientation of the reactants during the process. Within this context and supported by the results of the BOMD simulations, we draw the conclusion that for systems with null energy barrier, the most interfering factor in the reactive process is the stereodynamic effect. Once the reagents find a favorable orientation, the reaction occurs immediately, since there is no barrier that prevents the reaction from occurring. The Born-Oppenheimer simulations showed that for these systems the orientation process is more effective at low temperatures, and that for high temperatures this mechanism is hindered due to the high energy of the reactants. In this way, the reason for lower reactivity at high temperatures is intrinsically related to the difficulty of orientation of the reagents.

More specifically, for the OH + HCl reaction, the Born-Oppenheimer molecular dynamics simulation showed that the role of molecular orientation in promoting this reaction is minor than in the HBr and HI. The initial configurations of the system do not seem to have significant weight in the reactive process. Regardless of the simulated temperature, many initial configurations led to reactive trajectories. When making a connection between the potential energy surface and the reactional dynamic of this process, we observed that unlike the *anti*-Arrhenius reactions, in this system there is an energy barrier, and the fact that there is the effective orientation of reagents does not guarantee the reactive process. For low temperature, the long-range interaction forces provide the orientation of reactants for the formation of the OH---HCl complex. It was expected that the complex formation delayed the reactive process, since there is an energy barrier limiting the reaction, and the reactants would take time to acquire the energy needed to promote the reaction. However, this complex is generally born with an excess of internal energy, which may be used to overcome the reaction barrier. Additionally, if this internal energy it is not enough to overcome the barrier, it is increasing the probability of quantum tunneling and consequently, the probability of effective collisions increases. Thus, quantum tunneling can explain the fact that below cross-over temperature, the rate constants remain constant as temperature decreases.

In this study we also calculated the rate constants for the OH + HCl reaction by Born-Oppenheimer molecular dynamics and using high-level Transition-State-Theory modified to account for tunneling conditions. The Bell tunneling correction was in good agreement with experimental data in the entire temperature range of 200-2000 K, with minimal effort compared to much more elaborate treatments. From Born-Oppenheimer molecular dynamics it was necessary to calibrate the nanoreactor against experimental results. After calibration, the rate constants were also in good agreement with experimental data. Indeed, these results are indicative that our methodology provides at least a semi-quantitative route to the extraction of rate constants from first-principles molecular dynamics numerical experiments. Additionally, we observed that the best results were obtained for systems with higher reactivities, such as the OH + HI reaction. In this way, we conclude that the rarer and slower the reactive encounters, greater the need for calibration of the reactor.

Considering the limitations imposed by a *non*-adiabatic process and the lack of kinetic experimental values in the reaction between OH and HF, we adopted precautions to connect the *non*-Arrhenius behavior with the methodology used in this study and in previous ones. However, the understanding obtained with the analogous reaction strongly suggests a *sub*-Arrhenius behavior under moderate quantum tunneling.

Finally, we can conclude that the *non*-Arrhenius behaviors for reaction between OH radical and hydrogen halide came from the combination of stereodynamics and quantum tunneling effects. For all reactions we observed that the orientation effect is very important; however, the role of this effect has a different contribution in each system, since the kinetics of reactions is highly influenced by the potential energy surface profile.

REFERENCES

(1) Read, K. A.; Mahajan, A. S.; Carpenter, L. J.; Evans, M. J.; Faria, B. V. E.; Heard, D. E.; Hopkins, J. R.; Lee, J. D.; Moller, S. J.; Lewis, A. C.; *et al*. Extensive Halogen-Mediated Ozone Destruction over the Tropical Atlantic Ocean. *Nature* **2008**, *453* (7199), 1232–1235.

(2) Saiz-Lopez, A.; von Glasow, R. Reactive Halogen Chemistry in the Troposphere. *Chem. Soc. Rev.* **2012**, *41* (19), 6448–6472.

(3) Lilington, J. *Light Water Reactor Safety*; 1994.

(4) Zuo, J.; Zhao, B.; Guo, H.; Xie, D. Rate Coefficients of the HCl + OH → Cl + H_2O Reaction from Ring Polymer Molecular Dynamics. *J. Phys. Chem. A* **2016**, *120*, 3433–3440.

(5) Zuo, J.; Zhao, B.; Guo, H.; Xie, D. A Global Coupled Cluster Potential Energy Surface for HCl + OH ↔ Cl + H_2O. *Phys. Chem. Chem. Phys.* **2017**, *15*, 9770–9777.

(6) Ravishankara, A. R.; Wine, P. H.; Wells, J. R. The OH + HBr Reaction Revisited. **1985**, *447* (May 2012), 83–85.

(7) Sims, I. R.; Smith, I. W. M.; Clary, D. C.; Bocherel, P.; Rowe, B. R. Ultra-Low Temperature Kinetics of Neutral-Neutral Reactions - New Experimental and Theoretical Results For OH + HBr Between 295 K and 23 K. *J. Chem. Phys.* **1994**, *101*, 1748–1751.

(8) Atkinson, D. B.; Jaramillo, V. I.; Smith, M. a. Low-Temperature Kinetic Behavior of the Bimolecular Reaction OH + HBr (76−242 K). *J. Phys. Chem. A* **1997**, *101* (18), 3356–3359.

(9) Bedjanian, Y.; Riffault, V.; Le Bras, G.; Poulet, G. Kinetic Study of the Reactions of OH and OD with HBr and DBr. *J. Photochem. Photobiol. A Chem.* **1999**, *128* (1–3), 15–25.

(10) Jaramillo, V. I.; Smith, M. a. Temperature-Dependent Kinetic Isotope Effects in the Gas-Phase Reaction: OH + HBr. *J. Phys. Chem. A* **2001**, *105* (24), 5854–5859.

(11) Mullen, C.; Smith, M. A. Temperature Dependence and Kinetic Isotope Effects for the OH + HBr Reaction and H/D Isotopic Variants at Low Temperatures (53-135 K) Measured Using a Pulsed Supersonic Laval Nozzle Flow Reactor. *J. Phys. Chem. A* **2005**, *109* (17), 3893–3902.

(12) Jaramillo, V. I.; Gougeon, S.; Le Picard, S. D.; Canosa, A.; Smith, M. A.; Rowe, B. R. A Consensus View of the Temperature Dependence of the Gas Phase Reaction: OH + HBr → H_2O + Br. *Int. J. Chem. Kinet.* **2002**, *34* (6), 339–344.

(13) Takacs, G. A.; Glass, G. P. Reactions of Hydroxyl Radicals with Some Hydrogen Halides. *J.*

Phys. Chem. **1973**, *77* (16), 1948–1951.

(14) Leod, H. MAC; Balestra, C.; Jourdain, J. L.; Laverdet, G.; Bras, G. LE. Kinetic Study of the Reaction OH + HI by Laser Photolysis-Resonance Fluorescence. *Int. J. Chem. Kinet.* **1990**, *22* (1), 1167–1176.

(15) Lancar, I. T.; Mellouki, A.; Poulet, G. Kinetics of the Reactions of Hydrogen Iodide with Hydroxyl and Nitrate Radicals. *Chem. Phys. Lett.* **1991**, *177* (6), 554–558.

(16) Butkovskaya, N. I.; Setser, D. W. Dynamics of OH and OD Radical Reactions with HI and GeH4 Studied by Infrared Chemiluminescence of the H2O and HDO Products. *J. Chem. Phys.* **1997**, *106* (12), 5028--5042.

(17) Campuzano-Jost, P.; Crowley, J. N. Kinetics of the Reaction of OH with HI between 246 and 353 K. *J. Phys. Chem. A* **1999**, *103* (ii), 2712–2719.

(18) Takacs, G. a.; Glass, G. P. Reactions of Hydrogen Atoms and Hydroxyl Radicals With Hydrogen Bromide. *J. Phys. Chem.* **1973**, *77* (8), 1060–1064.

(19) Smith, I. W. M.; Zellner, R. Rate Measurements of Reaction of OH by Resonance Absorption. *J. Chem. Soc. Faraday Trans.* **1973**, *8*, 1045–1056.

(20) Wilson, W. E.; O'Donovan, J. T.; Fristrom, R. M. Flame Inhibition by Halogen Compounds. *12Th Symp. Combust.* **1969**.

(21) Mullen, C.; Smith, M. A. Temperature Dependence and Kinetic Isotope Effects for the OH + HBr Reaction and H/D Isotopic Variants at Low Temperatures (53-135 K) Measured Using a Pulsed Supersonic Laval Nozzle Flow Reaction. **2005**, *109* (2), 3893–3902.

(22) Bell, R. P. *The Tunnel Effect in Chemistry*; Champman and Hall: London, 1980.

(23) Tsai, P.; Che, D.; Nakamura, M.; Lin, K.; Kasai, T. Orientation Dependence in the Four-Atom Reaction of OH + HBr Using the Single-State Oriented OH Radical Beam. *Phys. Chem. Chem. Phys.* **2010**, *12*, 2532–2534.

(24) Tsai, P.-Y.; Che, D.; Nakamura, M.; Lin, K.; Kasai, T. Orientation Dependence for Br Formation in the Reaction of Oriented OH Radical with HBr Molecule. *Phys. Chem. Chem. Phys.* **2011**, *13* (4), 1419–1423.

(25) Che, D.-C.; Matsuo, T.; Yano, Y.; Bonnet, L.; Kasai, T. Negative Collision Energy Dependence of Br Formation in the OH + HBr Reaction. *Phys. Chem. Chem. Phys.* **2008**, *10* (10), 1419–1423.

(26) Che, D.-C.; Doi, A.; Yamamoto, Y.; Okuno, Y.; Kasai, T. Collision Energy Dependence for the Br Formation in the Reaction of OD+HBr. *Phys. Scr.* **2009**, *80* (4), 48110.

(27) Clary, D. C.; Stoecklint, T. S.; Wickham, A. G.; Stoecklin, T. S.; Wickham, A. G. Rate Constants for Chemical Reactions of Radicals at Low Temperatures. *J. Chem. Soc. Faraday Trans.* **1993**, *89* (13), 2185–2191.

(28) Clary, D. C.; Nyman, G.; Hernandez, R. Mode Selective Chemistry in the Reactions of OH with HBr and HCl. *J. Chem. Phys.* **1994**, *101* (5), 3704–3714.

(29) Nizamov, B.; Setser, D. W.; Wang, H.; Peslherbe, G. H.; Hase, W. L.; Nizamov, B.; Setser, D. W. Quasiclassical Trajectory Calculations for the OH (X2Π) and OD (X2Π) + HBr Reactions: Energy Partitioning and Rate Constants. *J. Chem. Phys.* **1996**, *105* (22), 9897–9911.

(30) Liu, J.; Li, Z.; Dai, Z.; Huang, X.; Sun, C. Direct Ab Initio Dynamics Calculations of the Reaction Rates for the Hydrogen Abstraction OH + HBr → H_2O + Br. *J. Phys. Chem. A* **2001**, *105* (32), 7707–7712.

(31) de Oliveira-Filho, A. G. S.; Ornellas, F. R.; Bowman, J. M. Quasiclassical Trajectory Calculations of the Rate Constant of the OH + HBr → Br + H_2O Reaction Using a Full-Dimensional Ab Initio Potential Energy Surface Over the Temperature Range 5 to 500 K. *J. Phys. Chem. Lett.* **2014**, *5* (4), 706–712.

(32) de Oliveira-Filho, A. G. S.; Ornellas, F. R.; Bowman, J. M. Energy Disposal and Thermal Rate Constants for the OH + HBr and OH + DBr Reactions: Quasiclassical Trajectory Calculations on an Accurate Potential Energy Surface. *J. Phys. Chem. A* **2014**, *118*, 12080.

(33) Ree, J.; Kim, Y. H.; Shin, H. K. Dependence of the Four-Atom Reaction HBr + OH → Br + H_2O on Temperatures Between 20 and 2000 K. **2015**.

(34) Zhang, M.; Hao, Y.; Guo, Y.; Xie, Y.; Schaefer, H. F. Anchoring the Potential Energy Surface for the Br + H_2O → HBr + OH Reaction. *Theor. Chem. Acc.* **2014**, *133* (8), 1513.

(35) Moise, A.; Parker, D. H.; Ter Meulen, J. J. State-to-State Inelastic Scattering of OH by HI: A Comparison with OH-HCl and OH-HBr. *J. Chem. Phys.* **2007**, *126* (12).

(36) Inada, Y.; Akagane, K. Non-Empirical Analysis of the Chemical Reactions of Iodine with Steam; I+H_2O → HI+OH and I+H_2O → IOH+H, in Severe Light Water Reactor Accidents. *J. Nucl. Sci. Technol.* **1997**, *34* (2), 217–221.

(37) Canneaux, S.; Xerri, B.; Louis, F.; Cantrel, L. Theoretical Study of the Gas-Phase Reactions

of Iodine Atoms (2P3/2) with H_2, H_2O, HI, and OH. *J Phys Chem A* **2010**, *114*, 9270–9288.

(38) Hao, Y.; Gu, J.; Guo, Y.; Zhang, M.; Xie, Y.; Schaefer III, H. F. Spin-Orbit Corrected Potential Energy Surface Features for the I (2P3/2) + H_2O → HI + OH Forward and Reverse Reactions. *Phys. Chem. Chem. Phys.* **2014**, *16* (6), 2641–2646.

(39) Zahniser, M. S.; Kaufman, F. Kinetics of the Reaction of OH with HCl. *Chem. Phys. Lett.* **1974**, *27* (4), 507–510.

(40) Keyser, L. F. High-Pressure Flow Kinetics. A Study of the Hydroxyl + Hydrogen Chloride Reaction from 2 to 100 Torr. *J. Phys. Chem.* **1984**, *88* (20), 4750–4758.

(41) Molina, M.; Molina, L.; Smith, C. The Rate of the Reaction of OH with HCl. *Int. J. Chem. Kinet.* **1984**, *16* (9), 1151–1160.

(42) Husain, D.; Plane, J. M. C.; Slater, N. K. H. Kinetic Investigation of the Reactions of OH(X2 Π) with the Hydrogen Halides, HCl, DCl, HBr and DBr by Time-Resolved Resonance Fluorescence (A2∑+-X2Π). *J. Chem. Soc. Faraday Trans. 2* **1981**, *77* (10), 1949.

(43) Ravishankara, A. R.; Wine, P. H.; Wells, J. R.; Thompson, R. L. Kinetic Study of the Reaction of OH with HCl from 240 to 1055 K. *Chem. Phys. Lett.* **1985**, *17*, 1281–1297.

(44) Smith, I. W. M.; Williams, M. D. Effects of Isotopic Substitution and Vibrational Excitation on Reaction Rates. *J. Chem. Soc., Faraday Trans. 2* **1986**, *80*, 1043–1055.

(45) Sharkey, P.; Smith, I. W. M. Kinetics of Elementary Reactions at Low Temperatures : Rate. *J. Chem. Soc., Faraday Trans.* **1993**, *89* (4), 631–638.

(46) Battin-Leclerc, F.; Kim, I. K.; Talukdar, R. K.; Portmann, R. W.; Ravishankara, A. R.; Steckler, R.; Brown, D. Rate Coefficients for the Reactions of OH and OD with HCl and DCl between 200 and 400 K. *J. Phys. Chem. A* **1999**, *103* (17), 3237–3244.

(47) Bryukov, M. G.; Dellinger, B. Kinetics of the Gas-Phase Reaction of OH with HCl. **2006**, 936–943.

(48) Aquilanti, V.; Mundim, K. C.; Cavalli, S.; Fazio, D. De; Aguilar, A.; Lucas, J. M. Exact Activation Energies and Phenomenological Description of Quantum Tunneling for Model Potential Energy Surfaces . The F + H2 Reaction at Low Temperature. *Chem. Phys.* **2012**, *398*, 186–191.

(49) Cavalli, S.; Aquilanti, V.; Mundim, K. C.; De Fazio, D. Theoretical Reaction Kinetics astride the Transition between Moderate and Deep Tunneling Regimes: The F + HD Case. *J. Phys.*

Chem. A **2014**, *118* (33), 6632–6641.

(50) Silva, V. H. C.; Aquilanti, V.; Oliveira, H. C. B. De; Mundim, K. C. Uniform Description of Non-Arrhenius Temperature Dependence of Reaction Rates , and a Heuristic Criterion for Quantum Tunneling vs Classical Non-Extensive Distribution. *Chem. Phys. Lett.* **2013**, *590*, 201–207.

(51) Carvalho-Silva, V. H.; Aquilanti, V.; de Oliveira, H. C. B.; Mundim, K. C. Deformed Transition-State Theory: Deviation from Arrhenius Behavior and Application to Bimolecular Hydrogen Transfer Reaction Rates in the Tunneling Regime. *J. Comput. Chem.* **2017**, *38* (3), 178–188.

(52) Bryukov, M. G.; Dellinger, B.; Knyazev, V. D. Kinetics of the Gas-Phase Reaction of OH with HCl. *J. Phys. Chem. A* **2006**, *110* (3), 936–943.

(53) Guo, Y.; Zhang, M.; Xie, Y.; Schaefer, H. F. Communication: Some Critical Features of the Potential Energy Surface for the Cl + H_2O → HCl + OH Forward and Reverse Reactions. *J. Chem. Phys.* **2013**, *139* (4), 10–14.

(54) Li, J.; Dawes, R.; Guo, H. Kinetic and Dynamic Studies of the Cl(2Pu) + H_2O($\tilde{X}$ 1A 1) → HCl($\tilde{X}$ 1Σ+) + OH($\tilde{X}$ 2Π) Reaction on an Ab Initio Based Full-Dimensional Global Potential Energy Surface of the Ground Electronic State of ClH_2O. *J. Chem. Phys.* **2013**, *139* (7).

(55) Zuo, J.; Li, Y.; Guo, H.; Xie, D. Rate Coefficients of the HCl + OH → Cl + H_2O Reaction from Ring Polymer Molecular Dynamics. *J. Phys. Chem. A* **2016**, *120* (20), 3433–3440.

(56) Zuo, J.; Xie, C.; Guo, H.; Xie, D. Accurate Determination of Tunneling Affected Rate Coefficients : Theory Aeesessing Experiment Accurate Determination of Tunneling Affected Rate Coefficients : Theory Assessing Experiment. *J. Phys. Chem. Lett.* **2017**, *8* (14), 3392–3397.

(57) Mallick, S.; Sarkar, S.; Bandyopadhyay, B.; Kumar, P. Effect of Ammonia and Formic Acid on the OH• + HCl Reaction in the Troposphere: Competition between Single and Double Hydrogen Atom Transfer Pathways. *J. Phys. Chem. A* **2018**, *122* (1), 350–363.

(58) Li, J.; Corchado, J. C.; Espinosa-Garcia, J.; Guo, H. Final State-Resolved Mode Specificity in HX + OH → X + H_2O (X = F and Cl) Reactions: A Quasi-Classical Trajectory Study. *J. Chem. Phys.* **2015**, *142*, 84314.

(59) Song, H.; Guo, H. Mode Specificity in the HCl + OH → Cl + H_2O Reaction: Polanyi's Rules vs Sudden Vector Projection Model. *J. Phys. Chem. A* **2015**, *119* (5), 826–831.

(60) Bonnet, L.; Larrégaray, P.; Duguay, B.; Rayes, J.-C.; Che, D.-C.; Kasai, T. Stereoselectivity as a Probe of Unexpected Reaction Pathways. *Chem. Soc. Japan* **2007**, *80* (4), 707–710.

(61) Cireasa, R.; Beek, M. C. Van; Moise, A.; Meulen, J. J. Inelastic State-to-State Scattering of OH (, J = 3 / 2 , F) by HCl. **2005**, *74319* (May 2013).

(62) Li, J.; Li, Y.; Guo, H. Communication: Covalent Nature of XH_2O (X F, Cl, and Br) Interactions. *J. Chem. Phys.* **2013**, *138* (14).

(63) Hao, Y.; Gu, J.; Guo, Y.; Zhang, M.; Xie, Y.; Schaefer III, H. F. Spin–orbit Corrected Potential Energy Surface Features for the I (2P3/2) + H_2O → HI + OH Forward and Reverse Reactions. *Phys. Chem. Chem. Phys.* **2014**, *16* (6), 2641.

(64) Tsai, S.-M.; Lyons, J. R.; Grosheintz, L.; Rimmer, P. B.; Kitzmann, D.; Heng, K. VULCAN : An Open-Source, Validated Chemical Kinetics Python Code for Exoplanetary Atmospheres. *Astrophys. J. Suppl. Ser.* **2017**, *228* (2), 20.

(65) Marx, D.; Hutter, J. Ab Initio Molecular Dynamics: Theory and Implementation. *Mod. methods algorithms quantum Chem.* **2000**, *1*, 301–449.

(66) Paranjothy, M.; Sun, R.; Zhuang, Y.; Hase, W. L. Direct Chemical Dynamics Simulations: Coupling of Classical and Quasiclassical Trajectories with Electronic Structure Theory. *WIRE Comput. Mol. Sci.* **2013**, *3* (3), 296–316.

(67) Marx, D.; Hutter, J. *Ab Initio Molecular Dynamics: Basic Theory and Advanced Methods*; Cambridge University Press, 2009.

(68) Wang, L.-P.; Titov, A.; McGibbon, R.; Liu, F.; Pande, V. S.; Martínez, T. J. Discovering Chemistry with an Ab Initio Nanoreactor. *Nat. Chem.* **2014**, *6*, 1044–1048.

(69) Martyna, G. J.; Klein, M. L.; Tuckerman, M. Nose–Hoover Chains: The Canonical Ensemble via Continuous Dynamics. *J. Chem. Phys.* **1992**, *97*, 2635–2643.

(70) NIST Chemistry Web Book. NIST Chemistry Web Book.

(71) Hoff, J. V. Etudes de Dynamique Chimique. **1884**.

(72) Denisov, E.; Sarkisov, O.; Likhtenshtein, G. I. *Chemical Kinetics: Fundamentals and Recent Developments*; 2003.

(73) Arrhenius, S. Ueber die Reaktionsgeschwindigkeit bei der Inversion von Rohrzucker durch Saeuren. *Zeitschrift fuer Phys. Chemie 4*, 226–248.

(74) Aquilanti, V.; Cavalli, S.; De Fazio, D.; Volpi, A.; Aguilar, A.; Lucas, J. M. Benchmark Rate

Constants by the Hyperquantization Algorithm. The F + H 2 Reaction for Various Potential Energy Surfaces: Features of the Entrance Channel and of the Transition State, and Low Temperature Reactivity. *Chem. Phys.* **2005**, *308* (3 SPEC.ISS.), 237–253.

(75) Limbach, H.-H.; Miguel Lopez, J.; Kohen, A. Arrhenius Curves of Hydrogen Transfers: Tunnel Effects, Isotope Effects and Effects of Pre-Equilibria. *Philos. Trans. R. Soc. Lond. B. Biol. Sci.* **2006**, *361* (1472), 1399–1415.

(76) Smith, I. W. M. The Temperature-Dependence of Elementary Reaction Rates: Beyond Arrhenius. *Chem. Soc. Rev.* **2008**, *37* (4), 812–826.

(77) Debenedetti, P.; Stillinger, F. Supercooled Liquids and the Glass Transition. *Nature* **2001**, *410* (6825), 259–267.

(78) Smith, R. S.; Kay, B. D. Breaking through the Glass Ceiling: Recent Experimental Approaches to Probe the Properties of Supercooled Liquids near the Glass Transition. *J. Phys. Chem. Lett.* **2012**, *3* (6), 725–730.

(79) Bazito, F. F. C.; Kawano, Y.; Torresi, R. M. Synthesis and Characterization of Two Ionic Liquids with Emphasis on Their Chemical Stability towards Metallic Lithium. *Electrochim. Acta* **2007**, *52* (23), 6427–6437.

(80) Monteiro, M. J.; Camilo, F. F.; Ribeiro, M. C. C.; Torresi, R. M. Ether-Bond-Containing Ionic Liquids and the Relevance of the Ether Bond Position to Transport Properties. *J. Phys. Chem. B* **2010**, *114* (39), 12488–12494.

(81) Peleg, M. . M.; Normand, M. D. M. D.; Corradini, M. G. The Arrhenius Equation Revisited. *Crit. Rev. Food Sci. Nutr.* **2012**, *52* (9), 830–851.

(82) Coutinho, N. D.; Silva, V. H. C.; Mundim, K. C.; de Oliveira, H. C. B. Description of the Effect of Temperature on Food Systems Using the Deformed Arrhenius Rate Law: Deviations from Linearity in Logarithmic Plots vs. Inverse Temperature. *Rend. Lincei* **2015**, *26* (2), 141–149.

(83) Tolman, R. C. Statistical Merchanics Applied To Chemical Kinetics. *J. Am. Chem. Soc.* **1920**, *42* (1889), 2506–2528.

(84) Benson, S. W.; Dobis, O. Existence of Negative Activation Energies in Simple Bimolecular Metathesis Reactions and Some Observations on Too-Fast Reactions. **1998**, *5639* (97), 5175–5181.

(85) Sealtins, P. W.; Pilling, M. J.; Krasnoperov, L. N. Kinetics and Thermochemlstry of R + HBr →

RH + Br Reactions: Determinations of the Heat of Formation of C_2H_5, /-C_3H_7, Sec-C_4H_9, and T-C4H9. **1992**, 9847–9855.

(86) Seetula, J. a; Russell, J. J.; Gutman, D. Kinetics and Thermochemistry of the Reactions of Alkyl Radicals (CH3, C2H5, I-C3H7, S-C4H9, and T-C4H9) with HI: A Reconciliation of the Alkyl Radical Heats of Formation. *J. Am. Chem. Soc.* **1990**, *112* (9), 1347.

(87) Timonen, R. S.; Seetula, J. A.; Gutman, D. Kinetics of the Reactions of Alkyl Radicals (CH_3, C_2H_5,i-C_3H_7,and T-C_4H_9) with Molecular Bromine. *J. Chem. Inf. Model.* **1990**, *94*, 3005–3008.

(88) Timonen, R. S.; Gutman, D. Kinetics of the Reactions of Methyl, Ethyl, Isopropyl, and Ferf - Butyl Radicals with Molecular Chlorine. *J. Chem. Inf. Model.* **1986**, *90* (13), 2987–2991.

(89) Wollenhaupt, M.; Carl, S. A.; Horowitz, A.; Crowley, J. N. Rate Coefficients for Reaction of OH with Acetone between 202 and 395 K. **2000**, *309*, 2695–2705.

(90) Wolfgang, R. Energy and Chemical Recovery. *Acc. Chem. Res.* **1969**, *3* (2), 48–54.

(91) Mozurkewich, M.; Lamb, J. J.; Benson, S. W. Negative Activation Energies and Curved Arrhenlus Plots. 2. OH + CO. **1984**, *2* (9), 6435–6441.

(92) Aquilanti, V.; Mundim, K. C.; Elango, M.; Kleijn, S.; Kasai, T. Temperature Dependence of Chemical and Biophysical Rate Processes: Phenomenological Approach to Deviations from Arrhenius Law. *Chem. Phys. Lett.* **2010**, *498* (1–3), 209–213.

(93) Rino, J. P.; Studart, N. Um Potencial de Interação Para O Estudo de Materiais E Simulações Por Dinâmica Molecular. *Quim. Nova* **2001**, *24* (6), 838–845.

(94) Aquilanti, V.; Coutinho, N. D.; Carvalho-Silva, V. H. Kinetics of Low-Temperature Transitions and Reaction Rate Theory from Non-Equilibrium Distributions. *Philos. Trans. R. Soc. London A* **2017**, *375*.

(95) Laidler, K. J.; Eyring, H. *The Theory of Rate Processes: The Kinetics of Chemical Reactions, Viscosity, Diffusion and Electrochemical Phenomena*; McGraw-Hill Book Company, I., Ed.; 1941.

(96) Eyring, H. The Activated Complex in Chemical Reactions. *J. Chem. Phys.* **1935**, *3* (2), 107–115.

(97) Roberto-Neto, O. Elementos Da Dinâmica Química Ao Nível Da Teoria Variacional Do Estado de Transição Com Correções Interpoladas. *Química Nova*. 1999, p 737.

(98) Laidler, K. J.; King, M. C. Development of Transition-State Theory. *J. Phys. Chem.* **1983**, *87*

(15), 2657–2664.

(99) Alder, B. J.; Wainwright, T. E. Studies in Molecular Dynamics. I. General Method. *J. Chem. Phys.* **1959**, *31*, 459.

(100) Karplus, M. Development of Multiscale Models for Complex Chemical Systems: From $H+H_2$ to Biomolecules (Nobel Lecture). *Angew. Chemie - Int. Ed.* **2014**, *53* (38), 9992–10005.

(101) Frenkel, D.; Smit, B. Understanding Molecular Simulation. *Understanding Molecular Simulation*. 2002, pp 63–107.

(102) Meller, J. Molecular Dynamics ˚. *Encycl. life Sci.* **2001**, 1–8.

(103) Hutter, J. Introduction to Ab Initio Molecular Dynamics. *Lect. Notes, Phys. Chem. Institute, Univ.* **2002**.

(104) Marx, D.; Ed, J. G.; Neumann, J. Von; Marx, D.; Hutter, J. *Ab Initio Molecular Dynamics: Theory and Implementation*; NIC Series, 2000; Vol. 1.

PUBLICATIONS AND EVENTS

➢ UNRELATED TO THESIS

- AQUILANTI, VINCENZO; **COUTINHO, NAYARA DANTAS**; CARVALHO-SILVA, VALTER HENRIQUE. Kinetics of low-temperature transitions and a reaction rate theory from non-equilibrium distributions. PHILOSOPHICAL TRANSACTIONS - ROYAL SOCIETY. MATHEMATICAL, PHYSICAL AND ENGINEERING SCIENCES, v. 375, p. 20160201, 2017.

- SANCHES-NETO, FLÁVIO OLIMPIO; **COUTINHO, NAYARA DANTAS**; CARVALHO-SILVA, VALTER HENRIQUE. A novel assessment of the role of the methyl radical and water formation channel in the CH3OH + H reaction. PHYSICAL CHEMISTRY CHEMICAL PHYSICS, v. 11, p. 1111, 2017.

- **COUTINHO, NAYARA DANTAS.**; CARVALHO-SILVA, VALTER HENRIQUE.; MUNDIM, KLEBER C.; DE OLIVEIRA, HEIBBE C. B. Description of the effect of temperature on food systems using the deformed Arrhenius rate law: deviations from linearity in logarithmic plots vs. inverse temperature. REND LINCEI-SCI FIS, v. 26, p. 141-149, 2015.

- ALLUM, LÓIDE O.; NAPOLITANO, HAMILTON B.; CARVALHO, PAULO DE SOUSA ; CIDADE, AMANDA FEITOSA ; DE AQUINO, GILBERTO LUCIO BENEDITO ; **COUTINHO, NAYARA DANTAS**; CAMARGO, ADEMIR J. ; ELLENA, JAVIER ; DE OLIVEIRA, HEIBBE C. B. ; CARVALHO-SILVA, VALTER HENRIQUE. Effect of the Methanol Molecule on the Stabilization of $C_{18}H_{18}O_4$Crystal: Combined Theoretical and Structural Investigation. The Journal of Physical Chemistry. A, v. 118, p. 10048-10056, 2014.

➢ RELATED TO THESIS

- **COUTINHO, NAYARA D**.; AQUILANTI, VINCENZO; CARVALHO-SILVA, VALTER HENRIQUE; CAMARGO, ADEMIR J; MUNDIM, KLEBER C.; DE OLIVEIRA, HEIBBE C. B. . Stereodirectional Origin of -Arrhenius Kinetics for a Tetraatomic Hydrogen Exchange Reaction: Born-Oppenheimer Molecular Dynamics for OH + HBr. The Journal of Physical Chemistry. A, v. 120, p. 5408-5417, 2016.

- **COUTINHO, NAYARA DANTAS**; CARVALHO-SILVA, VALTER HENRIQUE; DE OLIVEIRA, HEIBBE C. B; CAMARGO, ADEMIR J.; MUNDIM, KLEBER C; AQUILANTI, VINCENZO. Stereodynamical Origin of Anti-Arrhenius Kinetics: Negative Activation Energy and Roaming for a Four-Atom Reaction. Journal of Physical Chemistry Letters, v. 6, p. 1553-1558, 2015.

- **COUTINHO, ND, CARVALHO-SILVA,** VH, de OLIVEIRA, HCB, AQUILANTI, V. (2016). The HI + OH ⟶ H_2O + I Reaction by First-Principles Molecular Dynamics: Stereodirectional and anti-Arrhenius Kinetics. Lecture Notes in Computer Science. In International Conference on Computational Science and Its Applications. 2017, 10408 pp. 297–313.

- CARVALHO-SILVA, VALTER HENRIQUE; **COUTINHO**, **NAYARA DANTAS**; AQUILANTI, VINCENZO. Description of deviations from Arrhenius behavior in chemical kinetics and materials science. In: International Conference of Computational Methods In Sciences And Engineering 2016 (Iccmse 2016), 2016, Athens. Org.Crossref.Xschema._1.Title@11FD8AEF. P. 020006.

- **COUTINHO, NAYARA DANTAS**, SILVA, SANCHES-NETO, FO, CARVALHO-SILVA, VH, de OLIVEIRA, HCB, RIBEIRO-JUNIOR, AQUILANTI, V. Kinetics of the $OH + HCl \longrightarrow H_2O + Cl$ reaction: rate determining roles of stereodynamic and of quantum tunnelling. Submitted on Physical Chemistry Chemical Physics (PCCP).

- **COUTINHO, NAYARA DANTAS.** Origin of non-Arrhenius Kinetics for a Tetraatomic Hydrogen Exchange Reaction: Born−Oppenheimer Molecular Dynamics for OH + HX (X= Cl, Br and I). Palestra. Simpósio de química téorica e estrutura molecular, 2017.

- VI Simpósio de Estrutura Eletrônica e Dinâmica Molecular. How Stereodirectional effect reflects on non-Arrhenius behavior? Born-Oppenheimer molecular dynamic study of the OH + HCl → H_2O + Cl and OH + HBr→ H_2O + Br reaction. 2016. (Simpósio).

- Workshop on Sterodynamics of Molecular Chirality: Quantum, Classical and Molecular Dynamics. 2016

- XVIII Simpósio Brasileiro de Química Teórica.Simulation of Reactive channels for Inorganic Cycle SNP2 Formation: A Study via *ab Initio* Molecular Dynamics. 2015.

- V Simpósio de Estrutura Eletrônica e Dinâmica Molecular.Stereodynamical Origin of Anti-Arrhenius kinetics and of Negative Activation Energy for the OH +HBr → H_2O + Br reaction.